ADDIS ABABA UNIVERSITY

SCHOOL OF GRADUATE STUDIES

SOLAR ENERGY CONVERSION BASED ON ORGANIC AND ORGANIC/INORGANIC HYBRID SOLAR CELLS

ASSEFA SERGAWIE

April 2007

SOLAR ENERGY CONVERSION BASED ON ORGANIC AND ORGANIC/INORGANIC HYBRID SOLAR CELLS

By

ASSEFA SERGAWIE

A Thesis Submitted to the

School of Graduate Studies of Addis Ababa University

In Partial Fulfillment of the Requirements for the Degree Of

Doctor of Philosophy in Chemistry

Addis Ababa University

April 2007

ADDIS ABABA UNIVERSITY

SCHOOL OF GRADUATE STUDIES

SOLAR ENERGY CONVERSION BASED ON ORGANIC AND ORGANIC/INORGANIC HYBRID SOLAR CELLS

BY: Assefa Sergawie Asemahegne

Department of Chemistry

Faculty of Science

Approved by the Examining Board

Prof. Dieter Meissner External Examiner	
Dr. Teketel Yohannes Advisor	
Prof. Theodros Solomon Advisor	
Dr. Mesfin Redi Examiner	
Dr. Shimelis Admassie Examiner	
Dr. Wendimagegn Mammo Examiner	

DECLARATION

This thesis is my original work and has not been presented for a degree in any other university, and that all sources of material used for the thesis have been dully acknowledged.

Name: Assefa Sergawie

Signature: _____

The thesis has been submitted for examination with our approval as university advisors.

Teketel Yohannes	Theodros Solomon
Associate professor of chemistry	Professor of chemistry
Addis Ababa University	Addis Ababa University

Place and date of submission: School of Graduate Studies

Addis Ababa University

April 2007

TABLE OF CONTENTS

ACKNOWLEDGEMENTS ……..…...…..…v
LIST OF FIGURES ……..…….…..……vii
LIST OF TABLES …….……... xiii
ABSTRACT ……...…..……...…… xiv

1. INTRODUCTION …….…..... 1

2. ELECTRONICALLY CONDUCTING POLYMERS ……...…….....…..... 5
2.1. Electronic structures of conjugated polymers ……...…..…...……..... 6
2.2. Structural distortions in conducting polymers: Solitons, Polarons and Bipolarons …….. 8
2.2.1. Soliton formation ……..……...……. 8
2.2.2. Polaron formation …….……...……..... 8
2.2.3. Bipolaron formation ……..…….……..... 9
2.3. Charge transport in polymeric organic semiconductors ……... 11
2.3.1. Conductivity of conducting polymers ……..…… 12
2.3.2. Charge Transport Mechanism ……..… 12
2.4. Electrochemistry of conducting polymers …….…….. 13
2.4.1. Electrochemical polymerization ……..…….…..…….. 13
2.4.2. Electrolytes and Electrodes ……..……...…….. 14
2.4.3. Cyclic voltammograms of conducting polymers ……..……... 16

3. IONICALLY CONDUCTING POLYMERS …….. 19
3.1. The thermodynamics of salt dissolution ……...…..... 20
3.2. Ion conduction in polymer electrolytes ……...……. 21
3.3. Factors affecting ionic conductivity in polymer electrolytes ……....….... 22
3.3.1. Effect of concentration and ionic mobility …….……..…… 22
3.3.2. Effect of temperature ……..…….……. 23

4. ELECTRONIC PROPERTIES OF INORGANIC SEMICONDUCTORS …. 24

4.1. Crystal structures of semiconductors ……..…..……..... 24

4.2. Band structure and chemical properties of inorganic semiconductors …..... 24

4.3. Buckminsterfullerene ……...……... 25

5. PHOTOELECTROCHEMICAL SOLAR ENERGY CONVERSION …..….. 27

5.1. Principle of operation ……...…….……... 27

5.2. Semiconductor/electrolyte interface ……. 28

5.3. Dye sensitized photoelectrochemical cells ……... 29

5.3.1. Working principle of dye-sensitized photoelectrochemical cells 29

5.3.2. Electron transport in nanostructred dye-sensitized photo-electrochemical cells. ……...…... 31

5.4. Current-voltage behavior for a semiconductor/liquid interface ……...…… 32

5.5. Characteristics of photovoltaic cells ……...……. 34

5.5.1. Open-circuit Voltage ……..…….. 36

5.5.2. Short-circuit Current ……..…….. 38

5.5.3. Fill Factor ……..…….…….. 38

5.5.4. Power Conversion Efficiency ……..…….……... 39

5.5.5. Incident Photon-to-current Conversion Efficiency …...…..……..… 39

5.6. Factors affecting the efficiency of an organic solar cell ……...…….. 40

5.6.1. Polymer Absorption ……..……... 40

5.6.2. Polymer Energy Levels ……..…….…. 41

5.6.3. Charge Transport in a Conducting Polymer ……...…….. 44

5.6.4. Morphology ……..……..... 45

5.6.5. Selectivity of the Electrodes ……...……..…..….. 46

REFERENCES ……...……..……...… 47

6. POLYMER-SENSITIZED PHOTOELECTROCHEMICAL CELLS …… 53

6.1. Background ……...…..….. 53

6.2. Polymer-sensitized Photoelectrochemical Cell Consisting of Eu^{2+}/Eu^{3+} Redox

Couple: A Photoelectrochemical Cell Based on Emeraldine Base Form of Polyaniline ……. 55

6.2.1. Background ……..…… 55

6.2.2. Experimental ……..…….. 56

6.2.2.1. Preparation of Nc-TiO_2 film electrode …...…… 56

6.2.2.2. Preparation of polyaniline ……..…...…… 57

6.2.2.3. Photoelectrochemical studies ……..…….. 57

6.2.3. Results and discussion ……..…….……... 58

6.2.3.1. Current – Voltage characteristics …….…… 58

6.2.3.2. The photocurrent action spectra …….…….. 63

6.2.3.3. Conclusion ……..……..... 65

6.3. Polymer-sensitized Photoelectrochemical Cells Consisting of I_3^-/I^- Redox Couple…….……..…….…….…. 66

6.3.1. Background ……..…… 66

6.3.2. Experimental ……..……..... 67

6.3.2.1. Device preparations and characterizations ……..... 67

6.3.2.2. The photoelectrochemical cell construction …..….... 70

6.3.2.3. Experimental setup ……...…… 71

6.3.3. Results and discussion ……...……... 73

6.3.3.1. A Comparative Study on Liquid-state Photoelectro-chemical Cells Based on Poly(3-hexylthiophene) and a Composite Film of Poly(3-hexylthiophene) and Nano-crystalline Titanium Dioxide …….……..... 73

6.3.3.2. Synthesis and Characterization of Poly[3-(2',5'-diheptyloxyphenyl)thiophene] for use in Photo-electrochemical Cells …….……... 81

6.3.3.3. Effect of Side Chain Length on the Electrochemical and Photoresponse Characteristics of Poly[3-(2',5'-dialkoxyphenyl)thiophenes] …….……..... 90

6.3.3.4. The Photoresponse Behavior of a Solid-state MEH-PPV - Sensitized Titanium Dioxide Photoelectrochemical Cell. ……...…102

6.3.3.5. A Comparative Study on Solid-state Photoelectrochemical Solar Energy Conversion Based on Poly[2-methoxy-5-(2'-ethylhexyloxy)-1,4-phenylenevinylene], MEH-PPV, and a blend of MEH-PPV and C_{60} ……..... 111

REFERENCES ……..……..…. 120

ACKNOWLEDGEMENTS

I am greatly indebted to my research advisors Dr. Teketel Yohannes and Prof. Theodros Solomon for their guidance and encouragement while I carry out this research work and study for my PhD. I experienced the support of an advisor beyond responsibility under difficult circumstances.

I thank the Austrian Academic Exchange Service (ÖEAD) for giving me scholarship for a one year research work as part of my PhD work. I would like to thank Prof. N.S. Sariciftci for giving me the opportunity to do part of my research work under his supervision at Linz Institute for Organic Solar Cells (LIOS), Johannes Kepler University, Linz, Austria. He also donated the chemicals I needed to continue my research work at the Addis Ababa University. I would also thank Dr. H. Neugebauer for his guidance and members of the institution for their cooperation during my stay at LIOS.

I am grateful to Ethiopian Science and Technology commission, the Third World Academy of Sciences, Trieste, Italy and SIDA/SAREC for financial support. I am indebted to the Bahir Dar University for giving me the sponsorship and continuous support during my study. I greatly appreciate the department of Chemistry, Addis Ababa University, and staff members for their sincere cooperation during my study. I specially thank with gratitude Dr. Wendimagegn Mammo for generously providing the monomers of some of the polymers I studied in my research work. I am also thankful to Dr. Shimelis Admassie for his close assistance and Dr. Mesfin Redi for his genuine evaluation of my progress report.

With only limited access to research journals, getting literatures would have been very difficult had there not been the cooperation of my friend, Kahsay Gebre Medhin, from USA. I thank you very much.

I benefited from the pray of my mother to God, and from the continuous support and encouragement of my sisters, brothers, family members and friends. Thank you all.

Finally, I would like to express my sincere gratitude to the support and encouragement I got from my beloved wife Sr. Kibebework Haddis. You showed great endurance in taking care of me and our daughter, Bilien, while I go through the hard way. May God give you His rewards for your sacrifices!

LIST OF FIGURES

2.1. Chemical structures of some conjugated polymers, a): polythiophene (X = S); polyfuran (X = O); polypyrrole (X = NH), b) poly(*p*-phenylene), c) polyaniline. ….... 5

2.2. The development of a polyacetylene band structure from the molecular orbitals of ethylene. From left to right, the molecular orbitals progressively develop into a band structure as the length of the conjugation chain is increased. For shorter polyene chains, Δ represents the HOMO-LUMO energy gap. For the infinite polyene chain, VB and CB denote the valence band and the conduction band respectively and E_g is the band gap energy. ……...……..…..…….…….. 6

2.3. Chemical structure of a) *trans*-polyacetylene and solitons in *trans*-polyacetylene: b) neutral soliton, c) positive soliton, d) negative soliton. ……...……...…….. 8

2.4. Actual structures of polarons and bipolarons in polyhetrocyclic polymers (X = S, O, NH, etc). ……...……...……...… 9

2.5. Energy band diagrams showing polaron and bipolaron states in the non-degenerate polymer. The arrows indicated by the numbers 1, 2, 3, and 4, represents the possible optical transitions. …..……..… 10

2.6. Scheme for the generic electropolymerization pathway valid for many conducting polymers. 14

2.7. The Cyclic voltammogram for the electropolymerization of DHOPT on ITO-glass at a rate of 10 mV/s. The solution contains 1 mM DHOPT and 0.1 M $LiClO_4$ inCH_3CN. The inset is the voltammogram of the first cycle showing the crossover. 16

3.1. Schematic representation of cation motion in a polymer electrolyte. ……...… 22

4.1. The Chemical structure of C_{60}. ……..… 26

5.1. Schematic representation of a photoelectrochemical cell. ……...…… 27

5.2. Schematic representation of the formation of the Schottky junction between a p-type semiconductor and an electrolyte containing a redox couple O/R: a) before the contact, b) after the contact, considering the redox potential (E_0) of the electrolyte is higher than the semiconductor Fermi level (E_f). …… 29

5.3. Schematic of operation of dye-sensitized PEC. The photoanode, made of dye-sensitized nc-TiO_2, receives electrons from the photoexcited dye (path 1). The

oxidized dye is returned to its neutral state by receiving electrons from the reduced form (I^-) of the redox couple (I_3^-/I^-). The I^- is regenerated by the reduction of I_3^- at the counter electrode by the electrons circulated through the external circuit. Path 2 and path 3 refer to charge recombination processes. ΔV is the maximum attainable voltage under illumination. …… 31

5.4. I–V curves of an organic PV cell under dark (left) and illuminated (right) conditions. The open-circuit voltage (V_{OC}) and the short-circuit current (I_{SC}) are shown. The square $I_{max}V_{max}$ gives the maximum output. 35

5.5. The solar irradiance received on the surface of the earth. The spectrum includes data from both the diffuse and direct radiation and is measured at sea level with the sun at 37° to the vertical. This spectrum is known as the AM 1.5 solar spectrum. ….....… 41

5.6. Illustration of exciton dissociation at the donor/acceptor interface of organic solar cell. ΔV is the maximum cell voltage under illumination. ……..…….. 42

5.7. Illustration of competing energy and charge transfer processes. ……....…… 44

5.8. A schematic representation of the energy levels of two conjugated polymers and a hole trap site. For polymer 1, a hole in the HOMO level will see the hole trap species as a trapping site. However, a hole on polymer 2, which has a smaller HOMO energy, will not interact with the hole trap. ……..……..... 45

6.1. AFM picture of emeraldine base film on ITO-glass. ……...… 58

6.2. The UV-Vis absorption spectrum of EB film on ITO-glass. ……..…. 59

6.3. Cyclic voltammogram of EB film on Pt. Electrolyte: CH_3CN + 0.1M $(C_4H_9)_4NPF_6$, Reference electrode: quasi Ag/AgCl, Counter electrode: Pt, Scan rate: 5mV/s, E^{Ox}_{onset} = 0.82 V, E^{Red}_{onset} = -0.60 V. …….……..…… 60

6.4. Current density *vs*. voltage characteristics for ITO/EB/Electrolyte/Pt cell in the dark (open circles) and under 50 mW/cm^2 white light illumination from Xe lamp (closed circles). Electrolyte: CH_3OH + 0.02M $EuCl_2$ + 0.02M $EuCl_3$. ...……..…… 61

6.5. AFM picture of Nc-TiO_2/EB composite film on ITO-Glass. ……...……..…… 62

6.6. Current density *vs*. voltage characteristics for Glass/ITO/EB/Nc-TiO_2/Electrolyte/Pt cell in the dark (open circles) and under 50 mW/cm^2 white light illumination from Xe lamp (closed circles). Electrolyte: CH_3OH + 0.02M $EuCl_2$ + 0.02M $EuCl_3$. 62

6.7. The photocurrent action spectra for the system: Glass/ITO/Nc-TiO_2/Electrolyte/Pt (open circles) and Glass/ITO/EB/Nc-TiO_2/Electrolyte/Pt (closed circles). Electrolyte:

CH_3OH + 0.02M $EuCl_2$ + 0.02M $EuCl_3$. Inset: UV-Vis absorption spectra of emeraldine base film on ITO-glass. ……..……..…..… 63

6.8. A schematic energy level diagram for the device: Glass/ITO/EB/Nc-TiO_2/Electrolyte/Pt. The excitation of emeraldine base form of PAni at 660 nm is shown. ……. 64

6.9. Schematic layout of the (a) photoelectrochemical cells used and (b) chemical structure of the counter electrode, PEDOT. ……...……..……...… 71

6.10. General experimental set-up for the photoelectrochemical measurements. **a)** Power supply, **b)** Lamp housing, **c)** Monochromator, **d)** Sample holder, and **e)** Input/output measuring apparatus. ……..……..…… 72

6.11. The chemical structure of P3HT. ……..…… 73

6.12. Current density *vs.* voltage characteristics of the P3HT based liquid-state PEC. **a)** In the dark, **b)** Under white light illumination from the ITO/PEDOT side (front side) with light intensity of 100 mW/cm^2. ……...…. 74

6.13. Current density *vs.* voltage characteristics of the nc-TiO_2/P3HT based liquid-state PEC. **a)** In the dark, **b)** Under white light illumination from the ITO/nc-TiO_2/P3HT side (backside) with light intensity of 100 mW/cm^2. ……..…… 75

6.14. Short-circuit photocurrent action spectra of P3HT based liquid-state PEC under illumination from the front side (open triangles) and from the backside (closed triangles). ……..…….... 76

6.15. Short-circuit photocurrent action spectra of nc-TiO_2 /P3HT based liquid-state PEC under illumination from the front side (open squares) and from the backside (closed squares). ……..……. 76

6.16. Normalized optical absorption spectrum of P3HT (solid line) film on ITO-glass and normalized photocurrent action spectra of P3HT based (triangles) and nc-TiO_2/P3HT based (squares) devices for front side (open symbols) and backside (closed symbols) illuminations. ……..……..…… 78

6.17. Plot of V_{OC} *vs.* log I_{in} of P3HT based (open squares) and nc-TiO_2/P3HT based (closed squares) liquid-state PECs. ……..……..… 79

6.18. Plot of log I_{SC} *vs.* log I_{in} of P3HT based (open squares) and nc-TiO_2/P3HT based (closed squares) liquid-state PECs. ……..…… 80

6.19. The chemical structure of poly[3-(2’,5’-diheptyloxyphenyl)thiophene]. …...…..… 81

6.20. Cyclic voltammograms recorded for the electropolymerization of 1mM DHOPT on glassy carbon disk electrode in CH_3CN solution containing 0.1M of $LiClO_4$. The potential is scanned repetitively between 0.4 V and 1.2 V at a scan rate of 10 mV/s. ……..…….. 82
6.21. Cyclic voltammogram of PDHOPT on glassy carbon disk electrode recorded in a 0.1M TEATFB/CH_3CN solution at a scan rate of 10 mV/s. ……..……..… 83
6.22. UV-Vis absorption spectra of the undoped PDHOPT film on ITO-glass. ……..….. 83
6.23. Current density *vs*. voltage characteristics of the PDHOPT based liquid-state PEC. **a)** In the dark, **b)** Under white light illumination from the ITO/PDHOPT side (backside) with light intensity of 80 mW/cm^2. ……..……...…… 84
6.24. Current density *vs.* voltage characteristics of the nc-TiO_2/PDHOPT based liquid-state PEC. **a)** In the dark, **b)** Under white light illumination from the ITO/TiO_2/PDHOPT side (backside) with light intensity of 80 mW/cm^2. ……...… 85
6.25. Short-circuit photocurrent action spectrum of PDHOPT based liquid-state PEC under illumination from the front side. ……..……...…… 86
6.26. Short-circuit photocurrent action spectrum of nc-TiO_2 /PDHOPT based liquid-state PEC under illumination from the front side. ……...…… 86
6.27. Normalized optical absorption spectrum of PDHOPT (solid line) and normalized photocurrent action spectrum of PDHOPT based (open squares) and TiO_2/PDHOPT based (closed squares) devices for front side illuminations. ……...…… 87
6.28. Plot of V_{OC} *vs.* log I_{in} of PDHOPT based (open squares) and nc-TiO_2/PDHOPT based (closed squares) liquid-state PECs. ……..……... 88
6.29. Plot of log I_{SC} *vs.* log I_{in} of PDHOPT based (open squares) and nc-TiO_2/PDHOPT based (closed squares) liquid-state PECs. ……..….. 89
6.30. The chemical structures of: a) PDOOPT, b) PDHOPT and c) PDBOPT. …...…..... 90
6.31. Cyclic voltammograms for the electropolymerization of: (**a**) DOOPT, (**b**) DHOPT and (**c**) DBOPT on glassy carbon disk electrode in CH_3CN solution containing 1.0 mM of the monomers and 0.1 M of TEATFB recorded at a scan rate of 10 mV/s. …..……. 91
6.32. Cyclic voltammogram of: (**a**) PDOOPT, (**b**) PDHOPT and (**c**) PDBOPT on glassy carbon disk electrode recorded in a 0.1 M TEATFB/CH_3CN solution at a scan rate of 10 mV/s. ……..……..…… 93

6.33. UV-Vis Absorption spectra (normalized at 400 nm) of PDOOPT (closed squares), PDHOPT (open squares) and PDBOPT (closed triangles) films electrochemically coated on ITO-glass. ……..…….…… 94

6.34. Current density *vs.* voltage characteristics of the polymer/nc-TiO_2 based liquid-state PEC in the dark where the polymer is PDHOPT (dot line), PDOOPT (solid line) and PDBOPT (dash line). I-V characteristics of nc-TiO_2/polymer based PECs in the dark where the polymer is PDBOPT (dash line), PDHOPT (dot line) and PDOOPT (solid line). …… 96

6.35. Current density *vs.* voltage characteristics of the polymer/nc-TiO_2 based liquid-state PEC under white light illumination from the ITO/nc-TiO_2/polymer side (backside) with light intensity of 80 mW/cm^2 where the polymer is PDHOPT (dot line), PDOOPT (solid line) and PDBOPT (dash line). ……..…..……..…… 96

6.36. Action spectrum of PDOOPT/nc-TiO_2 (solid square), PDHOPT/nc-TiO_2 (open square) and PDBOPT/nc-TiO_2 (closed triangle) based liquid-state PEC under illumination from the backside. ……..……..……...…… 98

6.37. Plot of V_{OC} *vs.* log I_{in} of PDOOPT/nc-TiO_2 (solid squares), PDHOPT/nc-TiO_2 (open squares) and PDBOPT/nc-TiO_2 (closed triangles) based liquid-state PECs. ….…..... 99

6.38. Plot of log I_{SC} *vs.* log I_{in} of PDOOPT/nc-TiO_2 (solid squares), PDHOPT/nc-TiO_2 (open squares) and PDBOPT/nc-TiO_2 (closed triangles) based liquid-state PECs...…….... 100

6.39. The chemical structure of MEH-PPV. ……..……..…..…… 102

6.40. Current density *vs.* voltage characteristics of the nc-TiO_2/MEH-PPV based solid-state PEC a) In the dark and b) Under white light illumination from the backside at light intensity of 100 mW/cm^2. ……..… 103

6.41. Short-circuit photocurrent changes induced by switching illumination on and off from the backside of the nc-TiO_2/MEH-PPV based solid-state PEC with incident light intensity of 100 mW/cm^2. ……. 104

6.42. Open-circuit voltage response of the nc-TiO_2/MEH-PPV based solid-state PEC to switching illumination on and off from the backside with incident light intensity of 100 mW/cm^2. …… 105

6.43. Optical absorption spectrum of MEH-PPV film (solid line) on ITO-glass and the photocurrent action spectra of nc-TiO_2/MEH-PPV based PEC under illumination from the backside (solid squares) and front side (open squares). …….……. 106

6.44. Incident light intensity distribution (open triangles) and short-circuit photocurrent density spectra of the nc-TiO_2/MEH-PPV based solid-state PEC under illumination from the backside (solid squares) and front side (open squares). ……..…… 107
6.45. Dependence of short-circuit photocurrent on incident light intensity for illumination through the backside of the nc-TiO_2/MEH-PPV based solid-state PEC. ……..…..… 108
6.46. Dependence of photovoltage on incident light intensity for illumination through the backside of the nc-TiO_2/MEH-PPV based solid-state PEC. ……..…… 109
6.47. Current density *vs*. voltage characteristics of the MEH-PPV based solid-state PEC: a) In the dark and b) Under white light illumination from the ITO/PEDOT side (front side) at light intensity of 100 mW/cm^2. ……...……...… 112
6.48. Current density *vs*. voltage characteristics of the MEH-PPV/C_{60} based solid-state PEC: a) In the dark and b) Under white light illumination from the ITO/PEDOT side (front side) at light intensity of 100 mW/cm^2. ……..……...… 112
6.49. Schematic of operation of the MEH-PPV and MEH-PPV/C_{60} based solid-state PEC. ……...……. 114
6.50. Action spectra of MEH-PPV based solid-state PEC under illumination from the front side (closed triangles) and from the backside (open triangles). ……..……...… 115
6.51. Action spectra of MEH-PPV/C_{60} based solid-state PEC under illumination from the front side (closed squares) and from the backside (open squares). ……...…… 115
6.52. Normalized optical absorption spectrum of MEH-PPV/C_{60} film on ITO-glass (solid line) and normalized photocurrent action spectra of MEH-PPV based (closed triangles) and MEH-PPV/C_{60} based (closed squares) devices for front side illuminations. …. 117
6.53. Plot of log I_{SC} *vs.* log I_{in} of MEH-PPV based (open squares) and MEH-PPV/C_{60} based (closed squares) solid-state PECs. ……...……..…… 118
6.54. Plot of V_{OC} *vs.* log I_{in} of MEH-PPV based (open squares) and MEH-PPV/C_{60} based (closed squares) solid-state PECs. ……..…… 119

LIST OF TABLES

6.1. The performance of photoelectrochemical devices containing P3HT and nc-TiO_2/P3HT photoactive electrodes when illuminated with light intensity of 100 mW/cm^2. ……..… 75

6.2. The performance of photoelectrochemical devices containing PDHOPT and TiO_2/PDHOPT as photoactive electrodes when illuminated with light intensity of 80 mW/cm^2. …….. 85

6.3. Cyclic voltammetry data, estimated HOMO-LUMO energy levels and optical band gaps (E_g^{opt}) of PDOOPT, PDHOPT and PDBOPT films. ……..……..……...…..... 95

6.4. Photoelectrochemical cell performance parameters of PDOOPT/nc-TiO_2, PDHOPT/nc-TiO_2 and PDBOPT/nc-TiO_2 based devices depicted in Figures 6.35 and 6.36. ……...…….. 97

6.5. The performance of photoelectrochemical devices based on MEH-PPV and MEH-PPV/C_{60} photoactive electrodes when illuminated with white light intensity of 100 mW/cm^2. …….....….…… 113

6.6. The photocurrent action spectra (IPCE) for the MEH-PPV based and for the MEH-PPV/C_{60} based solid-state PECs. …….……..…… 116

ABSTRACT

Solar energy conversion based on organic and organic/inorganic hybrid solar cells has been studied in different types of photoelectrochemical cells (PECs). PECs that consist of Eu^{2+}/Eu^{3+} and I_3^-/I^- have been designed and studied for their photoresponse behavior. In devices that consist of Eu^{2+}/Eu^{3+} in methanol, liquid-state PECs using the emeraldine base form of polyaniline (EB) as a photoactive material have been fabricated and studied for their photoresponse behaviors. The photoresponse of EB:Nc-TiO_2-based PEC is significantly higher than that of EB-based and Nc-TiO_2-based PECs. A PEC with a structure: Glass/ITO/EB:Nc-TiO_2/Electrolyte/Pt produced an open circuit voltage (V_{OC}) of 0.205 V and short-circuit current (I_{SC}) of 105 μA/cm^2 under 50 mW/cm^2 white light illumination. The device showed an induced photon-to-current conversion efficiency (IPCE) of 80% and 8% at 370 nm and 700 nm, respectively. Different systems of devices that consist of I_3^-/I^- have been studied for their photoresponse behaviors. In liquid-state PECs, separate and comparative studies were conducted where the photoactive electrodes consist of chemically prepared poly[3-hexylthiophene], P3HT, and electrochemically prepared poly[3-(2',5'-dialkoxyphenyl)thiophenes]. In P3HT-based PECs, a comparative study was done between cells consisting of photoactive electrodes of P3HT and a composite of nc-TiO_2 and P3HT. P3HT based devices showed a V_{OC} of 160 mV, an I_{SC} of 2.4 μA/cm^2 and a fill factor (*FF*) of 0.42 when illuminated with white light intensity of 100 mW/cm^2. Nc-TiO_2/P3HT based devices showed better performance with a V_{OC} of 0.51 V, an I_{SC} of 0.31 mA/cm^2, and a *FF* of 0.51 when illuminated under the same condition. The *IPCE%* obtained at 550 nm for P3HT-based devices and for nc-TiO_2/P3HT-based devices were 0.18% and 4%, respectively. In P3HT-based devices, P3HT showed its p-type behavior while in nc-TiO_2/P3HT based devices, P3HT acted as a sensitizer to nc-TiO_2. In poly[3-(2',5'-dialkoxyphenyl)thiophenes] based cells, poly[3-(2',5'-dioctyloxyphenyl)thiophene], poly[3-(2',5'-diheptyloxyphenyl)thiophene] and poly[3-(2',5'-dibutyloxyphenyl)thiophene] were electrochemically deposited on nc-TiO_2 coated ITO-glass. The redox properties of the polymers were characterized using cyclic voltammetry. The energy levels of the highest occupied molecular orbitals (HOMO) and the lowest unoccupied molecular orbitals (LUMO) have been estimated from their cyclic voltammograms and UV-Vis absorption spectra. The poly[3-(2',5'-dialkoxyphenyl)thiophenes] sensitize nc-TiO_2 in liquid-state

photoelectrochemical cells. The investigated polythiophenes with longer dialkoxyphenyl substituents exhibited a lower photoelectrochemical cell performance. The results show that the expected better exciton and hole mobility of shorter polydialkoxyphenyl substituted thiophenes can be used for solar cell application by improving the film properties of the polymers. In solid-state polymer-sensitized photoelectrochemical cells, we have designed devices where poly[2-methoxy-5-(2'-ethylhexyloxy)-1,4-phenylenevinylene], MEH-PPV, was used as a sensitizer to TiO_2 and as electron donor to C_{60}. The ion-conducting polymer, poly[oxymethylene-oligo(oxyethylene)] complexed with I_3^-/I^- redox couple was used as a solid polymer electrolyte. It has been observed that PECs with a composite of the inorganic semiconductors/MEH-PPV photoactive electrodes exhibit improved cell performances when compared with MEH-PPV based PECs. Nc-TiO_2/MEH-PPV based devices produced an I_{SC} of 0.145 mA/cm^2, and a V_{OC} of 410 mV at light intensity of 100 mW/cm^2. The power conversion efficiency, the *FF* and the *IPCE%* were 0.03% and 0.5 and 1.8%, respectively. In PECs based on MEH-PPV/$C_{60,}$ an IPCE% of 0.32% and a V_{OC} of 281 mV and an I_{SC} of 13.4 μA cm^{-2} were obtained at light intensity of 100 mW/cm^2. Our results show that organic/inorganic hybrid PECs show improved performance when compared with organic based PECs and polymer-sensitized PECs could be alternates in designing solar energy conversion devices.

Keywords: Polymer-sensitized photoelectrochemical cell; Solar cell characteristics; Electrochemical polymerization; Semiconducting polymer; Nano-crystalline titanium dioxide; Buckminsterfullerene; Poly[oxymethylene-oligo(oxyethylene)]; Redox couple.

1. INTRODUCTION

Traditional fossil fuel energy sources are finite and release waste products into the atmosphere that threaten the earth's global environment. As a result, alternative energy sources, including wind, hydroelectric and solar energy are receiving increasing attention. In particular, solar energy is attractive due to the abundance and consistency of sunlight.

Photovoltaic cells are solid-state devices that convert solar illumination into electrical energy. The conventional silicon type solar cells are based on the *p*-*n* junction of *n*- and *p*-type solid semiconductors. Absorption of light generates electron-hole pairs that diffuse to the junction. The photogenerated electron-hole pairs are driven efficiently in opposite directions by an electric field existing at the boundary (*p*-*n* junction) [1]. This directs the electric current to flow in only one direction through an external circuit and to produce electrical power. The maximum conversion efficiency for crystalline Si solar cells that employ a single junction has reached 24% [2]. However, the relatively high cost of manufacturing these silicon solar cells has prevented them from widespread use. Another disadvantage of silicon solar cells is the use of toxic chemicals in their manufacture. These aspects prompted the search for less toxic and low cost solar cell alternatives.

The second type of solar energy conversion system is a photoelectrochemical cell. In a photoelectrochemical cell, a semiconductor electrode and a counter electrode are immersed into an electrolyte solution that contains a redox couple. When light is incident on the photoelectrochemical cell, the semiconductor electrode absorbs photons and creates excited electrons. These electrons sense the electric field present at the solid/liquid interface, and are either attracted or repelled by this field (depending on its sign), to produce a directional current through the cell [3]. A photoelectrochemical cell can produce electricity, chemical fuels or both. If the reactions at the counter electrode are the reverse of those at the semiconductor electrode, no net chemical change will take place and the light induced current will only result in the production of electrical power in the cell. If the cell reactions that follow light absorption result with net chemical changes, the photoelectrochemical cell will convert the incident solar energy into chemical fuels or into both chemical fuels and electrical energy.

Organic photovoltaic cells are solar energy conversion devices that convert light energy to electrical energy. In organic photovoltaic cells, the organic light-absorbing semiconductor polymer is sandwiched between two electrodes having different work functions. One of the electrodes is (semi-) transparent; often indium doped tin oxide (ITO). The other electrode is very often aluminum. When light is absorbed by a photovoltaic device, an electron is promoted from the highest occupied molecular orbital (HOMO) to the lowest unoccupied molecular orbital (LUMO) forming an exciton [4]. This process must be followed by exciton dissociation to electrons and holes. The electron must then reach one electrode while the hole must reach the other electrode. The asymmetry in the work functions of the electrodes directs the electron flow from the low work function electrode to the high work function electrode. The main advantages of organic photovoltaic cells are the easy preparation, low processing temperatures, low-cost materials and processing technology and the possibility to produce flexible devices on plastic substrates [5]. Up to now, their power conversion efficiencies are low compared to the silicon solar cells. The efficiency of these devices is limited by inefficient hopping charge transport [6] and the presence of structural electron traps in the form of incomplete pathways in the percolation network [7]. To improve the power conversion efficiency of organic photovoltaic cells, a heterojunction structure between a semiconducting polymer and an electron acceptor (such as fullerene and its derivative, phenyl C_{61}-butric acid methyl ester) have been made. In these devices only the polymer absorbs the light and the acceptor is used for the effective charge separation, transport and injection to the back contact. The power conversion efficiencies of these devices at light intensity of 100 mW/cm^2 have reached ~5% [8-10].

Bulk heterojunctions from blends of *n*-type and *p*-type semiconducting polymers have also been made. The benefit of this concept is that both the *p*-type and the *n*-type materials can absorb light. However because of the absence of good *n*-type semiconducting polymers and the diffusion of doping impurities from the *p*- to *n*-side (and *vice versa*) the efficiencies for these devices are below 1% [11,12].

Besides these fully organic photovoltaic devices, semiconducting polymers and oligomers can also be used in combination with inorganic semiconductors such as TiO_2, $CuInSe_2$ and $CuInS_2$ [13-18], a concept that is based on liquid-junction dye-sensitized solar cells. In these

hybrid organic/inorganic devices, the good electron accepting and conducting properties of the inorganic semiconductors can, in principle, be combined with cheap, solution processing of the semiconducting polymers. The semiconducting polymer replaces both the dye and the liquid electrolyte and it takes care of the absorption of the sunlight, charge injection into the inorganic semiconductor and the transport of holes after charge separation. The inorganic semiconductor serves as an electron accepting and transporting phase. The reported maximum efficiencies for such solid-state devices for bilayers and heterojunctions are below 0.5% [19,20]. The incomplete filling of the nano-pores of the inorganic semiconductor and the associated problems in charge separation and charge transport have a negative impact on the efficiencies of these types of devices.

Despite the high power conversion efficiencies of dye-sensitized photoelectrochemical cells, their commercial applications are limited due to problems like leakage of the electrolyte and the degradation of both the electrolyte [21] and the dye [22]. Various studies with different approaches have been carried out to alleviate the problems associated with liquid-state dye-sensitized photoelectrochemical cells. These include replacement of the liquid electrolyte by a polymer electrolyte [23] and by a hole-transporting material [24-27], replacement of the dye by a semiconducting polymer [28-30] and replacement of both the dye and the liquid electrolyte by a semiconducting polymer that plays the role of both a sensitizer and a hole-transporting medium [31,32].

In this work, we study conducting polymer-sensitized photoelectrochemical cells where the inorganic materials are nanocrystalline titanium dioxide (nc-TiO_2). Use of semiconducting polymers as sensitizers may be more advantageous than dye molecules with respect to the ease of large-scale production, cost and involvement of less toxic chemicals during the preparation of the polymers. Such systems may be advantageous since both the polymer and the redox couple can facilitate the transport of holes. The polymer absorbs light in the visible part of the spectrum. Following excitation, the excited electrons may be injected to the conduction band of the inorganic semiconductor. For charge transfer to occur, the polymers chosen should have their lowest unoccupied molecular orbitals above the conduction band of nc-TiO_2 and their highest occupied molecular orbitals above the valence band of TiO_2 but below the redox potential of the redox couples in the energy scale.

Our work has two major parts.

1. Polymer-sensitized photoelectrochemical cell that consists of Eu^{2+}/Eu^{3+}: Here a liquid-state photoelectrochemical cell based on emeraldine base form of polyaniline has been devised and studied for its photoresponse behavior.

2. Polymer-sensitized photoelectrochemical cells that consist of I_3^-/I^-: Different systems have been studied for their photoresponse behavior.

In liquid-state polymer-sensitized photoelectrochemical cells,

1. A comparative study was conducted where the photoactive electrodes consist of chemically prepared poly[3-hexylthiophene], P3HT, and a composite film of nc-TiO_2 and P3HT (nc-TiO_2/P3HT).

2. Separate and comparative studies were conducted where the photoactive electrodes consist of poly[3-(2',5'-dialkoxyphenyl)thiophenes], electrochemically prepared on indium doped tin oxide coated glass (ITO-glass) and on nc-TiO_2 coated ITO-glass. The investigated polymers are poly[3-(2',5'-dioctyloxyphenyl)thiophene], poly[3-(2',5'-diheptyloxyphenyl) thiophene] and poly[3-(2',5'-dibutyloxyphenyl)thiophene].

In solid-state polymer-sensitized photoelectrochemical cells, we have designed devices where poly[2-methoxy-5-(2'-ethylhexyloxy)-1,4-phenylenevinylene], was used as a sensitizer to nc-TiO_2. A solid-state photoelectrochemical cell that uses C_{60} as an electron acceptor has also been designed. The ion-conducting polymer, poly[oxymethylene-oligo(oxyethylene)], POMOE, complexed with I_3^-/I^- redox couple was used as a solid polymer electrolyte.

2. ELECTRONICALLY CONDUCTING POLYMERS

Conjugated polymers have been the focus of extensive research since the discovery of electrical conductivity in polyacetylene by Shirakawa, Heeger and MacDiarmid in 1977 [33,34]. Conjugated polymers have recently attracted a great amount of interest as conducting and semiconducting materials, and have been successfully applied to electroluminescent devices, field-effect transistors, and photovoltaic cells [35-38]. Because organic materials can be processed at low temperature, they can be fabricated into thin films onto plastic substrates. The extensive delocalization of π-electrons is well known to be responsible for the array of remarkable characteristics that these polymers tend to exhibit. These properties include non-linear optical behavior, electronic conductivity, and exceptional mechanical properties such as tensile strength and resistance to harsh environments [39]. A conducting polymer is an organic polymer that possesses the electrical, electronic, magnetic, and optical properties of a metal while retaining the mechanical properties, processibility, etc. commonly associated with a conventional polymer. Polymers composed of aromatic and heteroaromatic ring structures have been particularly outstanding from materials perspective [40,41]. Some examples of commonly used conjugated polymers are depicted in Figure 2.1.

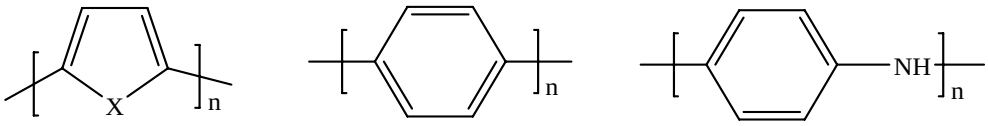

a) X = S, O, NH, etc. b) c)

Figure 2.1. Chemical structures of some conjugated polymers, (a): polythiophene (X = S); polyfuran (X = O); polypyrrole (X = NH), (b) poly(*p*-phenylene), (c) polyaniline.

Among the numerous conducting polymers that have been developed and studied, poly (3,4-ethylenedioxythiophene), PEDOT, has developed into one of the most successful materials from both a fundamental and practical perspective [42]. It posses several advantages as compared to other polythiophene derivatives: it combines a low oxidation potential (-0.13 V

vs. Ag/Ag^{+}) and moderate band gap (1.6 eV) with good stability in the oxidized state [42-45]. In addition to its high conductivity (400 – 600 S/cm for both chemically and electrochemically prepared samples) [42], PEDOT is found to be highly transparent in thin, oxidized films. As a result, PEDOT and its derivatives have found several applications including indium-doped tin oxide electrode modification and hole-conducting material in organic/polymer based light-emitting diodes and solar cells [46,47].

2.1. Electronic structures of conjugated polymers

Electronically conducting polymers have a conjugated structure, i.e. alternating single and double bonds between the carbon atoms of the main chain. Consider polyacetylene, which is formed from the repeating units of ethylene units (Figure 2.2).

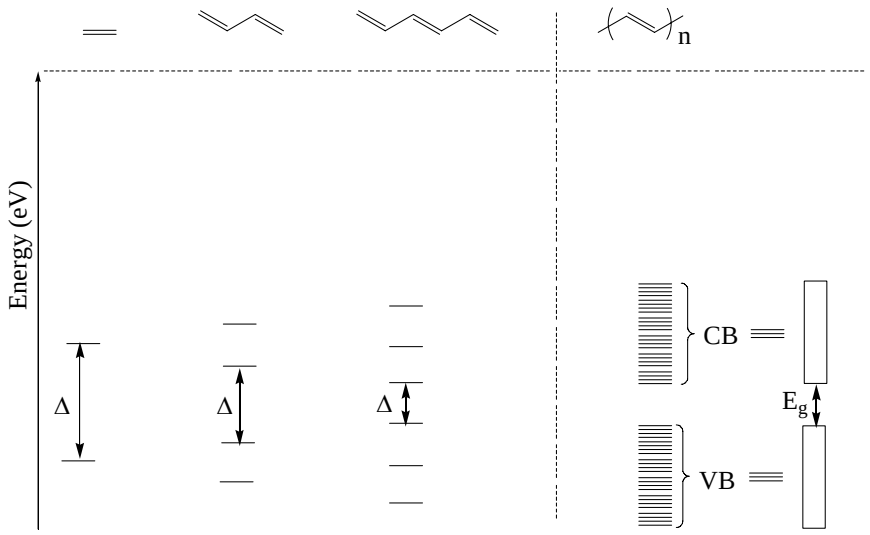

Figure 2.2. The development of a polyacetylene band structure from the molecular orbitals of ethylene. From left to right, the molecular orbitals progressively develop into a band structure as the length of the conjugation chain is increased. For shorter polyene chains, Δ represents the HOMO-LUMO energy gap. For the infinite polyene chain, VB and CB denote the valence band and the conduction band respectively and E_g is the band gap energy.

In ethylene molecule, the carbon atoms are sp^2 hybridized into a σ-orbital framework. The remaining p-orbitals of carbon interact to yield two orbitals of π-symmetry; one of which is bonding and the other is antibonding with respect to C-C interaction. In the ground state, the bonding π-orbital is occupied by two electrons, and this orbital is lower in energy than the empty antibonding orbital. A discrete optical transition exists between the highest occupied molecular orbital (HOMO) and the lowest unoccupied molecular orbital (LUMO) of ethylene, because these two orbitals are separated by a well-defined energy gap.

As the basic ethylene units are coupled together to form a larger molecule, the π-bonding will become more delocalized, and more atomic orbitals must be included in the overall molecular orbital description. In 1,3-butadiene, the four valence 2p orbitals of carbon that are not incorporated into the σ-bond will produce four π-type molecular orbitals. Two of these are bonding and are occupied by electron pairs, while the other two are antibonding and empty. The HOMO-LUMO gap of butadiene is slightly smaller than that of ethylene. This reduced gap is a consequence of the extended conjugation in this π-system relative to that of ethylene. Addition of another ethylene unit to 1,3-butadiene creates 1,3,5-hexatriene, a molecule with three fully occupied π-bonding orbitals and three empty π-antibonding orbitals. Again, the highest bonding molecular orbital and the lowest antibonding molecular orbital are separated by the HOMO-LUMO gap. As this process of adding ethylene units is continued, longer conjugated systems will be created until an infinite one-dimensional polyene chain has been formed. This chain will contain an infinite number of bonding and antibonding molecular orbitals. In this infinite chain, the bonding orbitals will tend to cluster together into a tightly packed group, and the antibonding orbitals will tend to cluster into another tightly packed group. The two groups are well separated producing a well-defined HOMO-LUMO energy gap. Even though each of the molecular orbital distributions consists of a large number of orbitals that are packed tightly together into a finite energy interval, for most purposes it is possible to ignore the difference and consider the orbitals as forming continuous bands of energy levels. The cluster of fully occupied π-bonding orbitals is referred to as the valence band (VB) and the cluster of vacant antibonding orbitals is called the conduction band (CB). Under this scheme, the HOMO-LUMO gap is called the band gap.

2. 2. Structural distortions in conducting polymers: Solitons, Polarons and Bipolarons

2.2.1. Soliton formation

When combining two chain segments of *trans*-polyacetylene (Figure 2.3) having different bond order (the ground states are degenerate), a defect in the form of an unpaired electron will be formed. Such a defect, having charge zero and spin 1/2, is called a soliton [48]. The unpaired electron is accompanied by bond length distortions in a region over about 15 carbon atoms [49,50]. The distortion of the chain results in the formation of a new localized energy level in the middle of the band gap that is occupied by the unpaired electron. There are also positively charged and negatively charged solitons with zero spin [51,52].

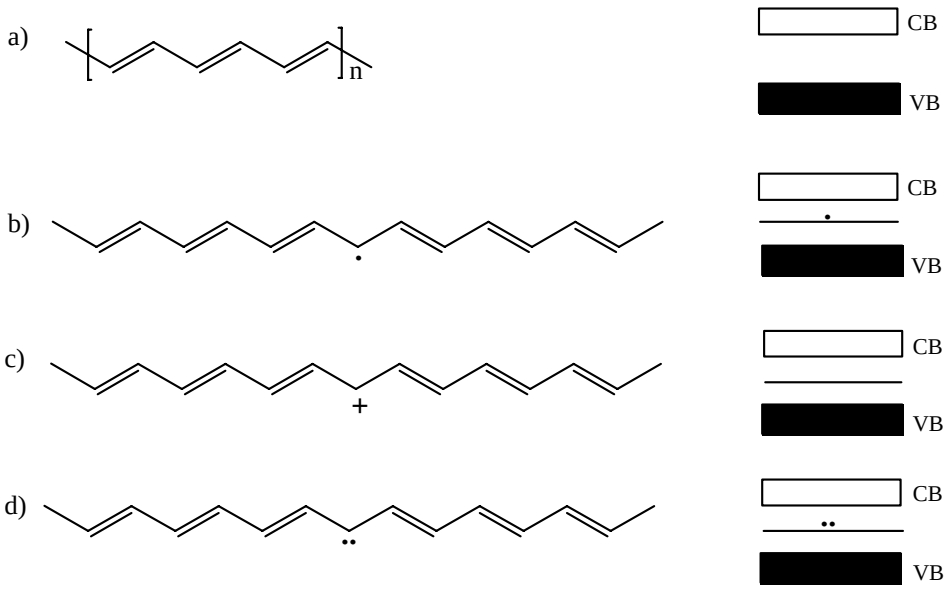

Figure 2.3. Chemical structure of a) *trans*-polyacetylene and solitons in *trans*-polyacetylene: b) neutral soliton, c) positive soliton, d) negative soliton.

2.2.2. Polaron formation

Localized distortion of a conducting polymer with non-degenerate ground states and possessing a standard semiconductor band structure gives rise to two localized electronic

states in the region between the valence and the conduction bands followed by a small local upward shift of the HOMO (i.e. the valence band) and downward shift of the LUMO (i.e. the conduction band). In a conducting polymer with non-degenerated ground states, removal of an electron from this localized state (i.e. oxidation or *p*-doping) forms an entity called a polaron [39]. A polaron is a radical cation (one unpaired electron), which is locally associated with a structural distortion in the conducting polymer (Figure 2.4). A *hole* polaron, created upon *p*-doping of the polymer has a charge of +1 and a spin of 1/2. The lower level of the sub-gap states is half occupied and the upper level is empty (Figure 2.5). In polaron formation the conduction band remains empty and the valence band remains full, there is no resulting high conductivity and the newly generated, half occupied electronic level remains quite localized in the gap.

2.2.3. Bipolaron formation

At higher doping levels, removal of electrons preferably forms a bipolaron (two positive charges) (Figure 2.4) rather than two polarons [53]. The stability of the bipolaron, despite the Coulombic repulsion between the two positive charges, is considered to arise from electron-phonon coupling [54]. A *hole* bipolaron has a charge of +2 and a zero spin. Both of the sub-gap states are empty (Figure 2.5).

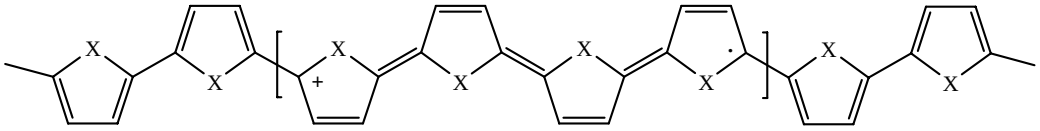

polaron

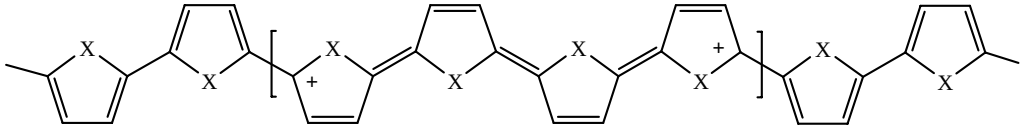

bipolaron

Figure 2.4. Actual structures of polarons and bipolarons in polyheterocyclic polymers (X = S, O, NH, etc).

We may also have *n*-doping, i.e. reduction or donation of electrons to the conducting polymer chain. We would then have negatively charged polarons and bipolarons. N-doping gives a doubly occupied lower level and a singly occupied upper level (for *n*-polaron) or a fully occupied higher level (for *n*-bipolaron) of the sub-gap states (Figure 2.5).

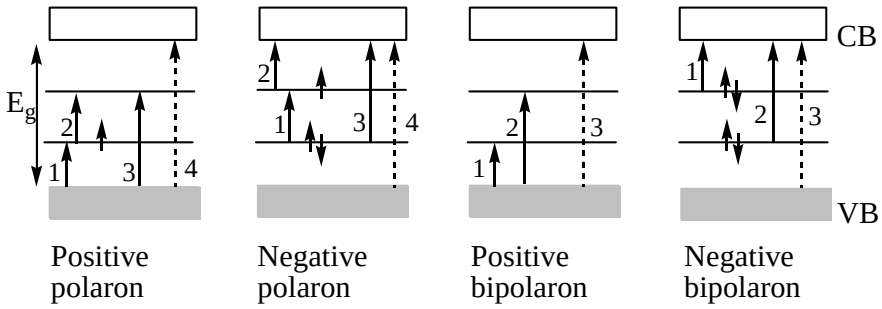

Figure 2.5. Energy band diagrams showing polaron and bipolaron states in the non-degenerate polymer. The arrows indicated by the numbers 1, 2, 3, and 4 represent the possible optical transitions [55].

Bipolarons can be mobile and can propagate along the conducting polymer chain. Thus at sufficient concentration levels, they can function as charge carriers. They are delocalized over some (6 to 8) monomer units [56]. As one progresses further to very high doping levels, the individual bipolaron states coalesce into bipolaron bands. At these high dopant concentrations, the bipolarons can become mobile under the application of an electric field, thus giving rise to the high conductivity observed in conducting polymers. At maximum doping levels, the bipolaron bands of conjugated polymers with low band gaps (~ 2 eV), such as polythiophenes, can merge with the valence and conduction bands, producing metal-like conduction stemming from the lower, half-filled valence/bipolaron band [57].

Polarons, bipolarons and other structural distortions in conducting polymers may be most commonly generated by electrochemical or chemical doping with appropriate counter ions then taking their place in the vicinity of these for charge neutrality [49]. Another method of generating these sub-gap states is through irradiation, which is called photodoping. When conducting polymers are irradiated with light of energy greater than or equal to the band

gap, electrons will be excited to the conduction band leaving a hole in the valence band. The electrons and holes remain bound forming an *electron–hole* pair. This bound *electron-hole* pair in a polymer chain is called an exciton. An exciton may recombine (thermally or radiatively) or separate to give free charges.

2.3. Charge transport in polymeric organic semiconductors

Charge transport in conducting polymers occurs *via* thermally activated hopping of charges either along a polymer chain or across the neighboring chains [5]. This mechanism of charge transport is very different from the coherent charge transport observed in crystalline semiconductor and is due to the very small amount of wave function overlap between adjacent transport sites. This small overlap produces electronic bands that are so narrow that, through the Heisenberg uncertainly principle, they lead to a mean free path smaller than the distance between the transport sites. Hence the charges have to hop between these sites. This hopping process is hindered further by the distribution of energy levels observed in conjugated polymers. This distribution can be caused by a spread in conjugation lengths, the presence of impurities and by local structural variations. Hopping transport also has to overcome positional variation encountered in thin polymer films. The cumulative result of these effects is to produce a low charge carrier mobility, μ, (10^{-3} – 10^{-5} cm^2/Vs [58,59]) that is dependent both on the temperature, *T*, and the electric field strength, *E*. Equation 2.1 describes the theoretical dependence on these externally controlled parameters where ε_a is the average activation energy of the hop, *k* is the Boltzmann constant, *n* is an exponent that varies between different theories (usually taken to be between 1/4 and 2) and γ is a pre-factor that correlates with the spatial energetic disorder within the polymer.

$$\mu \propto \exp\left(\frac{-\varepsilon_a}{kT^n}\right)\exp\left(\gamma\sqrt{E}\right) \tag{2.1}$$

According to the equation, the mobility of charges increases with increasing temperature (opposite to crystalline inorganic semiconductors) and is strongly dependent on the electric field strength.

2.3.1. Conductivity of conducting polymers

The conductivity (σ) of a conducting polymer is related to the number of charge carriers, n and their mobility (μ) [60].

$$\sigma \propto n\,\mu \tag{2.2}$$

Because the band gap of conjugated polymers is usually fairly large, n is very small under ambient conditions. Consequently, conjugated polymers are insulators in their neutral state and no intrinsically conducting organic polymer is known. A polymer can be made conductive by oxidation (*p*-doping) and/or, less frequently, reduction (*n*-doping) of the polymer generating the mobile charge carriers described earlier. Most conducting polymers have conductivities in the range of 10^{-6} to 10^{2} S/cm [5]. The highest conductivity measured at room temperature is in the order of 10^{5} S/cm for trans-polyacetylene doped with iodine [61].

2.3.2. Charge Transport Mechanism

The pre-requisite for charge transport is the presence of mobile charge carriers. In conducting polymers the conductivity is due to the presence of solitons, polarons and bipolarons, which are formed by self-localization of the carriers, induced into the π-electronic systems through doping [62]. Conductivity of materials depends on temperature. The temperature dependence of polymer conductivity is manifested opposite to that of metals. In case of conjugated polymers conductivity depends on doping level. At low doping levels the temperature dependence of the conductivity is high. As the doping level increases, the dependence of the conductivity on temperature becomes less [63]. There is no definite mechanism of charge transport and hence different models are suggested over the whole conductivity range [64,65]. In the undoped form of conjugated polymers, the charge

transport is similar to that of amorphous semiconductors. It is explained by hopping between localized states. At very low doping levels, the conductivity is mainly due to hopping. Its concept is generally deduced from ionic conduction to electronic conduction in amorphous and disordered non-metallic solids and polymers. In such materials we do not have free charge carriers, rather than localized electrons and so they can move between these localized states, which are distributed randomly. For polyacetylene, where solitons are dominant charge carriers, inter-soliton hopping is the dominant conductivity mechanism. The charged solitons are trapped by the dopant ions and neutral solitons are free to move. When a neutral soliton passes close by a charged soliton, an electron can hop between the mid-gap states belonging to the solitons [66].

2.4. Electrochemistry of conducting polymers

2.4.1. Electrochemical polymerization

Conducting polymers can be synthesized both chemically and electrochemically. Though electropolymerization is not the technique of choice for bulk industrial production, this technique is of utmost importance for fundamental studies [67]. Potentiostatic (constant potential) deposition technique in a three-electrode mode yields polymers with the most consistent morphology. Repeated potential cycling (cyclic voltammetry) is also used yielding conducting polymer films comparable to potentiostatic deposition. The potential is cycled within the potential window of the polymer in which the doping/dedoping process is reproducible, and beyond which oxidative or reductive decomposition of the polymer occurs. Galvanostatic (constant current) deposition can be used when control of charge is desired, but it usually yields polymers of poorer morphology and conductivity.

The electropolymerization of conducting polymers appear to follow a generic reaction pathway that prefers polymer linkage at the α-position for the monomers [56]. The common features of the pathway are the initiation, propagation and termination steps shown in Figure 2.6. The generic mechanism is denoted in electrochemical terminology as an $E(C_2E)_nC$ mechanism, that is, an initial electrochemical step (the radical cation generation), followed by polymer propagation *via* successive chemical (combination with monomer radical cation,

proton loss) and electrochemical (oxidation to generate oligomeric radical cations) steps, and likely termination *via* a chemical step. Recent research studies suggest the electropolymerization of thiophenes and pyrroles to involve a chain propagation process not with successive coupling steps of the starting radical cations, but rather via consecutive elimination steps [68].

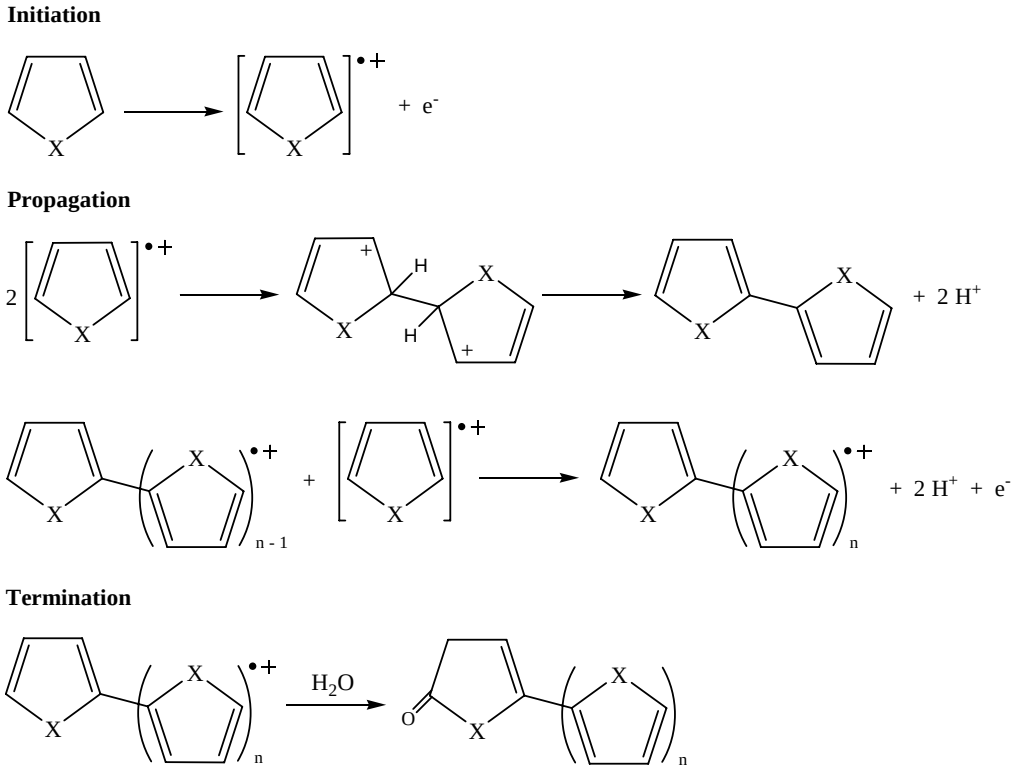

Figure 2.6. Scheme for the generic electropolymerization pathway valid for many conducting polymers (X = S, O, NH, etc).

2.4.2. Electrolytes and Electrodes

Electropolymerization of conducting polymers is carried out in an electrochemical cell that consists of the supporting electrolyte, the electrodes and the monomer. Electrolytes for electropolymerization are comprised of solvents and electrolyte salts. They are used to

decrease the resistance of the solution, to eliminate electromigration effects, and to maintain constant ionic strength. The solvent of electropolymerization is an important factor governing the conductivity, morphology, and subsequent chemical and electrochemical behavior of the conducting polymer obtained. For aqueous studies, mainly for conducting polymers such as polyaniline and other poly(aromatic amines), in which protons take part in the doping/dedoping processes, acids such as HCl, H_2SO_4 and $HClO_4$ are preferred. For non-aqueous liquid electrolytes, acetonitrile is the best preferred polymerization solvent for several reasons: facilitates proton removal in the polymerization; poor solubility or insolubility of many conducting polymers as well as oligomers; high inertness; greater volatility that leads to less solvent retention within the conducting polymer matrix (a distortive feature in electrochemistry); sufficient water content for effective polymerization without early termination. Solvents such as propylene carbonate exhibit high solubility of oligomers and of reduced polymer, and very high water content. Solvents with high nucleophilicity such as dimethyl formamide are also poor electropolymerization solvents. In case where the monomer has poor solubility in an otherwise good polymerization solvent, mixed solvents may be used primarily to facilitate solubility. Water or other nucleophilic impurities may serve as an effective counter electrode reaction during electropolymerization. The selection of electrolyte salts usable in electropolymerizations is varied and large. Tetrafluoroborate or perchlorate can be introduced as tetraethylammonium or lithium salts. The concentration of the electrolyte salt is from 100 to 1000 times that of the monomer and the minimum concentration of the monomer is usually 1.0 mM.

Any electrode which does not undergo oxidation at a potential equal to or less than the oxidation potential of the monomer can be used during electrochemical polymerization. For three electrode electrochemical studies, the customary reference electrode in aqueous medium is saturated calomel electrode (SCE), which is $Hg/Hg_2Cl_2/KCl$ (in water) and aqueous Ag/AgCl electrode (Ag/AgCl/KCl (in water). For non-aqueous medium, reference electrodes, which are in entirely solid–state, such as Ag wire coated with AgCl (Ag/AgCl) or in liquid-state, such as Ag/Ag^+ redox couple are used. For electrochromic and initial characterization studies, transparent working electrodes such as indium-doped tin oxide (ITO) and Au/Pt on glass are preferred. For pure electrochemical studies, Pt or glassy carbon working electrodes may be preferred. The most common counter electrode is

platinum wire or flag. When performing two-electrode measurements with a standard potentiostat/galvanostat, it frequently suffices to simply short the reference and the counter connections together as a single counter electrode connection.

2.4.3. Cyclic voltammograms of conducting polymers

Electrochemical monitoring of electropolymerizations is most effectively done using cyclic voltammetry that yields useful information, which can be applied to interpretation of electrochemical and electrochromic behavior of new conducting polymers. Figure 2.7 shows the preparation of a conducting polymer, poly[3-(2',5'-diheptyloxyphenyl)thiophene] (PDHOPT) *via* potential cycling.

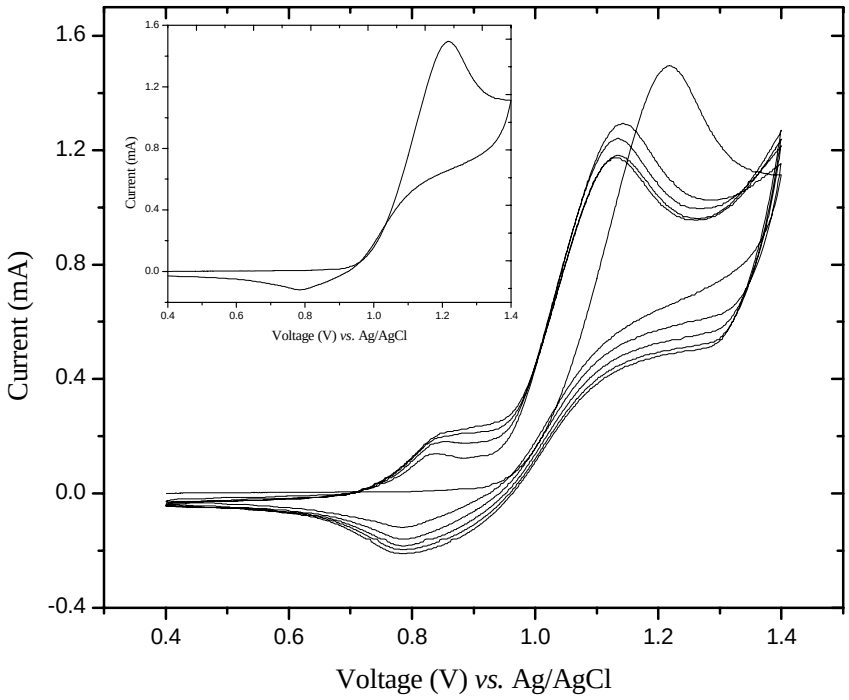

Figure 2.7. The Cyclic voltammogram for the electropolymerization of DHOPT on ITO-glass at a rate of 10 mV/s. The solution contains 1 mM DHOPT and 0.1 M $LiClO_4$ in acetonitrile. The inset is the voltammogram of the first cycle showing the crossover.

On the first anodic (to positive potential) scan, the oxidation current peak, corresponding to production of the monomer radical is observed. On the reverse, cathodic (to negative potential) scan, the reduction current peak corresponding to this oxidation is not observed, indicating that in the time scale of the experiment (the scan rate), the radical cation is rapidly consumed in the subsequent chemical reaction. Starting with the second scan, a redox couple is observed at lower positive potentials, increasing with every cycle, which corresponds to the redox process of the steadily growing conducting polymer film. The crossover of the reverse cathodic scan (Figure 2.3 inset) over the anodic scan in the first cycle of the voltammogram (typical of metal deposition processes, where nucleation is required [69]) has been associated with a process of conducting polymer nucleation for an initial deposition of a conducting polymer film. There are however observations where a conducting polymer film is produced with out showing the crossover in the cyclic voltammogram [70].

The cyclic voltammogram of a conducting polymer is recorded from the measurement of current resulting from application of voltage (potential) function with a fixed scan rate (expressed in mV/s) to the conducting polymer film in a monomer free electrolyte solution. The voltammogram (current-voltage curve) consists of doping/dedoping peaks for the oxidation and the reduction of a conducting polymer. Conducting polymers will electrochemically cycle well in the solvent of electropolymerization due to retention of solvent “affinity sites” [56]. Similarly, when a conducting polymer is electrochemically prepared in one salt, it may not always readily exchange with another, even if the latter is smaller. This appears to be due not to dopant ion size, but rather dopant affinity sites created in the particular morphology of the conducting polymer during polymerization. Dopant ions can also cause a substantial shift in the redox potential of a conducting polymer. Oxidation peaks unaccompanied by reduction peaks indicate that one is beyond the window. The problem on the dedoped side for p-type conducting polymers is the dissolution of this more soluble reduced form of the conducting polymer. According to well-established electrochemical treatments, for a behavior dominated by diffusion effects, the peak current (i_p) is proportional to the square root of scan rate ($\nu^{1/2}$). For a material localized on an electrode surface, such as a conducing polymer film, i_p is proportional to ν. This is true only if the polymer is not too thick and not doped by ions with small diffusion coefficients. If any

of the latter cases prevail, i_p can be proportional to $\nu^{1/2}$. Some other important parameters of the cyclic voltammograms of conducting polymers include: the symmetry of the peaks about the peak value; the cathodic and anodic separations and the background (residual) currents represented by the plateau following the peaks. For most conducting polymers, the background currents on the anodic side are much larger than the cathodic side. This stems from an increase in a capacitive current when a polymer is oxidized and conducting, and thus able to augment the effective electrode substrate mass. The peak in the oxidative scan is more symmetrical than that in the reductive scan implying that going from reduced to oxidized polymer appears more facile than the reverse path. This pattern is evident in the slopes of the i_p *vs.* ν *plots*, which are much larger for the anodic peaks. The peaks may be broad that results from the inequivalence sites in conducting polymer film. This phenomenon in turn can be associated with thick films as well as other factors such as polymer morphology and differing chain lengths. If a conducting polymer film is switching very slowly (for example if it is too thick), the film will not be able to follow the scan rate and hence the peak will be broad or otherwise distorted. In such instances, a slower scan rate may give well-defined peaks.

3. IONICALLY CONDUCTING POLYMERS

While electronic conductivity is the phenomenon related to the electrons-holes movement into solid conductors, ionic conductivity is described as the charge movement due to the ions motion. A polymer electrolyte is a solvent-free system where the ionically conducting phase is formed by dissolving salts in a high molecular weight polar polymer matrix. Polymer electrolyte materials should have adequate conductivity, low electronic conductivity, good mechanical properties, good chemical, electrochemical and photochemical stability and ease of processing. The interest in these solid-state ionic conductors comes from the possibility of using them to substitute the liquid electrolytes in electrochemical and photoelectrochemical devices [23,71-73]. The major challenge into replacing the liquid electrolyte by a polymeric one is to keep the high operation efficiency, similar to the electrochemical devices based on liquid junctions. Besides improving the stability of the active interface, hence allowing a long-term durability, a polymer electrolyte eliminates problems concerning evaporation or leakage of the solvent. Since 1978, when Michael Armand first introduced polyether-alkali-metal salt metal complexes to the solid-state community as potential materials for electrochemical devices, there has been enormous amount of research particularly on high molecular weight poly(ethylene oxide)-salt systems [74].

Poly(ethylene oxide), PEO, is the reference polymer for ionic conduction, since it is the best matrix for alkali salts because of the high Lewis base character of the oxygen atoms present in this polyether. Due to this reason, great efforts have been devoted to make polymer electrolytes based on PEO, combining it with several salts [75-77]. PEO is a linear polymer and the regioregularity of the $–(CH_2\text{-}CH_2O)–$ unit allows a high degree of crystallinity (70-85%). The melting point of the crystalline phase is 65^oC and the glass transition temperature (T_g) is low, approximately -60^oC, which permits ion transport at ambient temperatures. The dielectric constant is low (~5-8). One of the most successful amorphous host polymers is an oxyethylene-oxymethylene structure in which medium length but randomly variable ethylene oxide units are interspersed with methylene oxide groups [78]. The methylene oxide groups break up the regular helical structure of polyethylene oxide, thus suppressing

crystallization. The amorphous polymer, sometimes known as aPEO, has the following general structural formula.

$$\left[(OCH_2CH_2)_m\, OCH_2\right]_n \quad , m = 5\text{-}10 \tag{3.1}$$

It is assumed that ions are transported by the semi-random motion of short polymer segments [79]. The segmental motions are thought to promote ion mobility by making and breaking the co-ordination bonds between cation and polymer and providing free volume into which the ion can diffuse under the influence of the electric field.

3.1. Thermodynamics of salt dissolution

Both entropy and enthalpy changes have to be considered when dissolving a salt in a polymer solvent [78]. The overall entropy change on dissolution is made up of:

1. A positive entropy change due to the break up of the crystal lattice and the subsequent disordering of the ions in the system;
2. A negative entropy change caused by the stiffening of the polymer chains as they coordinate the cation.

The major enthalpy changes on dissolution are:
1. A positive enthalpy change due to the lattice energy of the salt;
2. A negative enthalpy change due to cation solvation.

In polymer electrolytes the loss of the entropy of the polymer chains outweighs the entropy gain leading to negative entropy of dissolution. The overall entropy change in different polymer-salt systems is important at higher temperatures but is less significant than the enthalpy changes at lower temperatures. The lattice energy of the salt is expected to have the greatest influence on salt dissolution. A polymer that is capable of strongly coordinating cations is necessary for electrolyte formation. Thus, polyethers (-O-), polyimines (-NH-)

and polythiols (-S-), which have strong coordinating groups, dissolve salts easily. In higher molecular weight polymers, cations are more likely to be coordinated by atoms on the same chain with the possibility of some coordination by neighboring atoms and therefore the chain must wrap around the cation without excessive strain. For polyethers, $–(CH_2CH_2O)_n–$ provide the right spacing for maximum solvation while $–(CH_2CH_2CH_2O)_n–$ and $–(CH_2O)_n–$ are much weaker solvents.

The solvation enthalpy of a salt in a polymer solvent depends on the cation-polymer interaction. Solubility can be discussed in terms of the acid-base interactions between solute (Lewis acid) and solvent (Lewis base) molecules, each being classified as “hard” or “soft”. The strongest interactions occur by matching hard with hard or soft with soft. Thus the strongest solvation in polyethylene oxide (hard base) would be with a hard cation, e.g. Li^+ and Na^+. The stability of anions in polymers very much depends on the charge dispersion. Large anions with delocalized charge require little solvation. These can either be soft (e.g. I^-) or hard (e.g. $CF_3SO_3^-$) bases. Salts containing monoatomic anions may be soluble in poly(ethyleneoxide), provided they are large and polarizable. The larger I^- anion is required for less-solvated monovalent cations such as K^+.

3.2. Ion conduction in polymer electrolytes

Figure 3.1 shows the simplified schematic representation of cation movements in a polymer electrolyte [71]. Unlike classical solid electrolytes, both the anions and the cations are mobile in polymer electrolytes. The stronger cation bonding to the polymer chain liberates anions from cation association and thus results in higher anion mobility and conductivity. Cation mobility depends on the strength of the cation-polymer interactions; if these are strong, cation transport is suppressed. The criteria for the development of polymer electrolyte systems that can achieve good working conductivity, in the range 10^{-3}-10^{-6} S/cm, are established. The low ionic conductivity can be compensated by forming very thin films with large surface area. The polymer must be capable of dissolving the salt and ionizing it to produce sufficient number of charge carrying species. It must also be amorphous to allow easy movement of ions, and must have a flexible chain to assist the ion transport. In PEO the ionic conductivity was found to increase on departing from the stoichiometric ether-

oxygen to cation ratio (O:M), as the number of vacant sites would increase on increasing the O:M ratio.

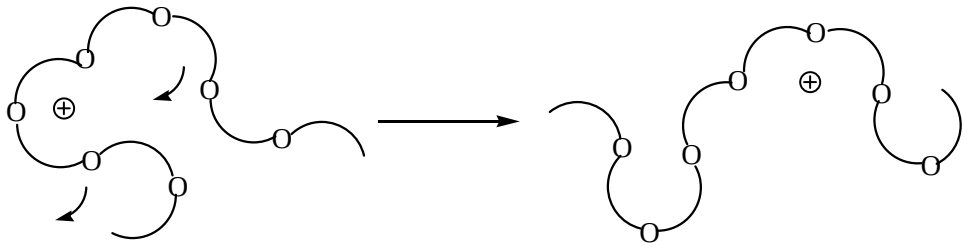

Intrachain hopping

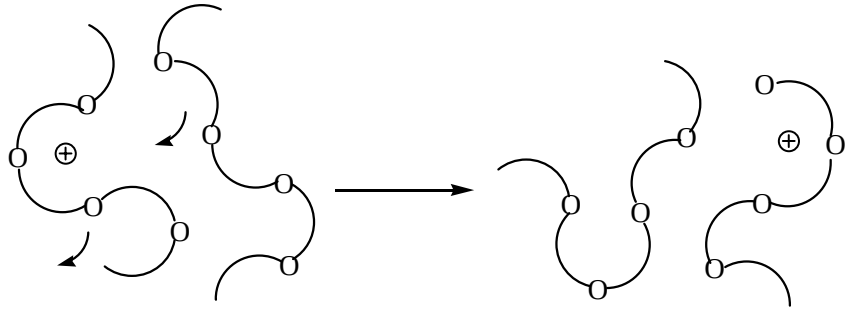

Interchain hopping

Figure 3.1. Schematic representation of cation motion in a polymer electrolyte.

3.3. Factors affecting ionic conductivity in polymer electrolytes

3.3.1. Effect of concentration and ionic mobility

For a given concentration of a salt, the concentration of ionic charge carriers in the polymer electrolyte is determined by the dielectric constant of the polymer and the lattice energy of the salt. Polymers with high dielectric constants and salts having low lattice energies generally promote greater dissociation of the salt, thereby providing higher concentration of free ions. The ionic conductivity, σ, of a homogeneous polymer electrolyte at a given temperature, T, is given by the summation of the products of the concentration of all ionic charge carriers and their mobilities as given in the following equation [80].

$$\sigma(T) = \sum_i n_i Z_i \mu_i \tag{3.2}$$

where Z_i is the ionic charge, n_i is the number charge carriers, and μ_i is the ion mobility.

When a salt is dissolved in a polymer matrix, the conductivity increases as a result of the addition of charge carriers. However, as the salt concentration is increased further, the conductivity reaches a maximum and then falls. This is thought to result from increasing cross-linking, either intra-chain or inter-chain, that reduces the segmental motion of the polymer electrolyte which in turn reduces the mobility of the ions. Formation of immobile aggregate species at higher concentrations may also lower the number of free charge carriers and contribute to the fall in the conductivity.

3.3.2. Effect of temperature

For many amorphous polymers the temperature dependence of the conductivity is related by the Vogel-Tamman-Fulcher (VTF) equation [81],

$$\sigma = \sigma_0 \exp\left[\frac{-B}{(T - T_0)}\right] \tag{3.3}$$

where $\sigma_0 = A/T^{1/2}$, A and B are parameters, assumed to be independent of temperature, that denote the number of charge carriers and an apparent activation energy for segmental motion. T_0 is a reference temperature that can be identified with the glass transition temperature, T_g.

According to the equation, as T_g decreases, the conductivity increases. Since lower T_g produces higher polymer flow and greater ion diffusibility, high ionic conductivity is obtained in polymers having highly flexible backbones and low glass transition temperatures.

4. ELECTRONIC PROPERTIES OF INORGANIC SEMICONDUCTORS

4.1. Crystal structures of semiconductors

In the semiconductor-based system, the ability of the semiconductor to transport charges in energy conversion scheme will depend on the electronic properties of the semiconductor solid. These properties can be explained from the knowledge of the crystalline structures of the semiconductors. Covalent semiconductors, such as Si and Ge, adopt the cubic diamond lattice, in which one of the tetrahedral holes in the face-centered cubic lattice is filled with atoms. Covalent, binary semiconducting solids, such as InAs and GaP, having elements of similar electronegativities adopt the zinc blend structure, a cubic diamond structure with adjacent atoms being of opposite type. Semiconductors, such as ZnO and CdSe, which are composed of elements with different radii and electronegativities, form a wurtzite structure, in which the atoms are hexagonally close-packed. The three structures, the cubic diamond, the zinc blend and the wurtzite are common to semiconductor materials and together they are known as adamantine structures. Steric or electronic factors can result in the adoption of non-adamantine structures. Semiconductors that adopt non-adamantine structures include TiO_2 and WS_2. TiO_2, an important semiconductor in photoelectrochemical applications mainly occur in rutile and anatase forms. The rutile lattice is derived from a body-centered cubic structure. To maintain a 1:2 cation-anion, stoichiometry, one-half of the trigonal sites are occupied by anions. The anatase structure is derived from the NaCl structure, but only one-half of the sites in one face-centered cubic lattice are occupied by Ti^{4+} cations. TiO_2 powders commonly contain both anatase and rutile components [82].

4.2. Band structure and chemical properties of inorganic semiconductors

An inorganic semiconductor is composed of a valence band and a conduction band. The top of the valence band and the bottom of the conduction band are called the valence band edge and the conduction band edge respectively. The corresponding energies are represented as E_{VB} and E_{CB}, respectively. The energy difference between these levels is called the band gap, E_g. Semiconducting solids have band-gaps in the range of 0.3 to 3.5 eV. The energy

positions of semiconductor band edges are scaled to the vacuum level. The vacuum level is defined as the energy of an electron in vacuum, and is taken to be 0 eV in the energy scale.

In general, semiconductors can have different types of valence band and conduction band structures. These differences can affect the chemical reactivity of the photogenerated carriers in the solids. In a covalent solid such as Si, the valence and the conduction bands are crystal orbitals that are either bonding or antibonding combinations of hybridized Si atomic orbitals. In ionic crystals, such as TiO_2, the valence band is composed of crystal orbitals that are derived from the filled 2p orbitals of O^{2-}, while the conduction band is composed of crystal orbitals that are derived from the empty 3d orbitals of Ti^{4+}. The band-gap in this case is obviously not an energy gap between bonding and antibonding bands of the same symmetry. This band structure has implications for the chemical behavior of the excited state of TiO_2. The band gaps of ionic semiconductors are usually very large (for TiO_2, E_g = 3.2 eV [83] and therefore less prone to undergo oxidation or corrosion reactions.

4.3. Buckminsterfullerene (C_{60})

The carbon allotropes, the fullerenes, are closed-cage carbon molecules with three-coordinate carbon atoms tiling spherical or nearly spherical surfaces. The best known of these molecules is Buckminsterfullerene, C_{60}, which has sixty carbon atoms forming a truncated-icosahedral structure with twelve pentagonal rings and twenty hexagonal rings, as shown in Figure 4.1 [84,85]. The coordination at every carbon atom is not planar but rather slightly pramidalised at every carbon atom. In other words some sp^3 character is present in the essentially sp^2 carbons of fullerene.

Because of its rich π-electron structure occupying 60 electrons, C_{60} displays complex electro-optical properties [86-88]. These constitute important applications for fullerenes and fullerene-based materials. Besides having a high electron affinity [89], C_{60} is fairly transparent and also has fair electron conductance (10^{-4} S/cm) [4]. Some exciting applications of the fullerenes involve their properties as dopants and electron acceptors in polymeric systems [89,90]. The electron transfer takes place within 300 fs after excitation, a process faster than any competing relaxation processes [91]. The photoinduced electron

transfer increases the yield of charged photoexcitatations on the polymer chain (polarons), resulting in an increase in the carrier lifetime and in the magnitude of the photoconductivity [91,92]. The photoinduced electron transfer has been used to fabricate semiconducting polymer/C_{60} (or its derivative) - based photovoltaic cells [93].

Figure 4.1. The Chemical structure of C_{60}.

5. PHOTOELECTROCHEMICAL SOLAR ENERGY CONVERSION

5.1. Principle of operation

A photoelectrochemical cell consists of two electrodes, an illuminated semiconductor electrode and a metallic counter electrode immersed in a solution containing an electroactive redox species, O/R, or an ion-conducting phase as a charge transport medium (Figure 5.1). In a cell that converts light into electricity, the counter electrode performs the reverse reaction of the photoelectrode, and the incident photon energy is harvested as electrical energy through an external circuit.

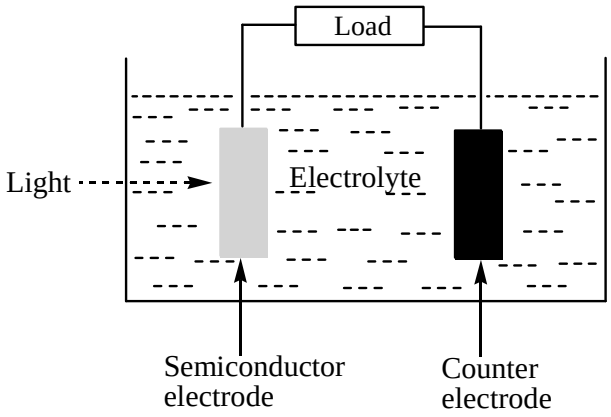

Figure 5.1. Schematic representation of a photoelectrochemical cell.

Inorganic semiconductors with large band gaps, like TiO_2, are the natural candidates for use in photoelectrochemical cells because of their chemical stability. The most promising candidates to replace the inorganic semiconductors in the assembly of solar cells are organic materials, due to their photosensitivity and photovoltaic effects. The most well-known and studied unconventional photovoltaic system is the Grätzel's dye-sensitized nano-structured TiO_2 solar cell [94].

5.2. Semiconductor/electrolyte interface [83]

Whenever two phases of different electrochemical potential are brought into contact, the phase that has the more negative electrochemical potential will tend to lose electrons to the phase with the more electropositive potential. Charge transfer between the two phases will occur until an equilibrium situation is established. At equilibrium, the phase that loses electrons will have excess positive charge starting from the surface. The region from which charges are removed is called the *depletion width*. The electric potential energy increases from zero value (in the bulk semiconductor) to the initial conduction band edge energy (at the interface) resulting in band bending. The difference between the two energy levels is called the *built-in potential*. The phase that accepted electrons would have an excess of negative charges. The electrochemical potential of a semiconductor is given by the value of its Fermi level (E_F) and the electrochemical potential of a solution is related to the redox potential of the redox couple. Since the number of the available states per unit energy in the solution far exceeds the number present in a semiconductor, the equilibrium positions of the Fermi level for both the semiconductor and the solution are essentially equal to the initial value of the solution electrochemical potential.

A schematic of the potential energy *versus* distance relationship for a *p*-type semiconductor/liquid junction (Schottky junction) is depicted in Figure 5.2. Illumination of a semiconductor with incident light energy greater than or equal to the band gap energy, promotes the valence band electrons to the conduction band, forming an excitons that dissociate into electrons and holes at the semiconductor/electrolyte interface. In *p*-type semiconductors, the minority carriers (electrons) migrate towards the interface, reducing the oxidized form of the redox couple. The majority carriers (*holes*) diffuse to the bulk of the semiconductor and to the external circuit, producing a photocurrent when the circuit is closed. The *holes* oxidize the reduced form of the redox couple at the counter electrode. There is therefore no net chemical reaction. For *n*-type semiconductors the majority carriers are the electrons and the inverse behavior occurs. These processes are the basic operation modes of regenerative photoelectrochemical cells. The potential where no excess of charge exists is called zero charge potential and, under these conditions, the space charge region

disappears and the bands do not bend. The potential where this situation occurs is known as *flat band* potential.

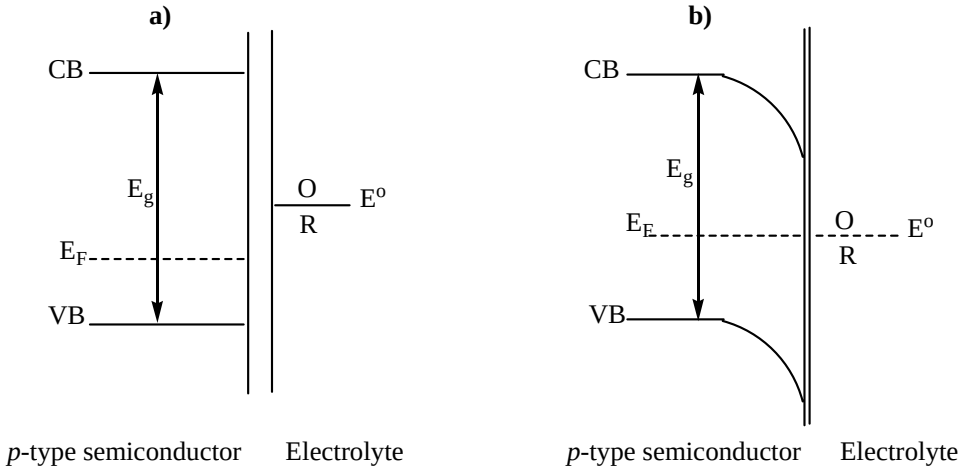

Figure 5.2. Schematic representation of the formation of the Schottky junction between a *p*-type semiconductor and an electrolyte containing a redox couple, O/R: a) before the contact, b) after the contact, considering the redox potential (E^o) of the electrolyte is higher than the semiconductor Fermi level (E_F).

5.3. Dye-sensitized photoelectrochemical cells

5.3.1. Working principle of dye-sensitized photoelectrochemical cells

A relatively narrow band gap, compatible with the photoconversion of visible light, is indicative of weaker chemical bonding in the semiconductor. It is therefore liable to photocorrosion, which is incompatible with a stable extended lifetime as an energy conversion device. The resolution of this dilemma lies in the separation of light absorption and charge separation functions, by sub-band gap sensitization of the semiconductor with an electroactive dye. A wide band gap, intrinsically stable semiconductor, such as titanium dioxide with its band gap of 3.1 eV, and which therefore normally exhibits a photovoltaic response only under ultraviolet irradiation, can then photorespond to visible light of wavelength 400 – 750 nm (1.6 – 3.0 eV). The sensitization process involves the excitation

of the dye from its charge-neutral ground state to an excited state by the absorption of the energy of a photon, followed by relaxation through electron loss to the semiconductor substrate. Only a monomolecular adsorbed film of the sensitizing dye can transfer charge to the substrate. The dye is left as a surface-adsorbed cation. This process is presented schematically in Figure 5.3 where it is associated with neutralization of the dye cation by reaction with a redox species in the contacting electrolyte, which in turn recovers an electron from a counter electrode, thereby constituting a closed regenerative cycle for the conversion of incident light into an electric current. The standard redox system is the iodide/triiodide couple, I_3^-/I^-. The maximum attainable voltage under illumination is given by the difference between the Fermi energy level of the TiO_2 and the electrochemical potential of I_3^-/I^-.

The dye sensitization technique made a breakthrough in the efficiency of dye-sensitized photoelectrochemical cells when it was discovered that it is possible to use rough polycrystalline metal oxide electrodes instead of single crystals [95]. The high internal area of such electrodes increases the amount of surface-bound dye, and thus the efficiency of the cell. The internal surface area of the electrodes was then increased even further, by using nanocrystals having a diameter of about 10 nm [94]. So-called nanostructured metal oxide films are made of such nanocrystals, sintered to form a mechanically stable, sponge-like structure in which the nanocrystals are in electrical contact with each other. The power conversion efficiency of dye-sensitized solar cells has reached around 10.4% [96].

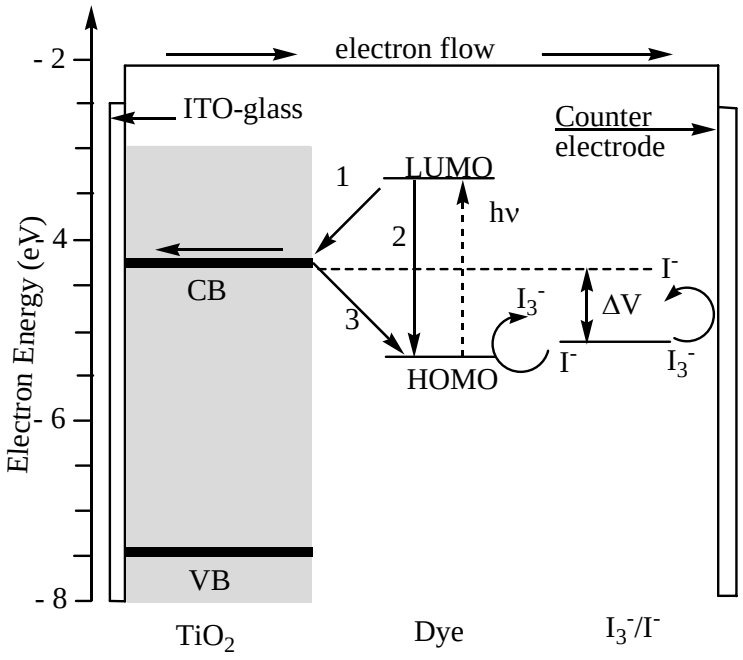

Figure 5.3. Schematic of operation of dye-sensitized TiO_2 PEC. The photoanode, made of dye-sensitized nc-TiO_2, receives electrons from the photoexcited dye (path 1). The oxidized dye is returned to its neutral state by receiving electrons from the reduced form (I^-) of the redox couple (I_3^-/I^-). The I^- is regenerated by the reduction of I_3^- at the counter electrode by the electrons circulated through the external circuit. Path 2 and path 3 refer to charge recombination processes. ΔV is the maximum attainable voltage under illumination.

5.3.2. Electron transport in nanostructred dye-sensitized photoelectrochemical cells

The high efficiency of dye-sensitized solar cells based on nanostructured metal oxide films was against expectations from semiconductor physics, since the structure contains a large number of defects (e.g. surface states and grain boundaries) that may act as recombination centers for electron - hole pairs. The film is also exposed directly to the electrolyte, increasing the recombination possibilities even further. In addition, there is no obvious electrical driving force for the electron to travel towards the back contact in a nanostructured film, since there is no internal electric field (band-bending) as in systems based on large crystals. Band-bending occurs when a single crystal semiconductor is in contact with an electrolyte and the Fermi level of the semiconductor adjusts to the redox

potential of the electrolyte. However, the dimensions of a nanocrystalline semiconductor particle are much smaller than the width of the band-bending zone (the depletion layer), and therefore band-bending does not occur. The electron transport mechanism in the nanocrystalline network has instead been described in terms of a diffusion model [97]. Thus, the electrons diffuse in the network due to the concentration gradient present in the film, and the conducting glass acts as a sink where the electrons leave the film. The rate of the electron transport is of the same order of magnitude as the diffusion of cations in the electrolyte. This was explained by a screening of the electron by cations in the electrolyte and by polar solvents [98,99]. The nanostructure is therefore not an obstruction for, but instead aids electron transport [100]. The ultra-fast kinetics of electron injection from the excited dye into the conduction band of TiO_2 has great contribution to the high performance of dye-sensitized nanocrystalline TiO_2 photoelectrochemical cells. The separation of charge carriers, associated with the majority carrier nature of the device where the electrons enter an *n*-type material, strongly inhibits charge carrier recombination losses. Electrons can be lost only through recapture by the dye cation or by the redox electrolyte after crossing a phase boundary – an inherently slow process. The energy level of the excited state, the LUMO, must lie higher than the conduction band edge of the semiconductor, so that an electron can be injected during the relaxation process. For optimum absorption of white light, therefore, the HOMO should be about 1.5 eV lower. Concerning the electrolyte, a compromise has in the past been required between viscosity, which simplifies the cell sealing process, and ionic mobility, since the redox cations must diffuse to the counter-electrode for the reduction reaction which maintains the regenerative characteristics of the cell. One consequence of low ionic mobility is a limitation of the cell efficiency under high intensity illumination, indicated by a reduced fill factor. The characteristics of the electrolyte must also accommodate the wide range of temperatures to which the cell is exposed in normal outdoor service.

5.4. Current - voltage characteristics of a semiconductor/liquid interface

A chemical equation that represents the interfacial charge transfer at a semiconductor electrode is given by Equation 5.1.

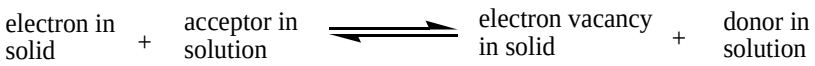

(5.1)

The forward reaction represents the behavior of a *p*-type semiconductor/electrolyte junction, and the reverse reaction represents an *n*-type semiconductor/electrolyte junction. The net current across the solid/liquid interface is given by the difference of the forward and reverse interfacial charge transfer rates. For an *n*-type semiconductor, a value of an applied voltage (V) greater than zero (reverse bias) lowers the rate of electrons leaving the semiconductor, but the rate of electrons entering the semiconductor remains unchanged. Therefore the net current will be independent of the applied voltage. In forward bias ($V < 0$ for an *n*-type semiconductor), the forward rate of charge transfer (as written in Equation (5.1)) increases exponentially with increasing bias. The net current will thus depend exponentially on the applied voltage. The dark current - voltage characteristic of a junction is given by Equation (5.2) [83].

$$I = I_o\left[\exp\left(\frac{qV}{nkT}\right) - 1\right] \tag{5.2}$$

where I is the total current density (dark current density), I_o is the inverse saturation current density which is the current density flowing under sufficiently high reverse bias, q is the charge on an electron, V is the applied voltage, n is the ideality factor of the diode (for an ideal diode $n = 1$), k is the Boltzmann constant and T is the absolute temperature.

Equation (5.2) is known as the diode equation. The current-voltage characteristic described by Equation (5.2), where the current predominantly flows in only one direction is called *rectification*. For an *n*-type semiconductor, more positive redox potentials of the electrolyte solution will yield smaller values of $I_{o,}$ and will produce highly rectifying diode behavior. The current-voltage characteristic of an illuminated semiconductor electrode is given by Equation (5.3) [83].

$$I = I_{ph} - I_o\left[\exp\left(\frac{qV}{nkT}\right) - 1\right] \qquad (5.3)$$

Where I_{ph} is the photogenerated minority carrier current (which is opposite in sign to the dark current) and is equal to the product of the absorbed photon flux and the charge on an electron.

5.5. Characteristics of photovoltaic cells

To characterize photovoltaic (PV) devices, two main measurements are made. First, the photocurrent response spectrum is measured. The wavelength of light illuminating the PV device is gradually stepped through out the visible spectrum, from infrared to ultra-violet (or the *vice versa*), while the photocurrent is measured at a certain wavelength interval. The same measurement is then performed on a calibrated silicon PV device, in order to calibrate the measurement on the organic device. This allows the induced photon-to-current conversion efficiency of the organic device to be determined across the complete spectrum. This data assists in the understanding of the processes that control device efficiency, and show how the devices sensitivity spectrum overlaps with the solar spectrum. Secondly, the current from the PV device is measured as a function of applied voltage, both in the dark, and under illumination. This data allows the device rectifying properties to be determined, and enables the amount of power that can be extracted from the cell to be calculated.

In Figure 5.4, some of the characteristics of a typical PV device are outlined. To the left, the $I - V$ curve of the cell in the dark is shown. When a positive potential is applied to the semiconductor, the Fermi energy of the semiconductor is lowered with respect to the Fermi energy of the metal. This results in a small potential drop across the semiconductor. The balance between the diffusion and the drift current is disturbed; as a result, more electrons diffuse towards the semiconductor than the number drifting to the metal. This leads to an anodic current. When a negative potential is applied to the semiconductor, its Fermi energy is raised with respect to the Fermi energy of the metal. The potential across the semiconductor increases while the barrier that restricts the electron flow to the semiconductor is unchanged. As a result, there is no current under a negative applied

potential; the cell shows a rectifying behavior. When the cell is illuminated, the semiconductor absorbs the photons with the right energy. The electrons from the valence band will acquire enough energy to jump to the conduction band. The conductivity of the semiconductor increases, primarily due to the higher number of photogenerated electrons in the conduction band and holes in the valence band. The cathodic current observed in Figure 5.4 (right) is a result of photogenerated charge carriers. The maximum photogenerated current flows under short-circuit condition; at the open-circuit voltage the photogenerated current is balanced to zero. For a PV device, the real area of interest is in the fourth quadrant, according to Figure 5.4 (right), in which power is extracted from the cell. When a load is connected across the contacts of a solar cell, the current and voltage values at which the cell is operating are constrained to be on the *I* - *V* curve in this fourth quadrant. A small load will result in operation of the PV device at a higher voltage and lower current, whereas a large load will result in a lower voltage and higher current. The square $I_{max}V_{max}$ is the maximum work the cell can yield.

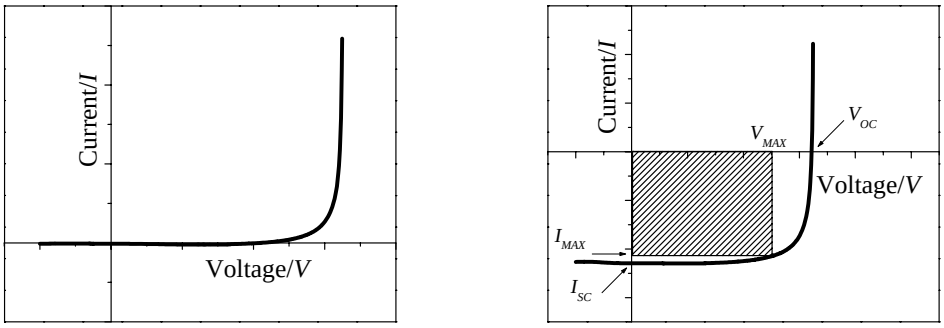

Figure 5.4. *I* – *V* curves of an organic PV cell under dark (left) and under illumination (right) conditions. The open-circuit voltage (V_{OC}) and the short-circuit current (I_{SC}) are shown. The square $I_{max}V_{max}$ gives the maximum power output.

The shapes of *I* - *V* curves in organic devices are determined by many different parameters, and it is difficult to predict how a particular polymer semiconductor will influence the fill factor value. Clearly what is required is for the horizontal section of the *I* - *V* curve be as shallow as possible, and for the vertical section to be as steep as possible. The vertical

section in the fourth quadrant is controlled by the rectifying characteristics of the device, and a sharp turn-on at the open-circuit voltage is preferred. This is controlled by the barriers to charge injection, which is in turn controlled by the offsets between the energy levels of the polymer semiconductors and the work functions of the electrodes. The charge mobility and series resistance of the contacts also play a role in determining this section of the *I* - *V* curve. The horizontal section is controlled by both the efficiency of exciton separation, and the mobility of the separated charges, both of which depend on the electric field and on the properties of the polymer semiconductors. To ensure a very shallow horizontal section of the *I* - *V* curve it is preferred that the field dependence of both of these parameters is as weak as possible. In the case of charge separation this can be achieved if excitons are separated efficiently at, say, the interface between two different polymer semiconductors.

5.5.1. Open-circuit Voltage (V_{OC})

It is the maximum voltage attainable in a solar energy conversion device. The cell is placed in an open-circuit and illuminated. Electrons and holes separate and flow towards the low and high work function materials, respectively. At some point the charge build-up will reach a maximum equal to the V_{OC}. Thus, the open-circuit voltage is a measure of the maximum Gibbs free energy that can be obtained from the cell. At open-circuit voltage, the net current, *I*, is zero. Therefore using Equation (5.3), the V_{OC} is given by Equation (5.4) [83].

$$V_{oc} = \frac{nkT}{q} \ln\left(\frac{I_{ph}}{I_0} + 1\right) \tag{5.4}$$

V_{OC} is determined from the *I* - *V* curve as the point at which the curve crosses the voltage axis ($I = 0$). There are different views concerning the maximum V_{OC} attainable in solar energy conversion devices.

1. There is a suggestion that the V_{OC} is limited by the difference in work functions of the two electrodes [101].

2. It has been shown that in some heterojunction cells V_{OC} is more dependent on the acceptor strength than on the electrode material [102,103].

3. According to Gregg [104], the photovoltage of a solar cell is suggested to be a function of both the built-in electrical and the photogenerated chemical potential energy differences across the cell. The dependence of V_{OC} on the built-in potential is approximately true for a specific photoconversion mechanism, that which governs conventional solar cells (where electrons and holes are photogenerated together in the same semiconductor phase).

In organic solar cells (including dye-sensitized photoelectrochemical cells) where the primary photoexcitations are excitons, the charge carrier pairs are already separated across an interface upon photogeneration, creating a large chemical potential gradient, which tends to separate them, further. An internal electric field is not required for charge separation, and thus the built-in potential does not set the upper limit to V_{OC}. Substantial photovoltaic effects can be achieved in both solid-state organic solar cells and in dye-sensitized photoelectrochemcial cells under conditions where the built-in potential is zero. The maximum possible photovoltage in any photovoltaic cell is thus given by the maximum splitting between the quasi-Fermi levels anywhere in the cell at open-circuit. In dye-sensitized nanocrystalline titanium dioxide photoelectrochemical cells, this corresponds to the difference in the Fermi level of the nanocrystalline titanium dioxide and the redox couple. The photovoltage, however, can be decreased because of dark current at the semiconductor/electrolyte interface that may arise from the reduction of triiodide by the conduction band electrons [105]. The decrease in the rate constant for triiodide reduction (k_{et}) in a photoelectrochemical cell results with an increase in the open-circuit voltage according to the equation [106]:

$$V_{OC} = \left(\frac{kT}{e}\right)\ln\left(\frac{I_{inj}}{n_{cb}k_{et}[I_3^-]}\right) \tag{5.5}$$

where I_{inj} is the flux of charge resulting from sensitized injection, n_{cb} the concentration of electrons at the TiO_2 surface, k the Boltzmann constant, T the absolute temperature and e the electronic charge.

5.5.2. Short-circuit Current (I_{SC})

The maximum current that can run through the cell is determined by the short-circuit current. This quantity is determined by connecting the two electrodes, whereby the potential across the cell is set to zero, and then illuminating the cell while the current flow is measured. It is obtained by substituting V = 0 into Equation (5.3). Ideally, it is equal to the current density, I_{ph}, generated by light [83].

$$I_{sc} = I_{ph} \tag{5.6}$$

The short-circuit current yields information about the charge separation and transport efficiency in the cell. Several factors can influence the value of the short-circuit current. Incident light may be absorbed by the solution, or it might be reflected at the various interfaces in the cell, or it may be absorbed by the semiconductor and then converted to photocurrent. The short-circuit current of organic and inorganic solar cells increases with incident light intensity (I_{in}) and is proportional to I_{in}^{α} [107] (Equation 5.7),

$$I_{SC} \alpha I_{in}^{\alpha} \tag{5.7}$$

where α is characteristic for the system studied. For inorganic solar cells, α has a value of 1. A non-linear relationship may result because of direct recombination of electrons and holes, quenching of excitons by free carriers and the effect of the series resistance of the device on the I_{SC} [108,109].

5.5.3. Fill Factor (*FF*)

It is a measure of the maximum work obtainable from a solar cell with reference to a hypothetical maximum power, i.e., the product, I_{SC} x V_{OC}. It is given by the following equation [83].

$$FF = \frac{I_{MAX}\ V_{MAX}}{I_{SC}\ V_{OC}} \tag{5.8}$$

For a high FF, two things are required: (i) that the shunt (parallel) resistance of the diode should be very large to prevent leakage currents and (ii) that the series resistance should be very small to get a sharp rise in the forward current. The series resistance simply adds up from all series resistance contributions in the device, that is, from bulk transport, from interface transfer and from transport through the contacts. The fill factor has values of 0.7 - 0.8 for an *I* - *V* relationship described by Equation (5.3). Often, however, resistive losses or recombination losses lower the value [109].

5.5.4. Power Conversion Efficiency (η):

The power conversion efficiency of a solar cell is defined as the maximum power produced by the cell (P_{MAX}) divided by the power (intensity) of the incident light on the representative area of the cell [83]. It is usually expressed in percent.

$$\eta\ (\%) = \frac{P_{MAX}}{I_{in}} = \frac{FF\ I_{SC}\ V_{OC}}{I_{in}}\ x100 \tag{5.9}$$

5.5.5. Incident Photon-to-current Conversion Efficiency (*IPCE*)

Incident photon-to-current conversion efficiency also called external quantum efficiency is defined as the ratio of the number of collected charge carriers to the number of incident photons at the device. It is given by the equation [110]:

$$IPCE\,\% = \frac{E_{ph}(\lambda) I_{SC}}{I_{in}\, e} = \frac{1240\, I_{SC}}{\lambda\, I_{in}} \tag{5.10}$$

Where $E_{ph}\ (\lambda)$ is the energy of a photon (Joule) as a function of the wavelength, *e* is the electronic charge, I_{SC} is short circuit current ($\mu A/cm^2$), λ is the excitation wavelength (nm)

and I_{in} the incident photon intensity (W/m^2). The ratio, E_{ph}/I_{in}, refers to the number of incident photons while; I_{SC}/e refers to the number of electrons that generate electricity. $1240/\lambda$ refers to the energy of photons in eV. *IPCE* is measured for a specific light wavelength. One advantage of analyzing the *IPCE* rather than photocurrent is that effects due to the spectral shape of the incident light, light source or measuring equipment are removed and the true response of the device is obtained. A plot of *IPCE vs.* wavelength illustrates the spectral operation range of a specific solar cell. For single layered organic photovoltaic cells, the *IPCE%* is typically in the order of 1% [111]. For high performance solar cells, the *IPCE* value can approach unity over a large spectral section. Light of different wavelength is absorbed at different depths of the photoactive electrode.

5.6. Factors affecting the efficiency of an organic solar cell

5.6.1. Polymer Absorption

The spectrum of the solar radiation reaching the surface of the earth has an envelope that extends from about 300 nm, in the UV, to beyond 4000 nm in the IR. Figure 5.5 shows the irradiance from the sun as a function of wavelength [112]. This spectrum includes both diffuse and direct light and is for light received at sea level with the sun at 37° to the vertical and is called the AM 1.5 solar spectrum. This is typically the spectrum used when characterizing solar cells. The proportion of this light that can be absorbed in a solar cell relates to the power conversion efficiency of the cell. The broader the absorption spectrum of the active solar cell material, the greater the efficiency of cells made from that material, although of course the absorption of light is only the first step in the charge extraction process. Inorganic semiconductors are considered to have fixed, well defined absorption spectra that can be modified slightly by the addition of dopant substituent atoms into their crystal structure. However, an elegant feature of organic semiconductors is that their absorption spectra can be changed, in some cases dramatically, simply by changing the molecular or polymeric chemical structure.

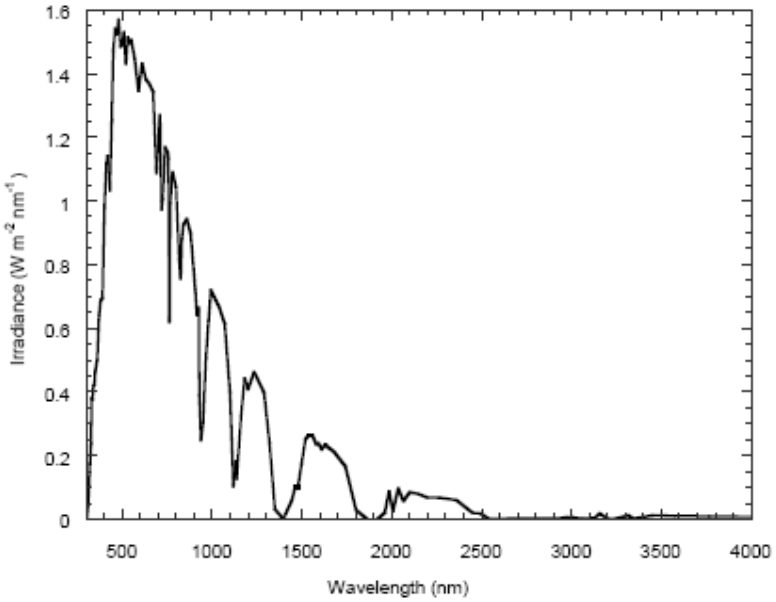

Figure 5.5. The solar irradiance received on the surface of the earth. The spectrum includes data from both the diffuse and direct radiation and is measured at sea level with the sun at 37° to the vertical. This spectrum is known as the AM 1.5 solar spectrum. Taken from Reference [112].

5.6.2. Polymer Energy Levels

The HOMO (highest occupied molecular orbital) is analogous to the valence band edge in a traditional semiconductor. Its energy is equivalent to the energy required to remove an electron from the polymer chain, and may also be termed the ionization potential. The LUMO (lowest unoccupied energy level) is analogous to the conduction band edge in an inorganic semiconductor, and is equal to the energy gained when an electron is added to the polymer chain. It is also referred to the electron affinity. The HOMO and LUMO levels of a material can be determined by cyclic voltammetry, which measures the potentials for electrochemical reduction and oxidation of a thin film sample.

One of the major challenges in a polymer photovoltaic device is to separate the bound charges (excitons), which are generated when a polymer semiconductor absorbs light. In most cases this is done by using two different semiconductors in either a double layer

(heterojunction) configuration, or as is usually preferred, a bulk heterojunction in which the two different semiconductors are mixed together and so present a larger interfacial surface area where charge separation may occur with a high efficiency [113]. The semiconductors are chosen to have different HOMO and LUMO levels, as shown in Figure 5.6.

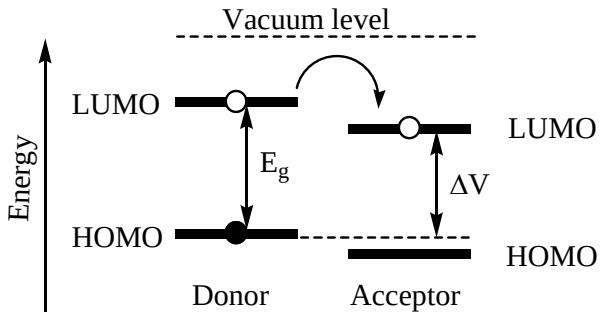

Figure 5.6. Illustration of exciton dissociation at the donor/acceptor interface of organic solar cell. ΔV is the maximum cell voltage under illumination.

The material with the deeper HOMO and LUMO levels is termed the acceptor, and the other material, the donor. The difference in the energy level between the HOMO of the donor and the LUMO of the acceptor corresponds to the maximum photovoltage of the cell under open-circuit condition. As shown in Figure 5.6, there is an energy gain in transferring an electron from the LUMO of the donor to the LUMO of the acceptor material. There is also an energy gain in transferring a hole to the donor from the acceptor. An exciton located on the donor may be split apart by transfer of the electron to the LUMO of the acceptor. This requires the energy gain in the electron transferring to the acceptor being sufficient to overcome the exciton binding energy, which is in the range of 0.1 to 0.5 eV [112]. Similarly, provided the HOMO offset is sufficient, excitons located on the acceptor may dissociate by transfer of a hole to the donor material.

In polymer photovoltaic devices based on blends of donor and acceptor polymers, the different materials phase separate when they are deposited from solution, giving a large surface area of interfaces distributed throughout the polymer film. Excitons photoexcited in both the donor and acceptor materials diffuse until they either find an interface where they

are dissociated, (allowing the charges to be extracted) or decay by some other means. It is clearly desirable for the probability of exciton separation to be as high as possible, once an exciton has found an interface. The greater the magnitude of the offsets between the donor and acceptor levels the greater the driving force for exciton separation. The necessary criteria for the selection of donor acceptor energy levels are [112]:

1. The donor and acceptor HOMO and LUMO offsets should be as large as possible (while considering the third point below). Work has shown that 0.5 eV or more is required for both the HOMO and LUMO offsets to ensure efficient bi-polar charge separation.

2. The donor and acceptor polymers should have similar band gaps. If this is not the case, there is a possibility that the entire exciton may transfer to the lower band gap material, from which it may decay radiatively, as shown in Figure 5.7.

3. There is a limit to the maximum desirable energy level offset. When the charges have separated the electron is sited on the acceptor LUMO and the hole on the donor HOMO. The difference in energies between these two levels dictates the chemical potential difference between the separated charges, which in turn imposes a limit on the open-circuit voltage the cell can produce. In a simple picture, if the donor and acceptor offsets are set at 0.5 V, and the materials each have band gaps of 1.5 eV, then the open circuit voltage would be pinned at around 1V. Increasing the offsets would increase the probability of charge separation, but would reduce the maximum sustainable open circuit voltage, as illustrated in Figure 5.6. Another way of looking at this is to note that energy is lost from the exciton when it separates by transfer of the electron or hole to a more stable level and this energy can not then be extracted as electrical energy, thus reducing the solar conversion efficiency.

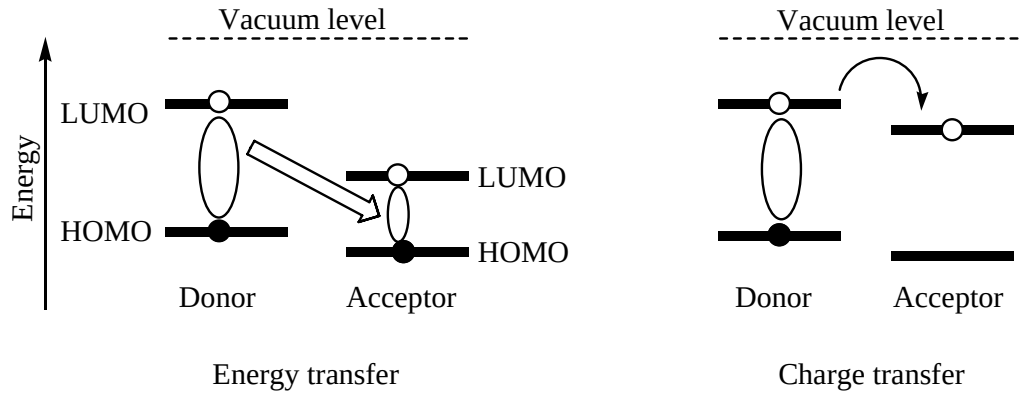

Figure 5.7. Illustration of competing energy and charge transfer processes.

5.6.3. Charge Transport in a Conducting Polymer

The mobility of charges in a polymer is reliant on favorable microscopic polymer morphology and a very low impurity/defect concentration. The morphologies that have shown the highest mobilities are those with polymer chains forming lamella structures and morphologies where the polymer chains are preferentially aligned. Impurities and defects can act as trap sites for charges depending on the relative energy levels of both the impurity/defect and the polymer. There are therefore two approaches to minimizing the reduction in mobility caused by these effects [113]. First, improvements can be made to the purity of the polymer thus reducing the density of impurities and defects. Second, it is possible to neutralize traps that are caused by impurities/defects with a known energy by selecting the polymer with a HOMO or LUMO such that the impurity/defect can no longer trap charges. An example of this is shown in Figure 5.8 where an impurity can act as a *hole*-trap for polymer 1 and not for polymer 2 because of the energy level alignment.

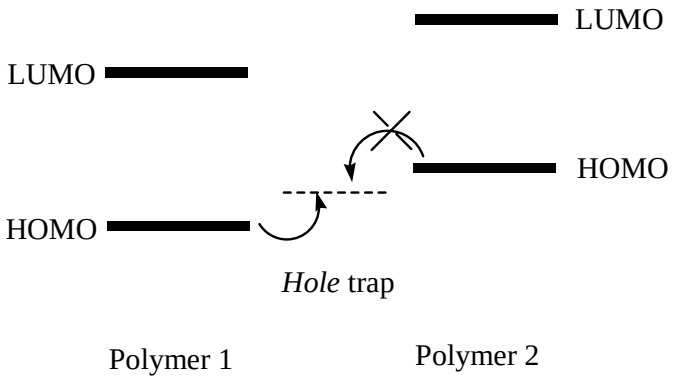

Figure 5.8. A schematic representation of the energy levels of two conjugated polymers and a *hole* trap site. For polymer 1, a *hole* in the HOMO level will see the *hole* trap species as a trapping site. However, a *hole* on polymer 2, which has a smaller HOMO energy, will not interact with the *hole* trap.

5.6.4. Morphology

The morphology of the polymer blend has a substantial impact on the performance of polymer device. A fine structured mixing of the donor and acceptor polymers is preferred, as the interfacial donor-acceptor interface area is then increased, and excitons have less far to diffuse to reach a dissociation site. However, the morphology also influences the transport of charges back to the collecting electrodes. Ideally, the two polymers mix to form an interpenetrating network, providing a complete path for transport of electrons to the cathode through acceptor domains and of holes through the donor domains to the anode. Breaks in the network can form trapping sites for charges, which can be detrimental to device performance. The morphology can be influenced through a wide variety of techniques during processing [5,114]. Choice of solvent boiling point and polarity, as well as the ambient conditions during deposition, can all influence the nature of the morphology. The nature of the polymers themselves will also affect the nature of the phase separation.

5.6.5. Selectivity of the Electrodes

The electrodes of photovoltaic devices have to be selective in the case of bulk heterojunctions. Since bulk heterojunction devices comprise a mixed layer of donor-acceptor systems, there is a prior in no symmetry breaking. Thus, by random diffusion processes, electrons and holes will also travel to the wrong electrode and recombine there, contributing to loss mechanisms. Such diffusion and recombination effects can be reduced by thin devices with different work function electrodes that induce an electric field across the photoactive layer. This electric field has been shown to be effective in thin layer metal-insulator-metal (MIM)-type devices [115]. In such a case, the charges are accelerated by the induced field and thus, the selective transport and charge collection of the electrodes are established by the work function asymmetry. However, in thick devices, as well as under intense light illumination conditions such as AM1.5 solar simulated irradiation, the charges generated exceed $10^{18}/cm^3$ and, thus, start to screen the electric field induced by the electrodes. In this case, the diffusion will become important and dominate once again. Therefore, electron-blocking layers on the hole-collecting electrode and hole-blocking layers on the electron-collecting electrodes become important. In state-of-the-art devices, the role of the poly(3,4-ethylenedioxythiophene): poly(styrene sulfonate) (PEDOT:PSS) layer on an ITO electrode [116-118] and the LiF layer under an Al electrode [119] can be rationalized in this manner.

REFERENCES

[1] M.A. Green, “Solar Cells”, Prentice-Hall, Inc., Englewood Cliffs, N.J., 1992.

[2] M.A. Green, Prog. Photovolt. Res. Appl. 9 (2001) 287.

[3] B. Miller, S.L. Licht, M.E. Orazem, P.C. Searson, Critical Reviews in Surface Chemistry 3 (1993) 29.

[4] H. Spanggaard, F.C. Krebs, Sol. Energy Materials Sol. Cells 83 (2004) 125.

[5] S.R. Forrest, Nature 428 (2004) 911.

[6] J.J. Dittmer, E.A. Marseglia, R.H. Friend, Adv. Mater. 12 (2000) 1270.

[7] H. Bässler, Molec. Crys. Liq. Crys. Sci. Technol. Sec. A 252 (1994) 11.

[8] G. Li, V. Shrotriya, J. Huang, Y. Yao, T. Moriarty, K. Emery, Y. Yang, Nature 4 (2005) 864.

[9] M. Reyes-Reyes, K. Kim, D.L. Carroll, Appl. Phys. Lett. 87 (2005) 083506.

[10] W. Ma, C. Yang, X. Gong, K. Lee, A.J. Heeger, Adv. Funct. Mater.15 (2005) 1617.

[11] A.C. Arias, J.D. MacKenzie, R.Stevenson, J.J.M. Halls, M. Inbasekaran, E.P. Woo, D.Richards, R.H. Friend, Macromolecules 34 (2001) 6005.

[12] G.Yu, A.J. Heeger, J. Appl. Phys. 78 (1995) 4510.

[13] D. Gebeyehu, C.J. Brabec, F. Padinger, T. Fromherz, S. Spiekermann, N. Vlachopoulos, F. Kienberger, H. Schindler, N.S. Sariciftci, Synth. Met. 121 (2001) 1549.

[14] A.C. Arango, L. Johnson, H. Horhold, Z. Schlesinger, S.A. Carter, Adv. Mater. 12 (2000) 1689.

[15] W.U. Huynh, J.J. Dittmer, A.P. Alivisatos, Science 295 (2002) 2425.

[16] G.P. Smestad, S. Spiekermann, J. Kowalik, C.D. Grant, A.M. Schwartzberg, J. Zhang, L.M. Tolbert, E. Moons, Sol. Energy Mater. Sol. Cells 76 (2003) 85.

[17] E. Arici, H. Hoppe, F. Schäffler, D. Meissner, M.A. Malik, N.S. Sariciftci, Thin Solid Films 451-452 (2004) 612.

[18] W.J.E. Beck, M.M. Wienk, R.A.J. Janssen, Adv. Mater. 16 (2004) 1009.

[19] A. J. Breeze, Z. Schlesinger, S. A. Carter, P. J. Brock, Phys. Rev. B 64 (2001)125205.

[20] Y. Song, J.K. Kim, A.Y. Kim, Synth. Met. 137 (2003) 1387.

[21] A. Hinsch, J.M. Kroon, R. Kern, I. Uhlendorf, J. Holzbock, A. Meyer, J.A. Ferber, Prog. Photovolt: Res. Appl. 9 (2001) 425.

[22] R. Grünwald, H. Tributsch, J. Phys. Chem. B 101 (1997) 2564.

[23] A.F. Nogueira, J.R. Durrant, M.A. De Paoli, Adv. Mater. 13 (2001) 826.

[24] B. O'Regan, D.T. Schwartz, J. Appl. Phys. 80 (1996) 4749.

[25] U. Bach, D. Lupo, P. Comte, J.E. Moser, F. Weissörtel, J. Salbeck, H. Spreitzer, M. Grätzel, Nature 395 (1998) 583.

[26] D. Gebeyehu, C.J. Brabec, N.S. Sariciftci, D. Vangeneugden, R. Kiebooms, D. Vanderzande, F. Kienberger, H. Schindler, Synth. Met. 125 (2002) 2797.

[27] D. Gebeyehu, C.J. Brabec, F. Padinger, T. Fromherz, S. Spiekermann, N. Vlachopoulos, F. Kienberger, H. Schindler, N.S. Sariciftci, Synth. Met. 121 (2001) 1549.

[28] G.K.R. Senadeera, T. Kitamura, Y. Wada, S. Yanagida, Sol. Energy Mater. Sol. Cells 88 (2005) 315.

[29] Y. Hao, M. Yang, C. Yu, S. Cai, M. Liu, L. Fan, Y. Li, Sol. Energy Mater. Sol. Cells 56 (1998) 75.

[30] P.A. van Hal, M.M. Wienk, J.M. Kroon, R.A.J. Janssen, J. Mater. Chem. 13 (2003) 1054.

[31] P.A. van Hal, M.M. Wienk, J.M. Kroon, W.J.H. Verhees, L.H. Slooff, W.J.H. van Gennip, P. Jonkheijm, R.A.J. Janssen, Adv. Mater. 15 (2003) 118.

[32] T.J. Savenije, J.M. Warman, A. Goossens, Chem. Phys. Lett. 287 (1998) 148.

[33] H. Shirakawa, E.J. Louis, A.G. MacDiarmid, C.K. Chiang, A.J. Heeger, J. Chem. Com. 16 (1977) 578.

[34] C.K. Chiang, C.R. Fincher, Y. W. Park, A.J. Heeger, H. Shirakawa, E.J. Louis, A.G. MacDiarmid, Phys. Rev. Lett. 39 (1977) 1098.

[35] M.T. Bernius, M. Inbasekaran, J. O'Brien, W.S. Wu, Adv. Mater., 12 (2000)1737.

[36] M. Shtein, J. Mapel, J.B. Benziger, S.R. Forrest, Appl. Phys. Lett., 81 (2002) 268.

[37] P. Peumans, S. Uchida, S. R. Forrest, Nature 425 (2003) 158.

[38] P. Peumans, S. R. Forrest, Appl. Phys. Lett. *79* (2001) 126.

[39] G. Hadziioannu, P.F. van Hutten; "Semiconducting Polymers, Chemistry Physics and Engineering"; Wiley, Weinheim, 2000.

[40] R.D. McCullough, Adv. Mater. 10 (1998) 93.

[41] A. Zen, J. Pflaum, S. Hirschmann, W. Zhuang, F. Jaiser, U. Asawapirom, J.P. Rabe, U. Scherf, D. Neher, Adv. Func. Mater. 14 (2004) 757.

[42] L. Groenendaal, F. Jonas, D. Freitag, H. Pielartzik, J.R. Reynolds, Adv. Mater. 12 (2000) 481.

[43] F. Jonas, L. Schrader, Synth. Met. 41-43 (1991) 831.

[44] G. Heywang, F. Jonas, Adv. Mater., 4 (1992) 116.

[45] G. Heywang, F. Jonas, Chem. Phys. 194 (1995) 207.

[46] T. Kugler, W.R. Salaneck, H. Rost, A.B. Holmes, Chem. Phys. Lett. 310 (1999) 391.

[47] G. Greczynski, T. Kugler, W.R. Salaneck, J. Appl. Phys. 88 (2000) 7187.

[48] J. Rasmusson, S. Stafström, M. Lögdlund, W.R. Salaneck, U. Karlsson, D.B. Swanson, A.G. MacDiarmid, G.A. Arbuckle, Synth. Met. 41-43 (1991) 1865.

[49] A.G. Mac Diarmid, Angew. Chem. Int. Ed. 40 (2001) 2581.

[50] J.L. Bredas, R.R. Chance, R. Silbey, Mol. Crys. Liq. Crys. 77 (1981) 319.

[51] W.R. Salaneck, H.R. Thomas, C.B. Duke, E.W. Plummer, A.J. Heeger, A.G. Mac Diarmid, J. Chem. Phys. 71 (1979) 2044.

[52] J. Tanaka, C. Tanaka, T. Miyamae, K. Kamiya, M. Shimizu, M. Oku, K. Seki, J. Tsukamoto, S. Hasegawa, H. Inokuchi, Synth. Met. 55-57 (1993) 121.

[53] S. Kuroda, H. Shirakawa, Synth.Met. 17 (1987) 423.

[54] Y. Onodera, Phys. Rev. B 30 (1984) 301.

[55] A.O. Patil, A.J. Heeger, F. Wudl, Chem. Rev. 88 (1988) 183.

[56] P. Chandrasekhar, “Conducting Polymers, Fundamentals and Applications”, Kluwer Academic Publishers, USA, 1999.

[57] M. Mastragostino, C. Arbizzani, A. Bongini, G. Barbarella, M. Zambianchi, Electrochim. Acta 38 (1993) 135.

[58] P.W.M. Blom, M.J.M. de Jong, M.G. van Munster, Phys. Rev. B 55 (1997) R656.

[59] I.D. Parker, J. Appl. Phys. 75 (1994) 1656.

[60] A.J. Campbell, D.D.C. Bradley, H. Antoniadis, Appl. Phys. Lett. 79 (2001) 2133.

[61] M.G. Kanatzidis, Chem. Eng. News 68 (1990) 36.

[62] A.J. Heeger, S. Kivelson, J.R. Schrieffer, W.P. Su, Rev. Mod. Phys. 60 (1988) 782.

[63] A.B. Kaiser, “Electronic properties of conjugated polymers”, in: H. Kuzmany M. Mehring, S. Roth (ed.), Heidelberg: Springer Verlag, 1987.

[64] L. Pautmeier, U. Rauscher, H. Bässler, Chem. Phys. 146 (1990) 291.

[65] L.B. Schein, D. Glatz, J.C. Scott, Phys. Rev. Lett. 65 (1990) 472.

[66] S. Kivlson, Phys. Rev. B. 25 (1982) 3798.

[67] L. Groenendaal F. Jonas, D. Freitag, H. Pielartzik, J. R. Reynolds, Adv. Mater. 15 (2003) 855.

[68] J. Heinze, H. John, A. Rasche, Institute for Physical Chemistry, University of Freiburg, Germany, 2006.

[69] S. Asavapiriyanont, G.K. Chandler, G.A. Gunawardena, D. Pletcher, J. Electroanal. Chem. Interfacial Electrochem. 177 (1984) 245.

[70] M. Dierich, J. Heinze, G. Heywang, F. Jonas, J. Electroanal. Chem. 369 (1994) 87.

[71] J.R. MacCallum and C.A. Vincent, "Polymer Electrolyte Reviews-2", Elsevier Applied science, London, 1989.

[72] R.J. Latham, R.G. Linford, W.S. Schlindwein, Ionics, 9 (2003) 41.

[73] Teketel Yohannes, Theodros Solomon, O. Inganäs, Synth. Met. 82 (1996) 215.

[74] F.M. Gray, "Polymer Electrolytes", The Royal Society of Chemistry, UK, 1997.

[75] A. Valee, S. Besner, J. Prudhomme, Electrochim. Acta 37 (1992)1579.

[76] S. Neyetz, D. Brown, Electrochim. Acta. 43 (1998) 1343.

[77] T. Sreekanth, M. J. Reddy, U.V. Rao, J. Power Sources 93 (2001) 268.

[78] D.J. Wilson, C.V. Nicholas, R.H. Mobbs, C. Booth, Br. Polym. J. 22 (1990) 129.

[79] M.B. Armand, Solid State Ionics 9/10 (1983) 745.

[80] J.R. MacCallum, A.S. Tomlin, C.A. Vincent, Eur. Poly. J. 22 (1986) 787.

[81] M.A. Ratneer, In "polymer Electrolyte: Reviews-1", J.R. MacCallum, C.A. Vincent (Eds), Elsevier Applied Science, London, 1987.

[82] K.D. Karlin, "Progress in Inorganic Chemistry", Vol.41, John Wiley & Sons, Inc., California, 1994.

[83] A. Hagfeldt, M. Grätzel, Chem. Rev. 95 (1995) 49.

[84] W. Krataschmer, L.D. Lamb, K. Fostiropoulos, D.R. Hufman, Nature 347 (1990) 54.

[85] H.W. Kroto, J.R. Heath, S.C. O'Brien, R.F. Curl, R.E. Smalley, Nature 318 (1985) 162.

[86] A. Hirsch, "The Chemistry of Fullerenes", Gutmann & Co. GmbH, Germany, 1994.

[87] H.W. Kroto, A.W. Allaf, S.P. Balm, Chem. Rev. 91 (1996) 1213.

[88] Q. Xie, E.P. Cordero, L. Echegoyen, J. Am. Chem. Soc. 114 (1992) 3978.

[89] N.S. Sariciftci, L. Smilowitz, A.J. Heeger, F. Wudl, Science 258 (1992) 1474.

[90] L. Smilowitz, N.S. Sariciftci, R. Wu, C. Gettinger, A.J. Heeger, F. Wudl, Phys. Rev. B 47 (1993)13835.

[91] B. Kraabel, D. McMranch, N.S. Sariciftci, D. Moses, A.J. Heeger, Phys. Rev. B 50 (1994) 18543.

[92] C.H. Lee, G. Yu, D. Moses, K. Pakbaz, C. Zang, N.S. Sariciftci, A.J. Heeger, F. Wudl Phys. Rev. B 48 (1993) 15425.

[93] N.S. Sariciftci, D. Braun, C. Zhang, V. Srdanov, A.J. Heeger, G. Stucky, F. Wudl, Appl. Phys. Lett. 62 (1993) 585.

[94] B. O'Regan, M. Grätzel, Nature 353 (1991) 737.

[95] J. Desilvestro, M. Grätzel, L. Kavan, J. Moser, J. Augustynski, J. Am. Chem. Soc. 107 (1985) 2988.

[96] A. Hagfeldt, M. Grätzel, Acc. Chem. Res. 33 (2000) 269.

[97] S. Södergren, A. Hagfeldt, J. Olsson, S-.E. Lindquist, J. Phys. Chem. 98 (1994) 5552.

[98] A. Solbrand, A.Henningsson, S. Södergren, H. Lindström, A. Hagfeldt, S-. E. Lindquist, J. Phys. Chem. B 103 (1999)1078.

[99] N. Kopidakis, A. Schiff, N-. G. Park, J. van de Langemaat, A.J. Frank, J. Phys. Chem. B 104 (2000) 3930.

[100] D. Cahen, G. Hodes, M. Grätzel, J.F Guillemoles, I. Riess, J. Phys. Chem. B 104 (2000) 2053.

[101] R.N. Marks, J.J. M. Halls, D.D.C. Bradley, R.H. Friend, A.B. Holmes, J. Phys.: Condens. Matter. 6 (1 994) 1379.

[102] C.J. Brabec, A. Cravino, D. Meissner, N.S. Sariciftci, M.T. Rispens, L. Sanchez, J.C. Hummelen, T. Fromherz, Thin Solid films 403 (2002) 368.

[103] V.D. Mihailetchi, P.W.M. Blom, J.C. Hummelen, M.T. Rispens, Appl. Phys. Lett. 94 (2001) 841.

[104] B.A. Gregg, "Organic-Based ("Excitonic") Solar Cells", National Renewable Energy Laboratory, 1617 Cole Blvd., Golden, CO 80401-3393, Colorado, 2003 .

[105] M.K. Nazeeruddin, A. Kay, I. Rodicio, R. Humphry-Baker, E. Müller, P. Liska, N. Vlachopoulos, M. Grätzel, J. Am. Chem. Soc. 115 (1993) 6382.

[106] A. Kumer, P.G. Santangelo, N.S. Lewis, J. Phys. Chem. 96 (1992) 835.

[107] H. Meier, "Organic Semiconductors", Verlag Chemie, Germany, 1974.

[108] D. Gebeyehu, C.J. Brabec, F. Padinger , T. Fromherz, J.C. Hummelen, D. Badt, H. Schindler, N.S. Sariciftci, Synth. Met. 118 (2001) 1.

[109] Y. Fang, S.-An. Chen, M.L. Chu, Synth. Met. 52 (1992) 261.

[110] N. Vlachopoulos, P. Liska, J. Augustynski, M. Grätzel, J. Am. Chem. Soc. 110 (1988) 1216.

[111] R.N. Marks, J.J.M. Halls, D.D.C. Bradley, R.H. Friend, A.B. Holmes, J. Phys.: Condensed Matter 6 (1994) 1379.

[112] J. Halls, R. Wilson, “Plastic cells for energy from the sun”, Crown, UK, 2004.

[113] G. Yu, C. Zhang, A.J. Heeger, Appl. Phys. Lett. 64 (1994) 1540.

[114] W. Geens, T. Aernouts, J. Poortmans, G. Hadziioannou, Thin Solid Films, 403-404 (2002) 438.

[115] N.S. Sariciftci, “Matrials Today”: Review, Elsevier Ltd., 2004, p.36.

[116] A.C. Arias, M. Granström, D.S. Thomas, K. Petritsch, R.H. Friend, Phys. Rev. B 60 (1999) 1854.

[117] M. Granström, K. Petritsch, A.C. Arias, A. Lux, M.R. Andersson, R.H. Friend, Nature 395 (1998) 257.

[118] P. Peumanns, S.R. Forrest, Appl. Phys. Lett. 79 (2001) 126.

[119] C.J. Brabec, S.E. Shaheen, C. Winder, N.S. Sariciftci, P. Denk, Appl. Phys. Lett. 80 (2002) 1288.

6. POLYMER-SENSITIZED PHOTOELECTROCHEMICAL CELLS

6.1. Background

Dye-sensitized photoelectrochemical cells (PEC) are considered low cost alternatives to the inorganic photovoltaic cells [1]. The cells are composed of nanocrystalline TiO_2 film deposited on a transparent conductive electrode (anode), a dye, chemically anchored on TiO_2 nanoparticles, an electrolyte bearing the I_3^-/I^- redox couple and a platinized transparent conductive electrode (cathode). Following light absorption by the dye, electrons are excited from the HOMO to the LUMO followed by relaxation through electron loss to the semiconductor. The dye cation is neutralized by the chemical reaction with the redox couple in the electrolyte solution which in turn gains an electron from a counter electrode, making the process regenerative for the conversion of incident light to electric current. For effective electron transfer to the TiO_2, the energy level of the LUMO of the dye (electron donor) should be higher than the conduction band edge of the semiconductor (electron acceptor) and the HOMO energy level should lie above the valence band of the semiconductor but below the electrochemical potential of the redox couple. The power conversion efficiency of such cells has reached 10.4% [2]. Despite their high power conversion efficiencies, their commercial applications are limited due to problems like leakage of the electrolyte and the degradation of both the electrolyte [3] and the dye [4]. Various studies with different approaches have been carried out to alleviate the problems associated with liquid-state DSSCs. These include replacement of the liquid electrolyte by a polymer electrolyte [5] and by a hole-transporting material [6-9], replacement of the dye by a semiconducting polymer [10-12] and replacement of both the dye and the liquid electrolyte by a semiconducting polymer that plays the role of both a sensitizer and a hole-transporting medium [13-15].

The donor-acceptor system of organic solar cells has been studied in solid-state organic photovoltaic cells based on conjugated polymers. Heterojunctions based on blends of conjugated polymers (electron donors following photoexcitation) with fullerene and its derivative (electron acceptors) are the best-studied devices and they have yielded the highest power conversion efficiencies reaching around 5% [16-18]. In such photovoltaic cells, the semiconducting polymer takes care of the absorption of the sunlight, charge injection into

the fullerene or its derivative and the transport of holes after charge separation. Besides these fully organic photovoltaic devices, semiconducting polymers can also be used in combination with inorganic semiconductors such as TiO_2, ZnO and $CuInSe_2$ [9, 19-23]. In these hybrid organic/inorganic devices, the good electron accepting and conducting properties of the inorganic semiconductors can, in principle, be combined with cheap, solution processing of the semiconducting polymers. The disadvantages of many of these systems are the low hole-mobility in semiconducting conjugated polymers compared with the electron-mobility in inorganic semiconductors [24] and the incomplete filling of the pores of the inorganic semiconductor by the polymers [23]. The sensitizing effect of semiconducting polymers on inorganic semiconducting particles has been studied in different types of solar energy conversion devices. Polymer-sensitized solar cell construction requires choice of suitable polymer with appropriate band gap and band position (with respect to the inorganic semiconductor), and appropriate method of deposition. Photovoltaic cells based on composite films of nc-TiO_2 and MEH-PPV were studied [15, 25] where MEH-PPV was used both as a sensitizer to TiO_2 and as a hole-transporting medium. Such cells exhibited a monochromatic induced photon-to-current conversion efficiency of 6% at the maximum absorption of the polymer [25]. The sensitization of inorganic semiconductors by conjugated polymers [10-11] has also been investigated in liquid-state and solid-state PECs where the hole-mobility is facilitated by the redox couple. Liquid-state photoelectrochemical cells using poly(3-thiophenemalonic acid)-sensitized TiO_2 electrodes were assembled with power conversion efficiency reaching 1.8% [26].

In this work, we present different systems of liquid-state and solid-sate polymer-sensitized photoelectrochemical cells based on Eu^{2+}/Eu^{3+} and I_3^-/I^- redox couples where the inorganic materials are nanocrystalline titanium dioxide and fullerene. I_3^-/I^-, whose standard reduction potential is +0.53 V *vs.* NHE, is the common redox couple used in photoelectrochemical cells. The emeraldine form of polyaniline, however, does not show any photovoltaic effect in I_3^-/I^-. Accordingly, we used Eu^{2+}/Eu^{3+} whose standard redox potential is -0.36 V *vs.* NHE. Use of semiconducting polymers as sensitizers may be more advantageous than dye molecules with respect to the ease of large-scale production, cost and involvement of less toxic chemicals during the preparation of the polymers.

6.2. Polymer-sensitized Photoelectrochemical Cell Consisting of Eu^{2+}/Eu^{3+} Redox Couple: A Photoelectrochemical Cell Based on Emeraldine Base Form of Polyaniline

6.2.1. Background

The need for inexpensive, renewable energy sources has led to the development of photovoltaic cells based on organic molecules and conjugated polymers. For such applications photoactive materials that are stable and absorb light in the longer wavelength region of the solar spectrum are required. Polyaniline (PAni) is one such a material whose absorption can be switched to the longer wavelength region of the solar spectrum [27, 28]. Different researchers have studied the photoelectrochemical properties of PAni. Kaneko and Nakamura [29] reported that a PAni film gives a cathodic photocurrent response at negative applied potentials (*vs.* Ag/AgCl) and a low anodic photocurrent response at positive applied potentials when dipped into an aqueous electrolyte solution (pH = 6) containing $LiClO_4$. Fast transient photocurrent in response to a near-infrared light pulse has also been observed by Genies and Lapkowski [27, 30], which they associated with rapid modifications in PAni's electrical properties. The catalytic effect of PAni on the photoelectrochemical reduction of chloral (CCl_3CO) in NH_3/HF solution [30] and potassium peroxodisulphate ($K_2(SO_4)_2$) in aqueous H_2SO_4 solution [31] has been observed. Based on these preliminary results, PAni was considered as a p-type semiconductor that can be useful for the photoelectrochemical conversion of light to electricity and for photoassisted electrosynthesis. The effect of redox couples on the photoelectrochemical behavior of polyaniline at different applied potentials (between –0.2 V and +0.8 V vs. SCE) has been studied by Shen and Tian [31]. It was observed that the redox couples ($Fe(CN)_6^{3-}/Fe(CN)_6^{4-}$ and I_3^-/I^-) increase the magnitude and the stability of the photocurrent in aqueous acidic media.

In an effort to increase the photoresponse of PAni, PAni had been electropolymerized on cellulose acetate coated Pt electrode [32]. The porous structure of cellulose acetate membrane favored the swelling of the film thereby increasing the surface area of the conductive PAni exposed to the electrolyte solution. This has been reported to intensify the process of charge transfer and mass transport during the cyclic voltammetry of PAni under

illumination with concomitant increment in the photocurrent. The emeraldine base form of polyaniline (EB) has been used as a hole transporting material in solid-state dye-sensitized TiO_2 solar cells [33]. Emeraldine base that is protonated with different acids has been investigated as a hole-transporting layer in polymer light emitting diodes [34] and as a photoactive layer in Schottky diodes [35], as a sensitizer for nanocrystalline TiO_2 (Nc-TiO_2) film in the presence of I_3^-/I^- in an aqueous electrochemical cell [36] and in a solid-state photoelectrochemical cell [37]. In the later case the device consists of emeraldine base doped with dodecylbenzene sulphonic acid and blended with ethylene-propylene-diene terpolymer as a working electrode, poly(ethyleneoxide-co-epichlorohydrine)/NaI-I_2 as a polymer electrolyte and Pt as a counter electrode. According to the report, the V_{OC} was 0 V both in the dark and under illumination indicating the absence of photovoltaic effect. A cathodic current was observed in the dark at negative applied potentials the magnitude of which increased under illumination.

There has been no report on the photovoltaic effect of the emeraldine base form of polyaniline in a liquid junction photoelectrochemical cell. Here we report on the properties of photoelectrochemical cells that consist of emeraldine base form of polyaniline as a photoactive material and Eu^{2+}/Eu^{3+} redox couple in methanol as an electrolyte.

6.2.2. Experimental

6.2.2.1. Preparation of nc-TiO_2 film electrode

Sheets of indium-doped tin oxide coated glass (ITO-glass), each of dimension 4.5 x 0.8 cm, were cleaned successively with toluene, acetone and isopropanol and dried in air. A colloidal solution of nc-TiO_2 was prepared by the hydrolysis of titanium tetraisopropoxide following a literature procedure [24]. Accordingly, 0.5 mL titanium tetraisopropoxide (Aldrich, 99%) was slowly added with stirring to a mixture of 2.5 mL glacial acetic acid (Sigma Aldrich), 7.5 mL isopropanol (Sigma Aldrich) and 2.5 mL deionized water. The solution was stirred till a viscous solution was formed. The viscous solution was coated on ITO-glass by doctor blading and sintered at 450^oC for half an hour. A non-coated area of the ITO-glass was left at the edge of the longer side for electrical contact.

6.2.2.2. Preparation of Polyaniline

Cyclic voltammetry was used to prepare PAni in a three-electrode electrochemical cell. The working electrodes used were ITO-glass and nc-TiO_2 film. The reference and the counter electrodes were saturated calomel electrode (SCE) and Pt foil, respectively. The potential range used was between -0.15 V and +0.9 V. The potential was applied with a Jaissle Potentiostat/Galvanostat 1030PC.T. The polymerization was carried out in a solution of 1.0 M aqueous $HClO_4$ (Fluka), 0.1 M $NaClO_4$ (Fluka) and 0.1 M freshly distilled aniline (Fluka). The solution was purged with argon for 20 minutes before polymerization and left under argon atmosphere throughout the polymerization process. PAni was initially prepared in its emeraldine salt form by holding the potential at 0.4 V after polymer deposition. The emeraldine base (EB) form was prepared by washing the emeraldine salt form with 1.0 M $HClO_4$ and then treating it with excess 25% NH_3. The blue emeraldine base form was then dried under nitrogen. The UV-Vis spectrum was measured by Hewlett Packard 8453 spectrometer.

6.2.2.3. Photoelectrochemical studies

For photoelectrochemical studies, EB and a composite of EB and nc-TiO_2 on ITO-glass were used as photoactive materials. 0.02 M $EuCl_2$ (Aldrich) and 0.02 M $EuCl_3$ (Aldrich) in methanol (Baker) were used as a redox couple. EB did not show a photoresponse in the presence of KI/I_2 (E^o = 0.53 V *vs*. NHE). This may be due to a mismatch in the energy positions between the redox couple and the highest occupied molecular orbital of EB. Because of this, the redox couple Eu^{2+}/Eu^{3+} (E^o = -0.36 V *vs*. NHE) was chosen as electron mediator. Methanol was used as a solvent to avoid the protonation of EB and because both $EuCl_2$ and $EuCl_3$ are soluble in it. The photoactive electrode and the Pt counter electrode immersed in a cuvette that contains the electrolyte solution formed the photoelectrochemical cell.

The light source was a Xe arc lamp (Schoeffel). The intensity of the white light used for current – voltage studies was 50 mW/cm^2 (measured by a power meter Lasermate A, model LD-3, USA) without corrections for the absorption and scattering by the cuvette. Current -

voltage curves were measured using Keithley 2400 source meter at constant applied voltages (for EB-based cell) and during voltage scans at a rate of 5 mV/s (for EB:Nc-TiO_2-based cell). The device was illuminated from the solution/polymer interface side. The photocurrent action spectra were studied using a monochromator (Schoeffel) fitted to the Xe arc lamp. 345 nm and 520 nm filters were used during the measurement in the range 380 to 540 nm and in the range from 550 to 800 nm, respectively. All measurements were made when the open-circuit voltage came to a steady state.

6.2.3. Results and discussion

6.2.3.1. Current – Voltage characteristics

a) Polyaniline grown on ITO-glass electrode

Figure 6.1 shows the atomic force microscope (AFM) picture of the emeraldine base film on ITO-glass.

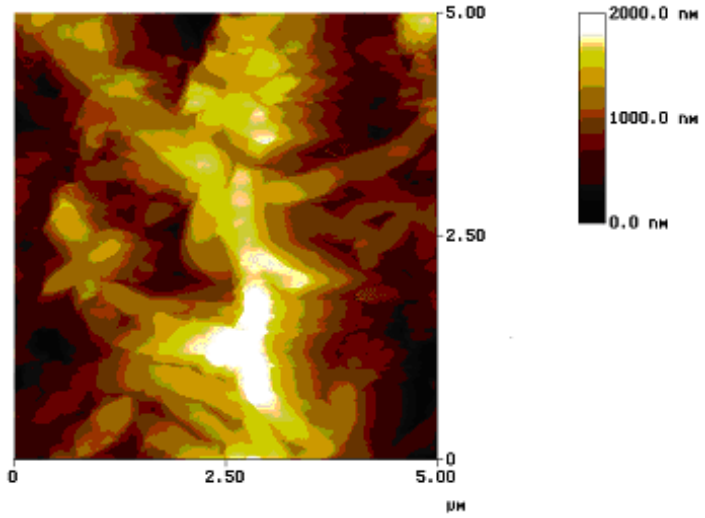

Figure 6.1. AFM picture of emeraldine base film on ITO-glass.

The film grew in bundles of fibers and its average thickness was in the range 2 – 3 µm. The PAni adhered poorly on the ITO-glass and its thickness was not uniform. Thick films

detached rather easily while thin films showed a very weak photocurrent response. The UV-Vis absorption spectrum of the film is shown in Figure 6.2. There are two absorption maxima at 330 nm (3.76 eV) and 665 nm (1.86 eV). The absorption extends to the infra red regions.

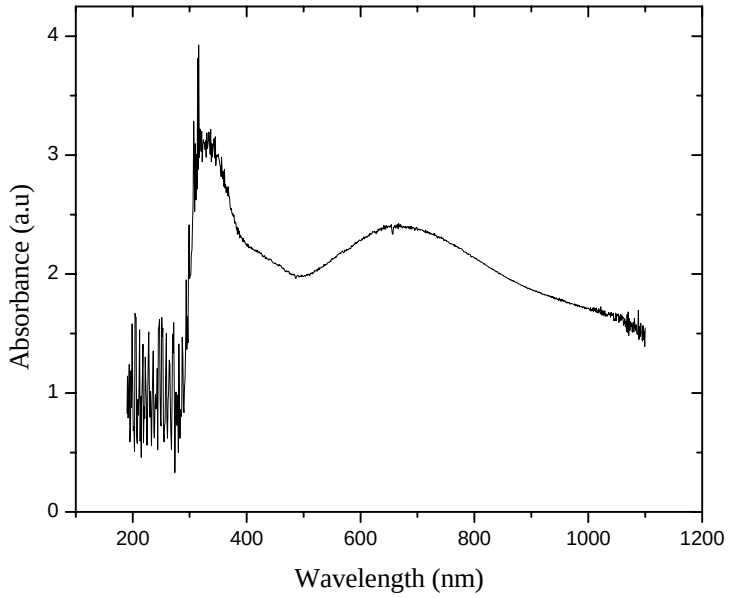

Figure 6.2. The UV-Vis absorption spectrum of EB film on ITO-glass.

Figure 6.3 shows the cyclic voltammogram of the emeraldine base form of PAni film on Pt. The onset potentials for the oxidation ($E^{ox}_{onset)}$ and reduction (E^{Red}_{onset}) were found to be 0.82 V and -0.6 V *vs.* quasi Ag/AgCl reference electrode, respectively. These values, after calibrating the quasi reference electrode with ferrocene, were equivalent to 0.8 V and -0.62 V *vs.* SCE, respectively. The onset potentials were determined from the intersection of the two tangents drawn at the rising oxidation (or reduction) current and background current in the cyclic voltammograms. The electrochemical HOMO – LUMO energy gap (1.42 eV) closely matches with the optical band gap (1.43 eV) measured from the UV-Vis absorption onset (Figure 6.2).

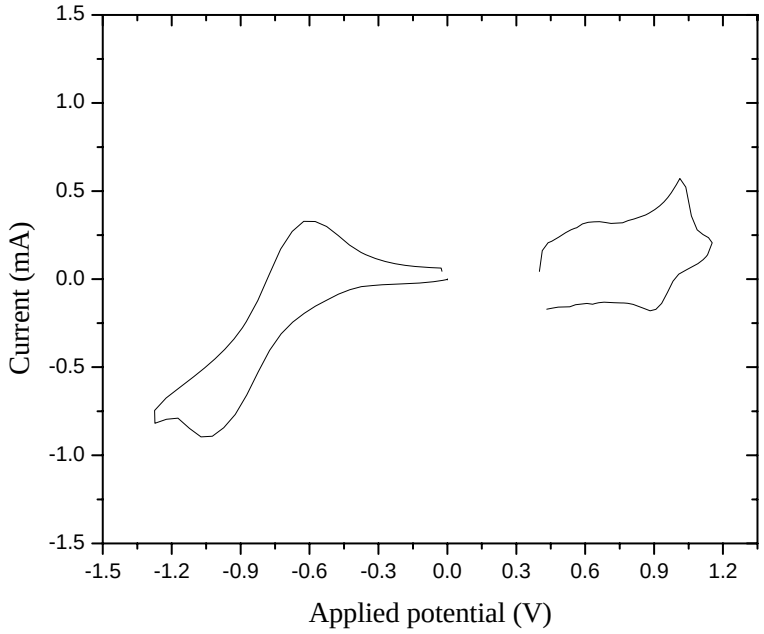

Figure 6.3. Cyclic voltammogram of EB film on Pt.
Electrolyte: acetonitrile + 0.1 M $(C_4H_9)_4NPF_6$, Reference electrode: quasi Ag/AgCl, Counter electrode: Pt, Scan rate: 5 mV/s, E^{Ox}_{onset} = 0.82 V, E^{Red}_{onset} = -0.60 V

Figure 6.4 shows the current – voltage (*I* – *V*) characteristics of the EB-based PEC in dark and under white light illumination with intensity of 50 mW/cm^2. Illumination of the PEC produced an anodic current under short-circuit condition and the negative value of the V_{OC} observed indicates that the photoactive electrode is higher in energy than the counter electrode. The V_{OC}, the I_{SC} and the fill factor (*FF*) obtained under illumination were -0.132 V, 0.64 μA/cm^2 and 0.35, respectively. The dark current may be a result of an electrochemical reaction on the EB film that involves the redox couple.

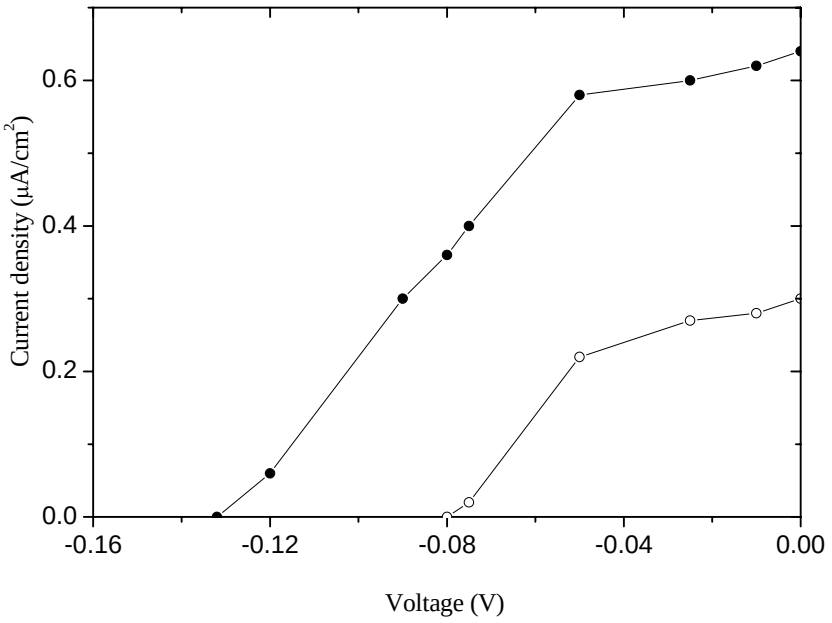

Figure 6.4. Current density *vs*. voltage characteristics for ITO/EB/Electrolyte/Pt cell in the dark (open circles) and under 50 mW/cm^2 white light illumination from Xe lamp (closed circles). Electrolyte: CH_3OH + 0.02 M $EuCl_2$ + 0.02 M $EuCl_3$.

b) Polyaniline grown on Nc-TiO_2 film electrode

In an effort to increase the photoresponse of emeraldine base (as observed by Neves *et. al*. for PAni film on cellulose acetate coated Pt [32]) and its possible use to sensitize TiO_2, aniline was electropolymerized on nc-TiO_2-coated ITO-glass. PAni started to grow on the ITO surface between the TiO_2 grains and extended between the pores to the surface of TiO_2. The electropolymerization process and the electrochromic properties of the PAni film were not affected by TiO_2 except that the rate of formation was slower than that on a bare ITO-glass. The PAni:Nc-TiO_2 composite film adhered strongly to the ITO-glass. The average thickness of the composite film was in the range 0.4 - 0.6 μm. Figure 6.5 shows the AFM picture of nc-TiO_2/EB composite film on ITO-glass.

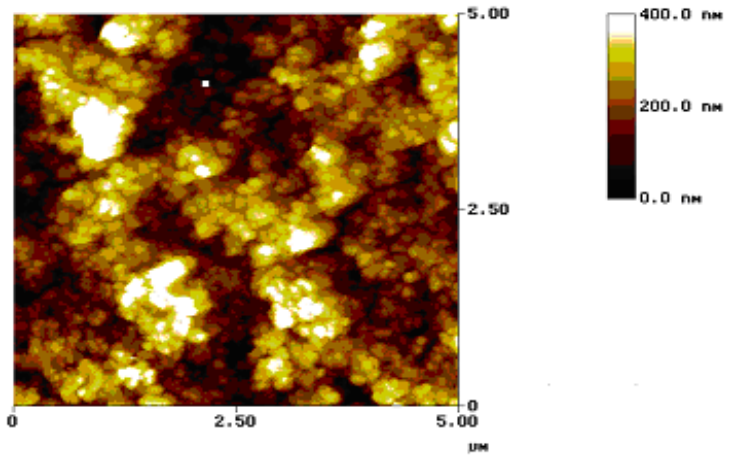

Figure 6.5. AFM picture of nc-TiO_2/EB composite film on ITO-Glass.

Figure 6.6 shows the *I* – *V* characteristics of the photoelectrochemical cell, Glass/ITO/EB:Nc-TiO_2/Electrolyte/Pt, in dark and under white light illumination with intensity of 50 mW/cm^2.

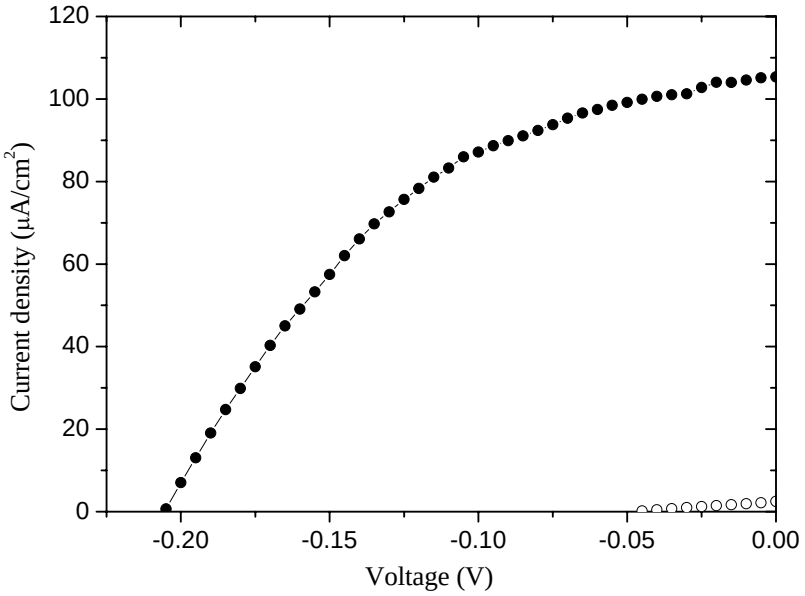

Figure 6.6. Current density *vs*. voltage characteristics for Glass/ITO/EB/Nc-TiO_2/Electrolyte/Pt cell in the dark (open circles) and under 50 mW/cm^2 white light illumination from Xe lamp (closed circles). Electrolyte: CH_3OH + 0.02 M $EuCl_2$ + 0.02 M $EuCl_3$.

Illumination of the PEC produced an anodic current under short-circuit condition and the negative value of the V_{OC} observed indicates that the photoactive electrode is higher in energy than the counter electrode. The cell has a V_{OC} of -0.205 V, a I_{SC} of 105 μA/cm^2 and a calculated *FF* of 0.44. The photoresponse of the PEC and its stability were more than the EB-based PEC. The $I - V$ curves have similar features with a solid-state dye-sensitized photoelectrochemical cell observed by Peter C. Searson *et al.* [38].

6.2.3.2. The photocurrent action spectra

The photocurrent action spectrum for the EB:Nc-TiO_2-based PEC is shown in Figure 6.7. The action spectrum for nc-TiO_2-based cell is also shown for comparison. The inset shows the UV-Vis absorption spectra of EB film.

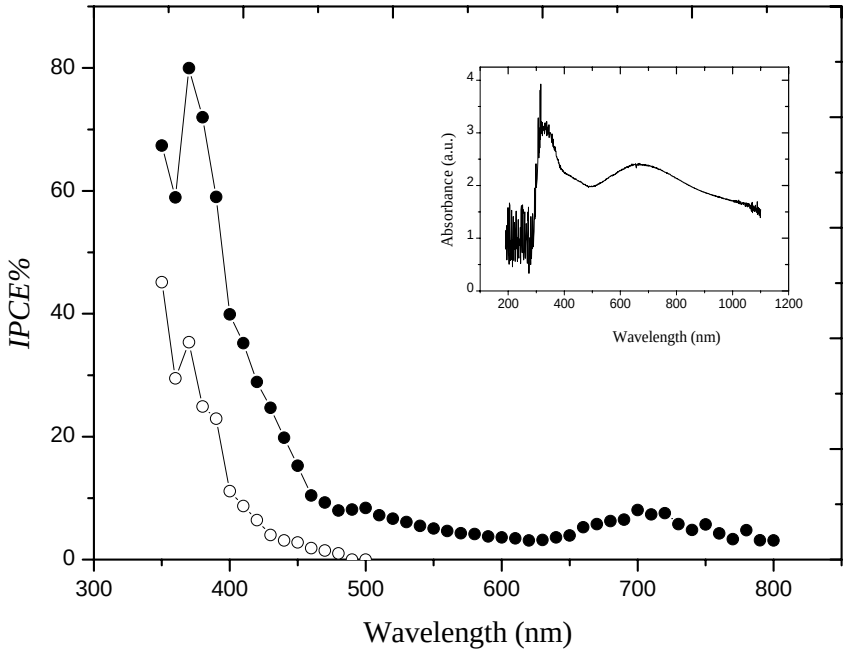

Figure 6.7. The photocurrent action spectra for the system: Glass/ITO/Nc-TiO_2/Electrolyte/Pt (open circles) and Glass/ITO/EB/Nc-TiO_2/Electrolyte/Pt (closed circles). Electrolyte: CH_3OH + 0.02 M $EuCl_2$ + 0.02 M $EuCl_3$. Inset: UV-Vis absorption spectra of emeraldine base film on ITO-glass.

The maximum incident photon-to-current conversion efficiency (*IPCE*) for the EB:Nc-TiO_2 - based cell was 80%. The high value corresponds to the absorption of light both by EB and TiO_2 at 370 nm. The *IPCE%* due to absorption by EB at 700 nm was 8%. The photoresponse of nc-TiO_2 is negligible above 420 nm.

A schematic energy level diagram for the device: Glass/ITO/EB/Nc-TiO_2/Electrolyte/Pt is shown in Figure 6.8.

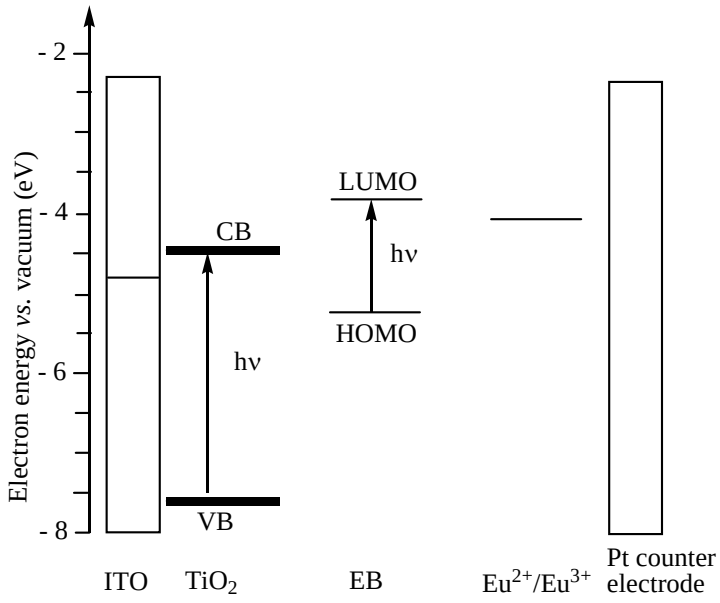

Figure 6.8. A schematic energy level diagram for the device: Glass/ITO/EB/Nc-TiO_2/Electrolyte/Pt. The excitation of emeraldine base form of PAni at 660 nm is shown.

The onset potentials for oxidation (E^{ox}_{onset}) and reduction (E^{red}_{onset}) can be used to estimate the energies of the highest occupied molecular orbitals (E_{HOMO}) and the lowest unoccupied molecular orbitals (E_{LUMO}) of conducting polymers [39,40]. According to de Leeuw *et al*. [41] E_{HOMO} (eV) = -(E^{ox}_{onset} + 4.4) and E_{LUMO} (eV) = -(E^{red}_{onset} + 4.4), where the onset potentials are in V *vs*. SCE. Using cyclic voltammetry, E^{ox}_{onset} and E^{red}_{onset} of the EB film were found to be 0.8 V and -0.6 V *vs*. SCE, respectively. This yields an estimated energy

level of -5.2 eV for the HOMO and -3.8 eV for the LUMO of EB. The position of Eu^{2+}/Eu^{3+} redox system (E^o = -0.36 V *vs*. NHE) is approximately at -4.14 eV (0 V *vs*. NHE = -4.5 eV).

From the results observed above, it is possible to suggest that the emeraldine base form of polyaniline shows photovoltaic effect in the presence of Eu^{2+}/Eu^{3+}. An anodic photocurrent has been produced when a voltage is applied between zero and the open-circuit voltage. This observation indicates that upon illumination, electrons from the HOMO of EB excite to its LUMO from which they are transferred to the ITO (in EB-based cell) or to the conduction band edge of nc-TiO_2 and then to the ITO (in EB:Nc-TiO_2-based cell). In the mean time holes can be transferred from EB^+ to Eu^{2+}. The Eu^{2+} is recovered at the counter electrode where Eu^{3+} accepts electrons. Such transfer of charges can however take place only if the Fermi energy levels of the ITO (-4.7 eV) and the nc-TiO_2 (-4.4 eV [2]) are raised to a level higher than the energy of the counter electrode probably by pinning with the excited state of the polymer. The nc-TiO_2 layer, in addition to its use as a matrix for the growth of PAni, participates in the light absorption (in the short wavelength region) and in the injection of electrons to the ITO contact. The photocurrent observed in the longer wavelength region is due to the absorption of light by EB.

6.2.3.3. Conclusion

A photoelectrochemical cell has been fabricated using the emeraldine base form of polyaniline as a photoactive material in the presence of Eu^{2+}/Eu^{3+} in methanol. The photoresponse of EB:Nc-TiO_2-based PEC is significantly higher than that of EB-based and nc-TiO_2-based PECs. The EB/Nc-TiO_2-based cell shows a V_{OC} of -0.205 V and an I_{SC} of 105 µA/cm^2 under 50 mW/cm^2 white light illumination from a Xe lamp. The cell shows an *IPCE%* of 80% and 8% at 370 nm and 700 nm, respectively. Though the performances of the PECs under the present experimental conditions are low, the results indicate that we can make use of the high environmental stability of PAni for solar cell application.

6.3. Polymer-sensitized Photoelectrochemical Cells Consisting of I_3^-/I^- Redox Couple

6.3.1. Background

The photoresponse behaviors of polymer-sensitized photoelectrochemical cells that consist of I_3^-/I^- have been studied in different systems.

In liquid-state photoelectrochemical cells,

1. A comparative study was conducted where the photoactive electrodes consist of chemically prepared poly[3-hexylthiophene], P3HT, and a composite film of nc-TiO_2 and P3HT (nc-TiO_2/P3HT). P3HT was chosen since it is known to have good solubility, good film giving properties [38] and suitable HOMO-LUMO energy level positions with respect to TiO_2 and I_3^-/I^- redox couple [42].

2. Separate and comparative studies were conducted where the photoactive electrodes consist of poly[3-(2',5'-dialkoxyphenyl)thiophenes], electrochemically prepared on ITO-glass and on nc-TiO_2 coated ITO-glass. The investigated polymers are poly[3-(2',5'-dioctyloxyphenyl)thiophene] (PDOOPT), poly[3-(2',5'-diheptyloxyphenyl)thiophene] (PDHOPT) and poly[3-(2',5'-dibutyloxyphenyl)thiophene] (PDBOPT).

Conducting polymers have been electrochemically deposited on large band-gap n-type semiconducting metal oxides for the formation of hybrid organic-inorganic heterojunctions for applications in photovoltaic cells, light emitting diodes and electrochromic devices [43-48]. Polymers that are electrochemically grown on nc-TiO_2 coated ITO-glass improve the filling of the pores of TiO_2 by the polymers, resulting with increased contact surface between the polymers and the TiO_2 particles that leads to a better charge transfer.

In solid-state photoelectrochemical cells, we have designed solid-state polymer-sensitized nc-TiO_2 photoelectrochemical cells where poly[2-methoxy-5-(2'-ethylhexyloxy)-1,4-phenylenevinylene], MEH-PPV, was used as a sensitizer to TiO_2 and as electron donor to C_{60}. MEH-PPV was chosen because of its light absorption in the visible region, suitable

energy positions of its highest occupied molecular orbital and lowest unoccupied molecular orbital for charge transfer to nc-TiO_2, to C_{60} and to the electrolyte [49] and its low intrinsic trap density [26]. The ion-conducting polymer, poly[oxymethylene-oligo(oxyethylene)], POMOE, complexed with I_3^-/I^- redox couple was used as a solid polymer electrolyte. As compared to liquid junction PECs, solid-state PECs have advantages like handling, portability and packaging.

6.3.2. Experimental

6.3.2.1 Device preparations and characterizations

a) Indium-doped tin oxide (ITO)

Transparent ITO is the material mostly used as a high-work function material in photovoltaic devices and light emitting diodes and as a back contact in photoelectrochemical cells. The ITO/polymer interface is not well understood or well controlled. There are large variations of the ITO morphology and work function from manufacturer to manufacturer and from batch-to-batch [50-53].

The uneven surface of ITO on glass results in local areas with high fields under operation that may cause rapid polymer degradation [54]. Different methods such as acid etching and ozone cleaning have been used to control the surface [55]. In this work, ITO-glass sheets (sheet resistance = 10 Ω/square), each of dimensions 1.5 cm x 2.5 cm were cleaned successively with deionized water, acetone and isopropanol and dried in air. Indium was also found to diffuse into the organic layer where it acts as trapping site for charge carriers [56]. One strategy used to minimize indium diffusion is to place an interfacial hole-transporting layer, such as poly(3,4-ethylenedioxythiophene) (PEDOT) [57-59], between the ITO and the active material. This layer also serves to smooth out the uneven surface of ITO.

b) Nanocrystalline TiO_2 (nc-TiO_2)

Nanocrystalline TiO_2 films were formed by the hydrolysis of titanium isopropoxide according to the literature [24, 60]. Thus, 0.5 mL of titanium isopropoxide (Aldrich, 99%) was slowly added with vigorous stirring to a mixture of 2.5 mL of glacial acetic acid (Sigma Aldrich), 7.5 mL of isopropanol (Sigma Aldrich) and 2.5 mL of deionized water under argon atmosphere. The solution was stirred for three days to obtain a viscous solution. The TiO_2 colloidal solution was applied on the surface of the ITO-glass and distributed with a glass rod sliding over an adhesive tape that covered the glass edges. The adhesive tape controlled the thickness of the TiO_2 film, which is in the range of few micrometers. A non-coated area (0.5 cm x 1.5 cm) was left for electrical contact. After drying in air, the TiO_2 was sintered at 450^oC for 30 minutes in a furnace (Carbolite, ELF 11/14B model, England) and then cooled slowly.

c) Electrochemical synthesis of semiconducting polymers

The electrochemical synthesis of poly[3-(2',5'-dioctyloxyphenyl)thiophene] (PDOOPT), poly[3-(2',5'-diheptyloxyphenyl)thiophene] (PDHOPT) and poly[3-(2',5'-dibutyloxyphenyl)thiophene] (PDBOPT) were carried out from their corresponding monomers using cyclic voltammetry on different substrates (ITO-glass, nc-TiO_2 coated ITO-glass and glassy carbon) in a three-electrode cell. The glassy carbon disk electrode (3 mm in diameter) was cleaned with Al_2O_3 powder (0.05 micron) prior to polymerization. The electrolyte solution contained 1.0 mM of the monomers in 0.1 M $LiClO_4/CH_3CN$ or 0.1 M $(C_2H_5)_4NBF_4/CH_3CN$ solutions. The solutions were purged with argon for 15 minutes and remained under argon through out the polymerization process. Ag/AgCl and Pt wire were used as quasi-reference electrode and counter electrode, respectively. The quasi-reference electrode was prepared by applying a voltage of 4.6 V from a dc source to an Ag wire dipped along with the counter platinum wire in a saturated aqueous solution of KCl. The cyclic voltammograms of the polymers were recorded in 0.1 M tetraethylammoniumtetrafluroborate (TEATFB)/CH_3CN solution. For solar cell applications, the polymers were dedoped to their neutral states at 0.4 V *vs.* Ag/AgCl quasi-

reference electrode in a monomer free electrolyte solution and then rinsed with acetonitrile and dried in air.

d) Electrochemical synthesis of poly[3,4-ethylenedioxythiophene] (PEDOT)

In all devices, oxidized poly(3,4-ethylenedioxythiophene) (PEDOT) that is electrochemically deposited on ITO-glass [61-63], is used as a counter electrode. It is prepared from a solution of 0.1 M 3,4-ethylenedioxythiophene, EDOT (Bayer), in acetonitrile that contained 0.1 M $LiClO_4/CH_3CN$ solution. The polymerization was carried out potentiostatically at 1.8 V (*vs.* Ag/AgCl quasi-reference electrode) for 2 seconds. The oxidized form of the polymer was rinsed with acetonitrile and dried in air. The film formed was semi-transparent. PEDOT improves the charge transfer between the ITO and the I_3^-/I^- redox couple [64,65]. It is chosen as a counter electrode, because it is less costly and can easily be prepared electrochemically to a desired transparency [65].

e) Electrolytes

In liquid-state photoelectrochemical cells, the electrolyte used is Iodolyte (Solaronix) that contains the I_3^-/I^- redox couple.

In solid-state photoelectrochemical cells, the electrolyte used is a polymer, amorphous poly(ethylene oxide), in the poly[oxymethylene-oligo(oxyethylene)] (POMOE) family, with a repeating unit of $CH_2O(CH_2CH_2O)_9$ complexed with I_3^-/I^-. It is known to have very good ionic conductivity at room temperature [66,67]. The I_3^-/I^- was prepared by dissolving 47.4 mg KI and 7.2 mg I_2 in 25 mL of methanol separately. Similarly, 304.2 mg of POMOE was dissolved in 25 mL of methanol. Finally, equal volumes of each solution were mixed to produce the polymer electrolyte complexed with I_3^-/I^-. The mole ratio of oxygen to potassium as calculated by taking into account both the oxymethylene and oxyethylene oxygen atoms was 25 and the mole ratio of KI to I_2 was 10:1.

6.3.2.2. The photoelectrochemical cell construction

The liquid-state photoelectrochemical cells consisted of the Iodolyte sandwiched between the photoactive electrodes and a PEDOT coated on ITO-glass counter electrode. The two electrodes were separated by a Teflon spacer to prevent shorting. The photoactive electrodes consisted of P3HT (Aldrich) and electropolymerized PDOOPT, PDHOPT and PDBOPT on either ITO-glass or on nc-TiO_2 coated ITO-glass. 1.25 mg of P3HT was dissolved in 1 mL of 1,2-dichlorobenzene (Aldrich). The solution was drop-casted on the nc-TiO_2-coated ITO-glass sheets and on ITO-glass sheets. After drying in air, the P3HT film at the edge was cleaned with 1,2-dichlorobenzene for an electrical contact area. The films were further dried in vacuum (LAB-LINE DUO-VAC OVEN, USA) for 24 hours. The devices were sealed with TG-50 sealant (Solaronix).

The solid-state photoelectrochemical cells consisted of the polymer electrolyte sandwiched between the photoactive electrodes and a PEDOT coated on ITO-glass counter electrode. The photoactive electrodes consisted of MEH-PPV (Aldrich) on nc-TiO_2 coated ITO-glass and a composite film of MEH-PPV and C_{60} or MEH-PPV alone on ITO-glass. To prepare a MEH-PPV/nc-TiO_2 composite film, 1.67 mg of MEH-PPV was dissolved in 1 mL of 1,2-dichlorobenzene (Aldrich, 99%). The MEH-PPV solution was drop-casted on the nc-TiO_2-coated ITO-glass. Similarly, a MEH-PPV film and a MEH-PPV/C_{60} composite films were formed on ITO-glass by drop casting solutions of 2.5 mg of MEH-PPV and a mixture containing 2.5 mg of MEH-PPV and 2.5 mg of C_{60}, respectively, each dissolved in 1 mL 1,2-dichlorobenzene. The films were then dried in air at room temperature. The slow evaporation of the solvent at room temperature resulted in the formation of uniform films of MEH-PPV. After drying in air, the polymer films at the edges were cleaned with 1,2-dichlorobenzene for an electrical contact. The films were further dried in vacuum for 24 hours. The polymer electrolyte (POMOE) complexed with I_3^-/I^- redox couple was then drop-casted on the top of the photoactive films from methanol solution and dried in air. Contact between the electrodes was ensured by the application of pressure using a spring attached to a sample holder.

All the devices were then mounted in a sample holder inside a metal box having a 1 cm x 1 cm light entrance window, which determined the illumination area. The schematic layout of the photoelectrochemical cells used and the chemical structure of PEDOT, the polymer used as a counter electrode on ITO-glass, are depicted in Figure 6.9.

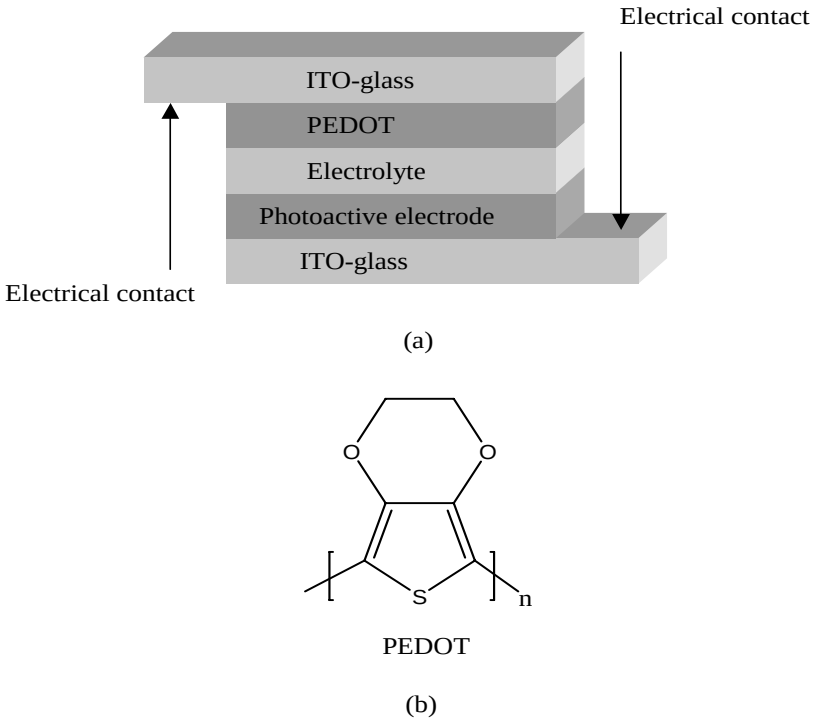

Figure 6.9. Schematic layout of the (a) photoelectrochemical cells used and (b) chemical structure of the counter electrode, PEDOT.

6.3.2.3. Experimental setup

A 250 W tungsten-halogen lamp regulated by an Oriel power supply (Model 66182) was used to illuminate the PEC. The white light intensity was measured in the position of the sample cell with a Conrad electronic luxmeter (Model LX-101). For intensity dependence measurements a series of neutral density filters were placed between the light source and the sample holder to vary the light intensity incident on the sample. A grating monochromator (Model 77250) was used to select a wavelength manually between 300 nm and 800 nm at an

interval of 10 nm. The steady-state currents were recorded after illuminating the devices for 60 seconds at each selected wavelength. All spectra were corrected for the spectral response of the lamp and the monochromator by normalization to the response of a calibrated silicon photodiode (Hamamatsu, model S-1336-8BK). The photoelectrochemical properties were studied using CHI600A Electrochemical Analyzer (IJ Cambria). Optical absorption measurements were carried out using a Lambda 19 UV/VIS/NIR spectrometer (Perkin-Elmer). A schematic of the experimental set-up used to measure the photoelectrochemical properties of the device is shown in Figure 6.10.

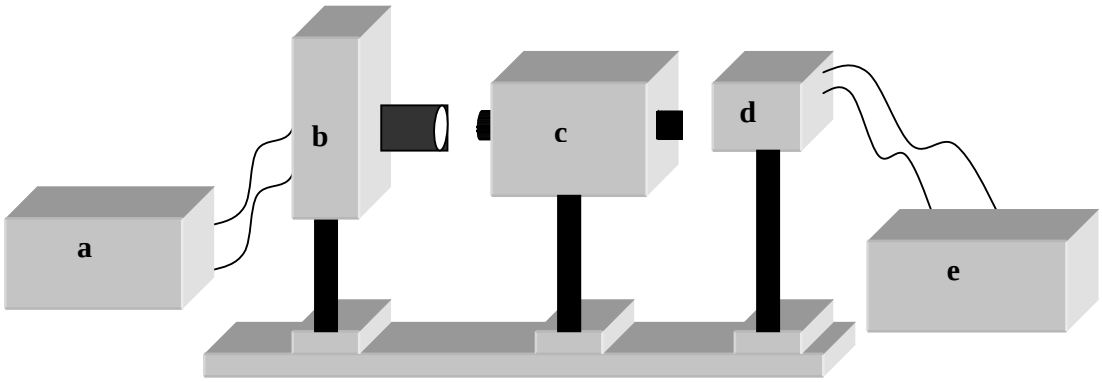

Figure 6.10. General experimental set-up for the photoelectrochemical measurements.
a) Power supply, b) Lamp housing, c) Monochromator, d) Sample holder, and e) Input/output measuring apparatus.

6.3.3. Results and discussion

6.3.3.1. A Comparative Study on Liquid-State Photoelectrochemical Cells Based on Poly(3-Hexylthiophene) and a Composite Film of Poly(3-Hexylthiophene) and Nanocrystalline Titanium Dioxide

The chemical structure of poly(3-hexylthiophene), P3HT, is depicted in Figure 6.11.

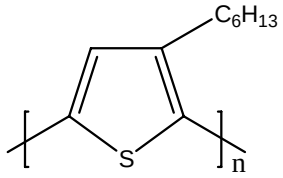

Figure 6.11. The chemical structure of P3HT.

a) Current-voltage characteristics

Figure 6.12 and Figure 6.13 show the current-voltage curves of P3HT and P3HT/nc-TiO_2, based PECs, respectively. The photoelectrochemical characteristics of the devices are compared in Table 6.1.

Illumination of P3HT based device produced a cathodic current under short-circuit condition. This indicates that electrons are transferred from the LUMO of P3HT (E_{LUMO} = –3.5 eV [42]) to the I_3^-/I^- redox mediator whose redox potential is around -4.9 eV [2]. Hence, P3HT exhibited its p-type behavior. On the other hand, illumination of nc-TiO_2/P3HT based devices produced an anodic current under short-circuit condition, indicating the transfer of electrons from the LUMO of P3HT to the conduction band edge ($E_{CB\ (nc\text{-}TiO2)}$ = -4.2 eV [68]) of nc-TiO_2. Hence P3HT played the role of a sensitizer in nc-TiO_2/P3HT based PECs. From Table 6.1, it can be seen that the devices containing nc-TiO_2/P3HT photoactive electrode exhibit higher V_{OC}, I_{SC}, FF and η when compared with

devices containing P3HT photoactive electrode. This is, most likely, due to a better charge separation and ease of charge transport through the nc-TiO_2 structure.

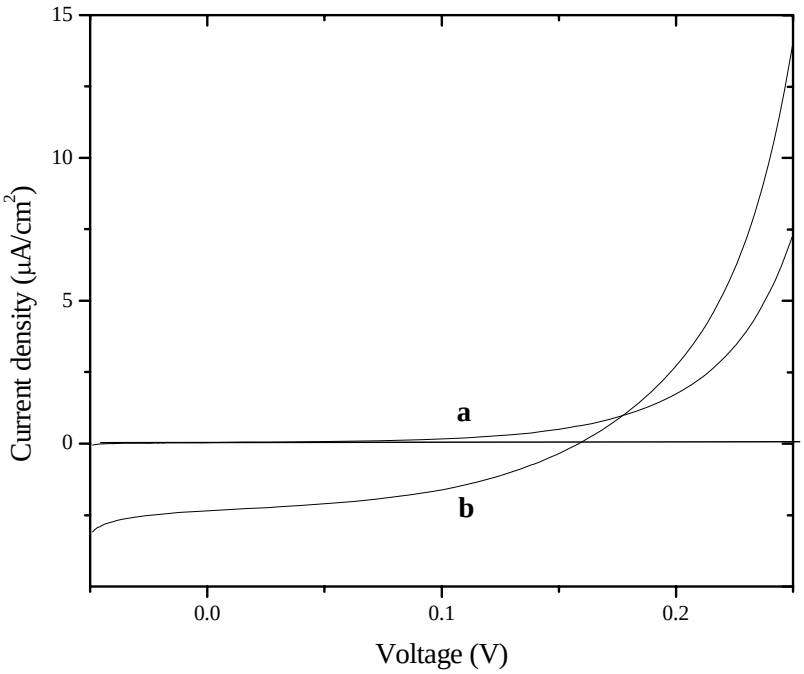

Figure 6.12. Current density *vs*. voltage characteristics of the P3HT based liquid-state PEC. **a)** In the dark, **b)** Under white light illumination from the ITO/PEDOT side (front side) with light intensity of 100 mW/cm^2.

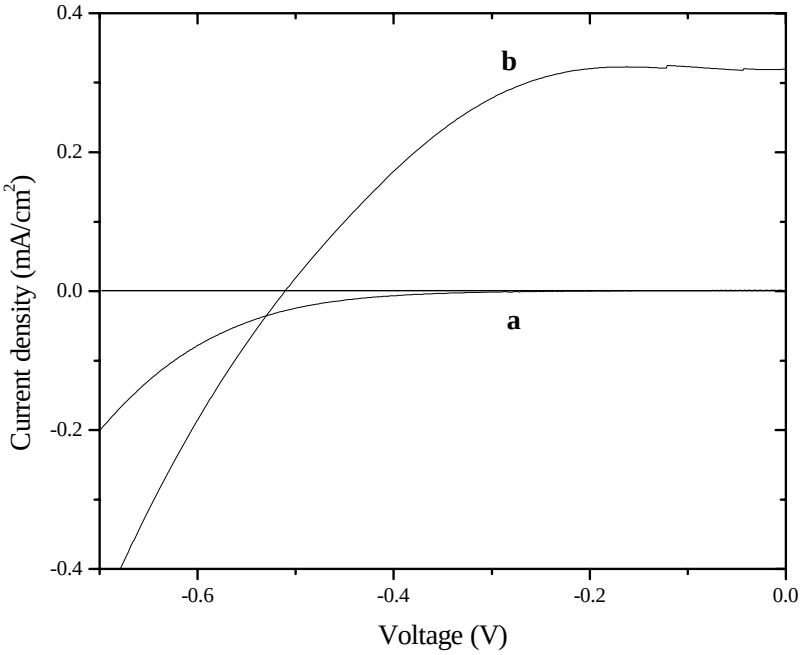

Figure 6.13. Current density *vs.* voltage characteristics of the nc-TiO_2/P3HT based liquid-state PEC. a) In the dark, b) Under white light illumination from the ITO/nc-TiO_2/P3HT side (backside) with light intensity of 100 mW/cm^2.

Table 6.1: The performance of photoelectrochemical devices containing P3HT and nc-TiO_2/P3HT photoactive electrodes when illuminated with light intensity of 100 mW/cm^2.

Photoactive electrode	V_{OC} (mV)	I_{SC} (μA/cm^2)	*FF*	η (%)
P3HT	160	2.4	0.42	1.6x10^{-4}
Nc-TiO_2/P3HT	-510	320	0.51	0.1

b) Spectral response

Figure 6.14 and Figure 6.15 show *IPCE%* of P3HT and nc-TiO_2/P3HT based PECs, respectively.

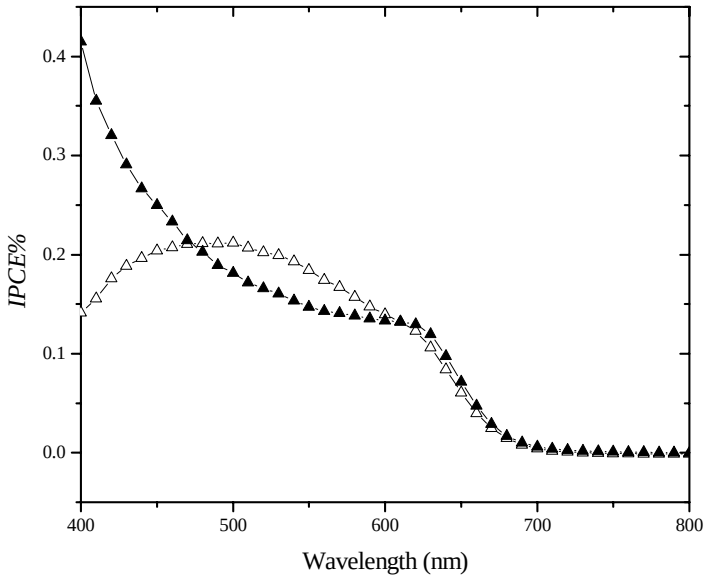

Figure 6.14. Short-circuit photocurrent action spectra of P3HT based liquid-state PEC under illumination from the front side (open triangles) and from the backside (closed triangles).

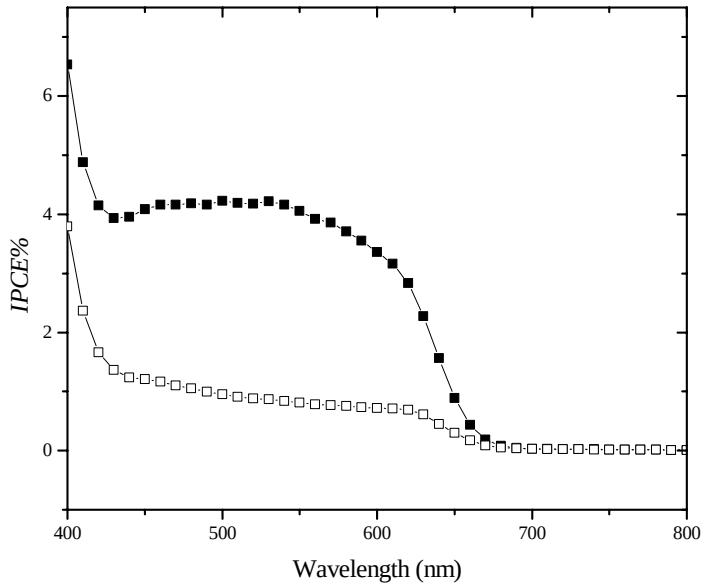

Figure 6.15. Short-circuit photocurrent action spectra of nc-TiO_2/P3HT based liquid-state PEC under illumination from the front side (open squares) and from the backside (closed squares).

The *IPCE*% obtained for the P3HT based PEC were 0.18% for front side and 0.15% for backside illumination at the maximum absorbance (550 nm). For nc-TiO_2/P3HT based device, due to better charge separation and charge transport, the *IPCE%* obtained at maximum absorbance were higher, 0.8% for front side and 4% for backside illuminations.

Comparison of the optical absorption spectrum and the spectral photoresponse can be used to identify the active junction responsible for the photoelectrochemical phenomena. If illumination through the front side of the PEC produces a spectral response that corresponds to the absorption spectrum of the conjugated polymer, then the conjugated polymer/electrolyte junction is responsible; if illumination from the backside produces a matching spectrum, then it is the conjugated polymer/ITO junction (in P3HT based devices) and the nc-TiO_2/ITO junction (in nc-TiO_2/P3HT based devices) that are active. The normalized absorption spectra of P3HT and the normalized photocurrent action spectra of front sides and backsides of P3HT based and nc-TiO_2/P3HT based devices are depicted in Figure 6.16.

The absorption spectrum of P3HT more or less matches the action spectra for the front side and for the backside illuminations of P3HT based and nc-TiO_2/P3HT based devices, respectively. Therefore, it can be concluded that the junctions responsible for the photocurrents observed in P3HT based and nc-TiO_2/P3HT based devices were the P3HT/electrolyte and the nc-TiO_2/ITO interfaces, respectively.

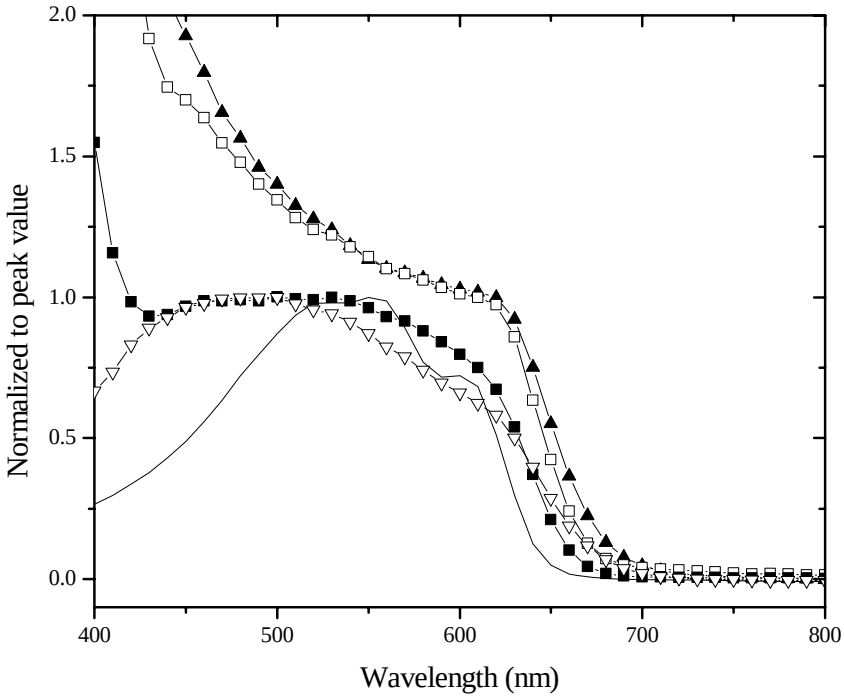

Figure 6.16. Normalized optical absorption spectrum of P3HT (solid line) film on ITO-glass and normalized photocurrent action spectra of P3HT based (triangles) and nc-TiO_2/P3HT based (squares) devices for front side (open symbols) and backside (closed symbols) illuminations.

c) Dependence of *Voc* and *Isc* on incident light intensity

The dependence of V_{OC} and I_{SC} on incident light intensity for P3HT and nc-TiO_2/P3HT based devices are shown in Figure 6.17 and Figure 6.18, respectively. From the figures it can be observed that in devices that contain nc-TiO_2/P3HT photoactive electrode, the V_{OC} and the I_{SC} increase more rapidly (greater slope) with increasing light intensity indicating better charge separation and collection.

For organic and inorganic solar cells, the short-circuit current density increases with incident light intensity and is proportional to I_{in}^{α} [69], where α is characteristic for the system studied. In Figure 6.18, the photocurrent increases less rapidly than the first power

(an ideal value) of the light intensity for both P3HT based (α = 0.74) and nc-TO_2/P3HT based (α = 0.85) devices. Such sub-linear dependence implies bimolecular recombination of excitons [70,71] and/or the presence of structural disorders and traps in the films that promote charge recombination [70,72].

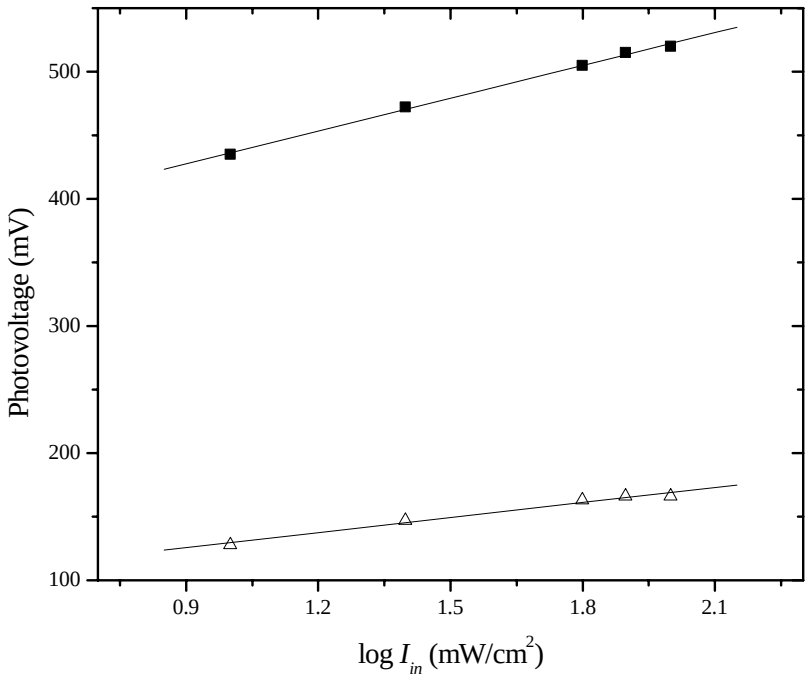

Figure 6.17. Plot of V_{OC} *vs.* log I_{in} of P3HT based (open triangles) and nc-TiO_2/P3HT based (closed squares) liquid-state PECs.

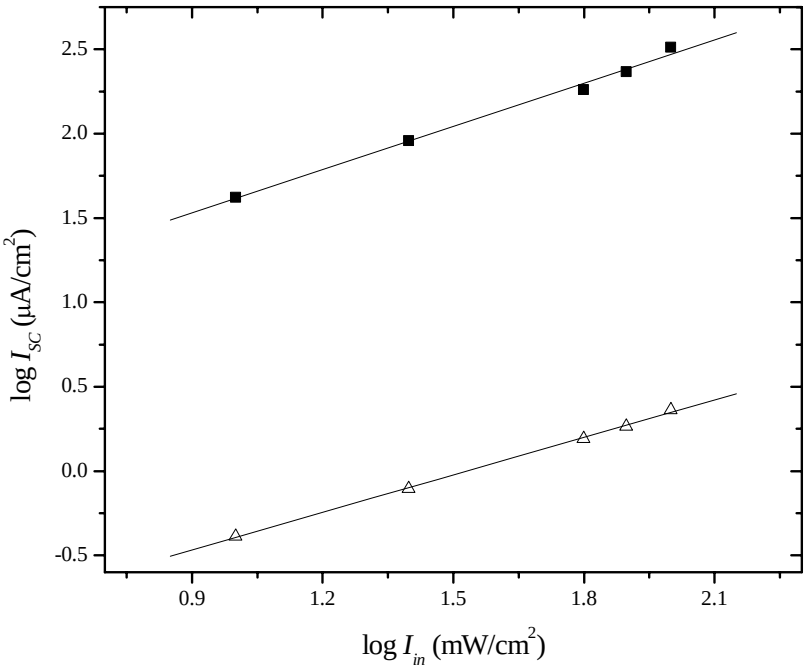

Figure 6.18. Plot of log I_{SC} *vs.* log I_{in} of P3HT based (open triangles) and nc-TiO_2/P3HT based (closed squares) liquid-state PECs.

d) Conclusions

Liquid-state photoelectrochemical cells based on P3HT and a composite film of nc-TiO_2/P3HT photoactive electrodes were constructed and studied for their photoresponse behavior. Devices where the photoactive electrode consists of nc-TiO_2/P3HT composite film showed improved cell performance over those that consist of P3HT alone. Nc-TiO_2/P3HT based devices exhibited a V_{OC} of -0.51 V, an I_{SC} of 0.32 mA/cm^2 and a *FF* of 0.51 when illuminated with light intensity of 100 mW/cm^2. It has been observed that in devices that contain nc-TiO_2/P3HT photoactive electrode, the V_{OC} and the I_{SC} increase more rapidly with increasing light intensity indicating better charge separation and collection.

6.3.3.2. Synthesis and Characterization of Poly[3-(2',5'-Diheptyloxyphenyl)Thiophene] for use in Photoelectrochemical Cells

The chemical structure of poly[3-(2',5'-diheptyloxyphenyl)thiophene] (PDHOPT) is shown in Figure 6.19.

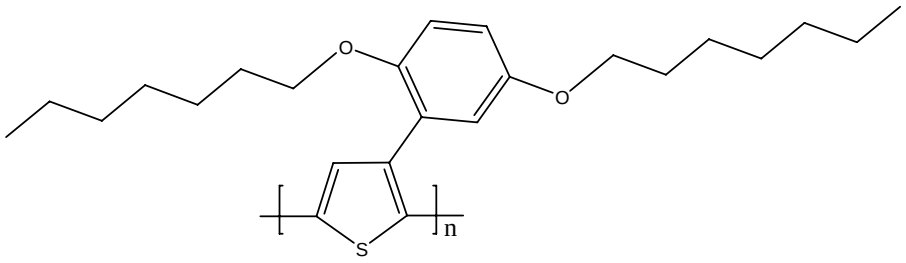

Figure 6.19. The chemical structure of poly[3-(2',5'-diheptyloxyphenyl)thiophene].

a) Electrochemical synthesis and characterization of poly[3-(2',5'-diheptyloxyphenyl) thiophene]

Figure 6.20 shows the cyclic voltammogram for the electrochemical polymerization of DHOPT on glassy carbon disk electrode. Oxidation of the monomer starts around 0.93 V with peak potential at 1.09 V. The oxidation of the monomer increases from cycle to cycle, giving more of its polymer film that gives peaks for p-doping (oxidation) and dedoping at 0.86 V. Upon continued cycles, the peak potentials shift slightly towards positive and negative directions, respectively, indicating a slightly slower kinetics for the electron transfer reactions with the deposition of more of the polymer. The polymerization on nc-TiO_2 coated ITO-glass takes place on the surface of the ITO and the film grows within the pores of the nc-TiO_2 film. The color of the polymer film changes between blue in its oxidized state and yellow in its neutral state. The polymer adheres strongly on nc-TiO_2 coated ITO-glass and on glassy carbon, but slightly less on ITO-glass.

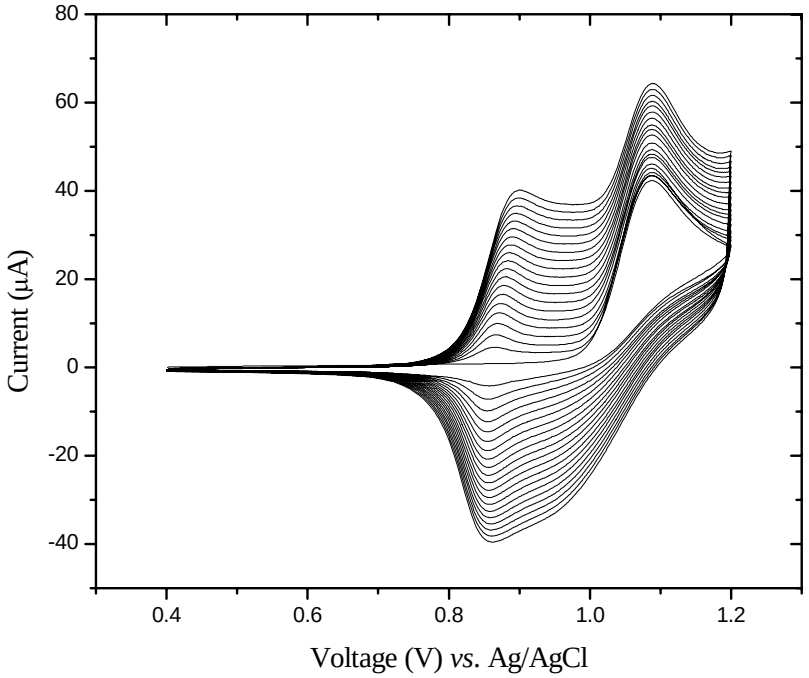

Figure 6.20. Cyclic voltammogram recorded for the electropolymerization of 1 mM DHOPT on glassy carbon disk electrode in CH_3CN solution containing 0.1 M of $LiClO_4$. The potential is scanned repetitively between 0.4 V and 1.2 V at a scan rate of 10 mV/s.

Figure 6.21 shows the cyclic voltammogram of PDHOPT in a monomer free electrolyte solution that contains 0.1 M tetraethylammoniumtetrafluroborate (TEATFB) in acetonitrile. The onset potential for the oxidation of PDHOPT is 0.86 V *vs.* Ag/AgCl. The HOMO level of the polymer is determined using the empirical equation proposed by Bredas *et al.* [73] by adding a value of 4.4 to the onset of oxidation measured against the Ag/AgCl reference electrode [41] which is found to be - (0.86 + 4.4) ≈ -5.3 eV. The optical band gap of the neutral polymer as determined from the onset of the UV-Vis absorption peak (580 nm) is 2.1 eV (Figure 6.22). Thus, The LUMO level of the polymer is estimated by subtracting the optical band gap from the HOMO level and is found to be -3.2 eV. These energy positions can allow the transfer of electrons from the excited state of the polymer to the conduction band edge of TiO_2 ($E_{CB\ (TiO2)}$ = -4.2 eV [68] and the transfer of holes from the HOMO of the polymer to I_3^-/I^- redox mediator whose redox potential is around -4.9 eV [2].

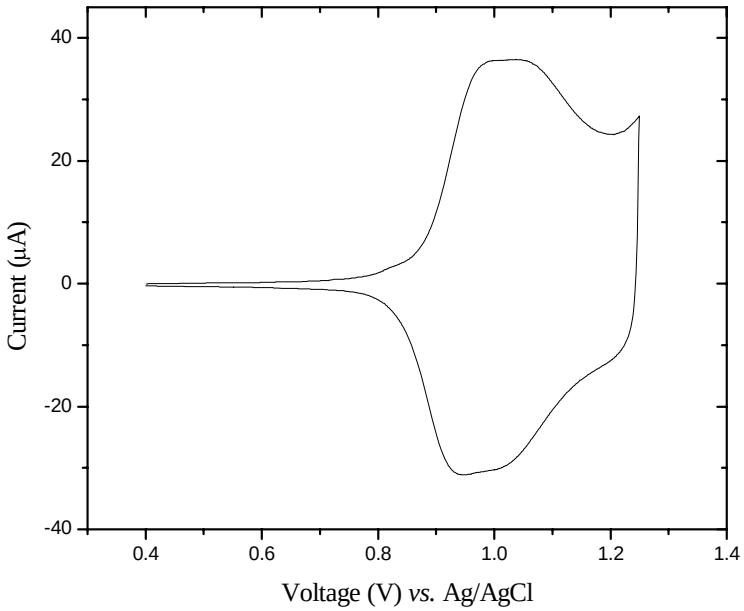

Figure 6.21. Cyclic voltammogram of PDHOPT on glassy carbon disk electrode recorded in a 0.1 M TEATFB/CH_3CN solution at a scan rate of 10 mV/s.

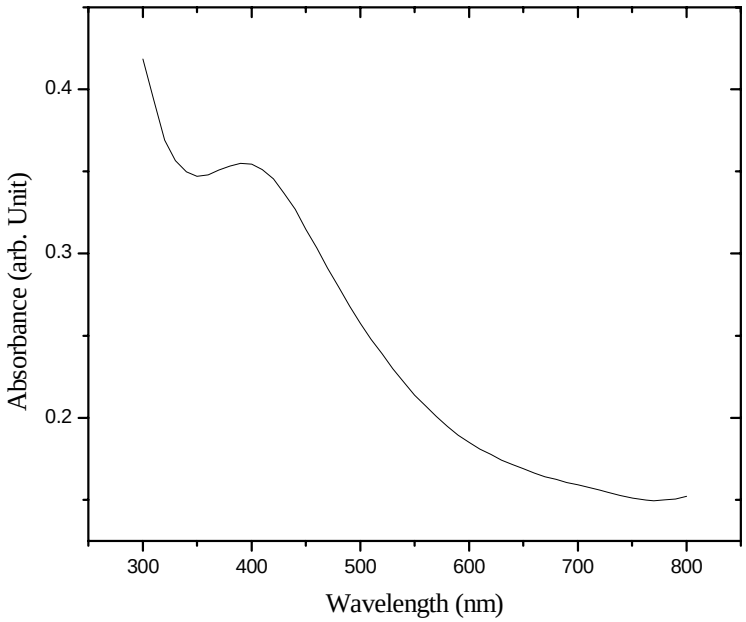

Figure 6.22. UV-Vis absorption spectra of the undoped PDHOPT film on ITO-glass.

b) The photoresponse behaviors of the photoelectrochemical cells

i) Current-voltage characteristics

Figure 6.23 and Figure 6.24 show the current voltage curves of the photoelectrochemical devices, both in the dark and under white light illumination where the photoactive electrode consists of a film of PDHOPT and a composite film of PDHOPT/TiO_2, respectively. The photoelectrochemical characteristics of the devices are compared in Table 6.2. Illumination of both devices produced anodic photocurrents due to photogenerated charge carriers. Devices containing TiO_2/PDHOPT photoactive electrode exhibit higher $V_{OC,}$ I_{SC} and *FF* when compared with devices containing PDHOPT only. Though the power conversion efficiencies of both types of devices are low, devices made from TiO_2/PDHOPT show improved performance by 3 orders of magnitude.

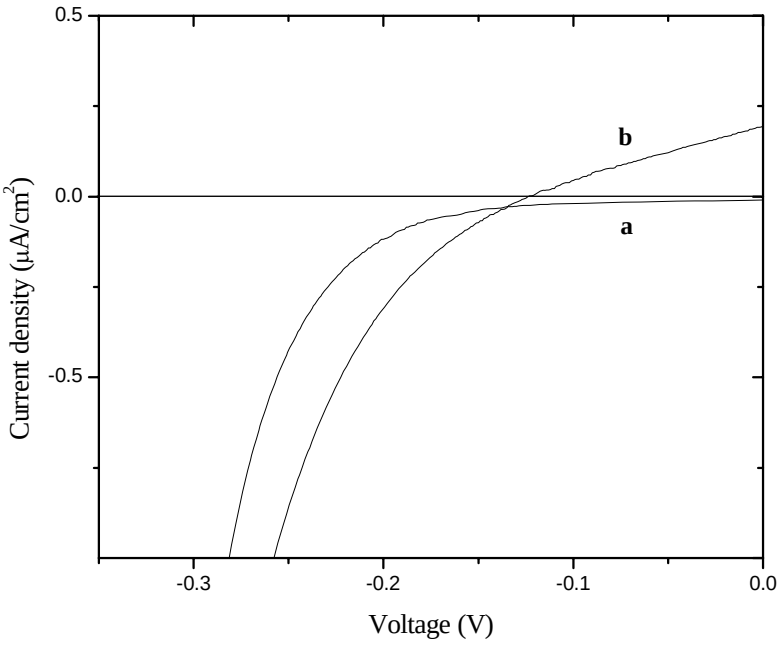

Figure 6.23. Current density *vs*. voltage characteristics of the PDHOPT based liquid-state PEC. a) In the dark, b) Under white light illumination from the ITO/PDHOPT side (backside) with light intensity of 80 mW/cm^2.

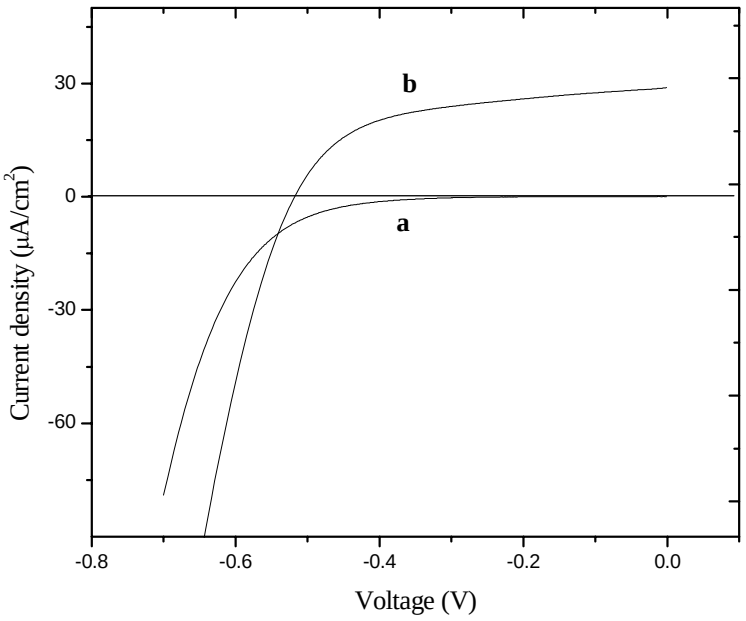

Figure 6.24. Current density *vs.* voltage characteristics of the nc-TiO_2/PDHOPT based liquid-state PEC. a) In the dark, b) Under white light illumination from the ITO/TiO_2/PDHOPT side (backside) with light intensity of 80 mW/cm^2.

Table 6.2: The performance of photoelectrochemical devices containing PDHOPT and nc-TiO_2/PDHOPT as photoactive electrodes when illuminated with light intensity of 80 mW/cm^2.

Photoactive electrode	V_{OC} (mV)	I_{SC} (μA/cm^2)	*FF*	η (%) (x10^{-5})
PDHOPT	-125	0.2	0.27	0.84
Nc-TiO_2/PDHOPT	-520	29	0.54	1018

ii) Spectral response

Figure 6.25 and Figure 6.26 show the incident photon-to-current conversion efficiencies (*IPCE*) of PDHOPT and nc-TiO_2/PDHOPT based devices, respectively. When compared with PDHOPT based devices, the nc-TiO_2/PDHOPT based devices have higher *IPCE%* values at each wavelength.

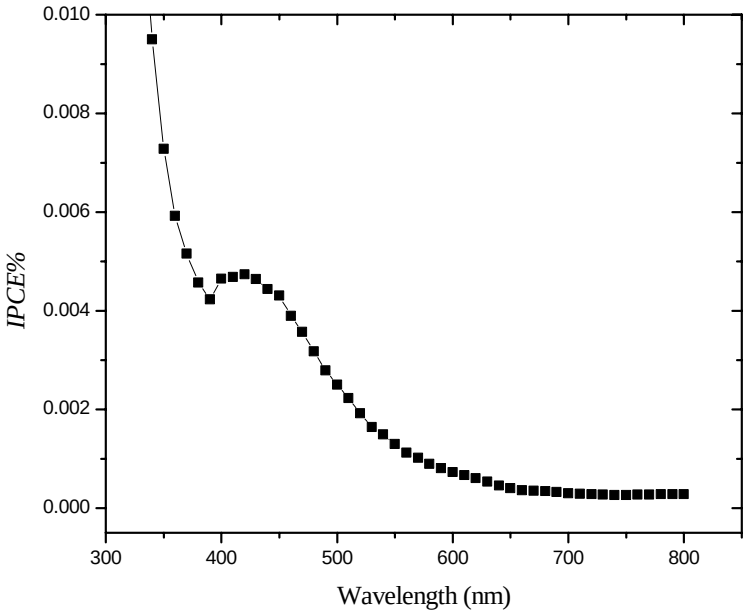

Figure 6.25. Short-circuit photocurrent action spectrum of PDHOPT based liquid-state PEC under illumination from the front side.

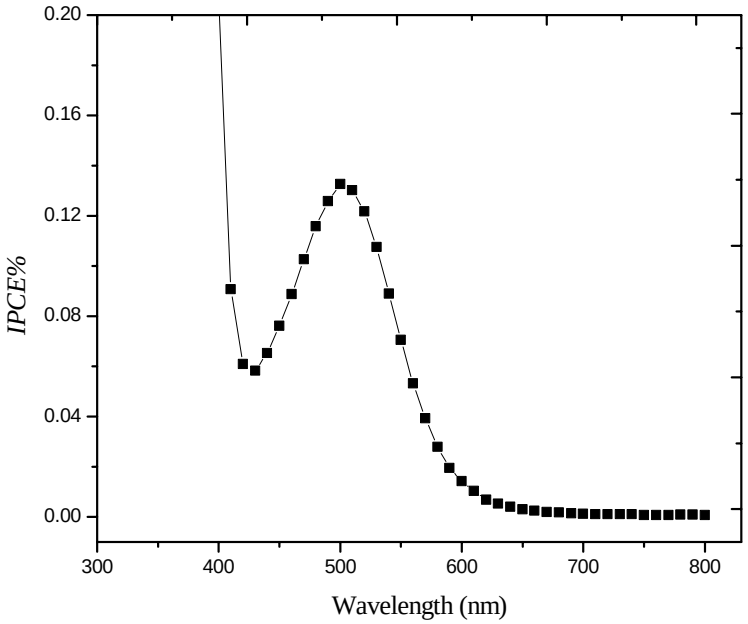

Figure 6.26. Short-circuit photocurrent action spectrum of nc-TiO_2/PDHOPT based liquid-state PEC under illumination from the front side.

The normalized photocurrent action spectra of PDHOPT and nc-TiO_2/ PDHOPT based devices along with the normalized absorption spectrum of PDHOPT are depicted in Figure 6.27. From the figure it can be observed that both types of devices follow similar pattern with the absorption spectrum of PDHOPT, PDHOPT based devices being more similar.

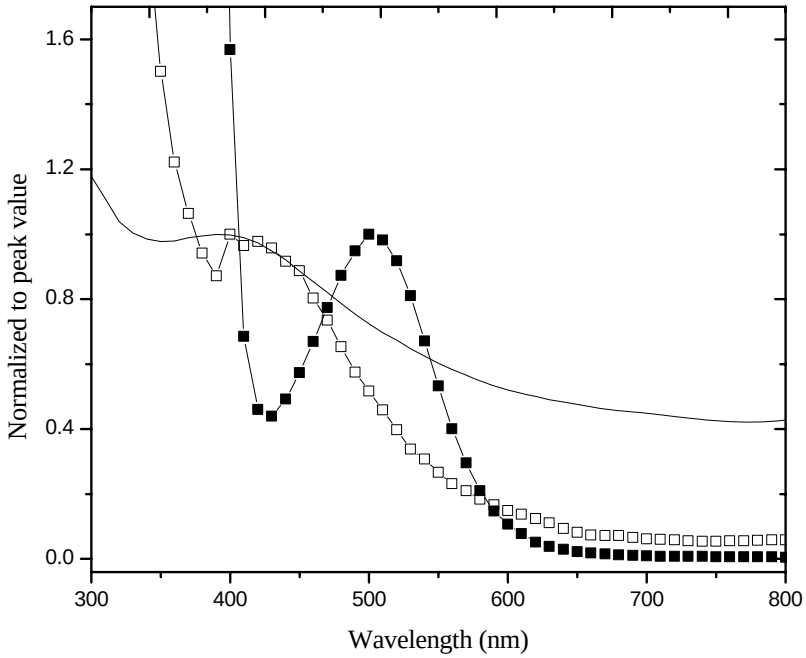

Figure 6.27. Normalized optical absorption spectrum of PDHOPT (solid line) and normalized photocurrent action spectrum of PDHOPT based (open squares) and nc-TiO_2/PDHOPT based (closed squares) devices for front side illuminations.

iii) Dependence of *Voc* and *Isc* on incident light intensity

The dependencies of V_{OC} and I_{SC} on incident light intensity for PDHOPT and nc-TiO_2/PDHOPT based devices are shown in Figures 6.28 and 6.29, respectively. From the figures it can be observed that the V_{OC} and the I_{SC} are more dependent on light intensity in devices that contain nc-TiO_2/PDHOPT photoactive electrode indicating better charge separation in the devices.

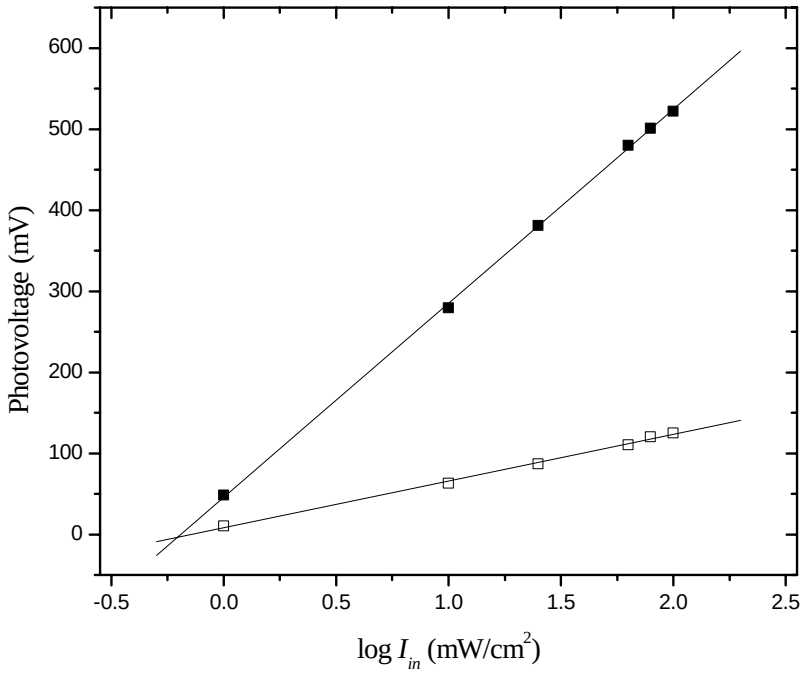

Figure 6.28. Plot of V_{OC} *vs.* log I_{in} of PDHOPT based (open squares) and nc-TiO_2/PDHOPT based (closed squares) liquid-state PECs.

In Figure 6.29, the photocurrent for both PDHOPT based and nc-TiO_2/PDHOPT based devices increases with increasing light intensity. The photocurrent for PDHOPT based devices increases less rapidly than the first power (an ideal value) of the light intensity (slope = 0.86), indicating the presence of bimolecular exciton recombination due to surface states that act as recombination centers. For TiO_2/PDHOPT based device, the photocurrent increases more rapidly than the first power of the light intensity (slope = 1.3), indicating an increase in the lifetime of the free charge carriers with their increasing density [74].

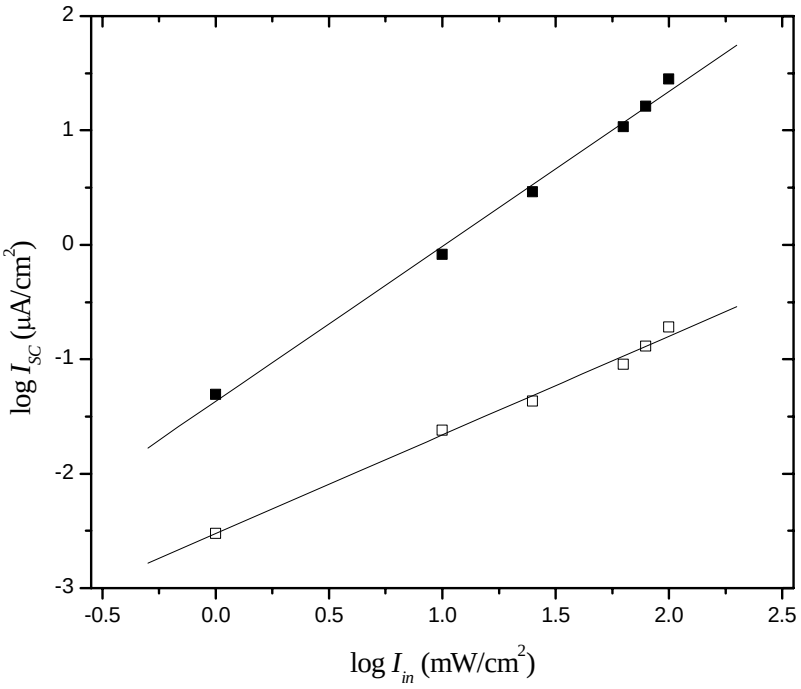

Figure 6.29. Plot of log I_{SC} *vs.* log I_{in} of PDHOPT based (open squares) and nc-TiO_2/ PDHOPT based (closed squares) liquid-state PECs.

c) Conclusions

Poly[3-(2',5'-diheptyloxyphenyl)thiophene], PDHOPT, has been prepared electro-chemically from its monomer for solar cell application. The estimated energy levels of the highest occupied molecular orbital and the lowest unoccupied molecular orbital of PDHOPT are -5.3 eV and -3.2 eV, respectively. PDHOPT sensitizes nanocrystalline titanium dioxide in liquid-state photoelectrochemical cells. Devices where the photoactive electrode consists of nc-TiO_2/PDHOPT composite film showed improved cell performance over those that consist of PDHOPT alone. It has been observed that the V_{OC} and the I_{SC} are more dependent on light intensity in devices that contain nc-TiO_2/PDHOPT photoactive electrode indicating better charge separation in the devices with increasing light intensities.

6.3.3.3. Effect of Side Chain Length on the Electrochemical and Photoresponse Characteristics of Poly[3-(2',5'-dialkoxyphenyl)thiophenes]

The structures of poly[3-(2',5'-dioctyloxyphenyl)thiophene] (PDOOPT) and poly[3-(2',5'-dibutyloxyphenyl)thiophene] (PDBOPT) are depicted in Figure 6.30. The structure PDHOPT has been shown in Figure 6.19.

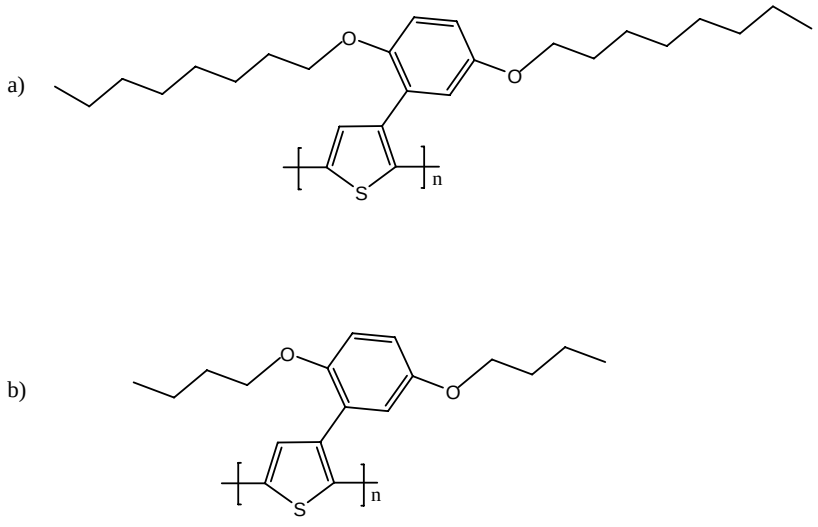

Figure 6.30. The chemical structures of: a) PDOOPT and b) PDBOPT.

a) Electrochemical synthesis and characterization of poly[3-(2',5'-dioctyloxyphenyl)thiophene], poly[3-(2',5'-diheptyloxyphenyl)thiophene] and poly[3-(2',5'-dibutyloxyphenyl)thiophene]

Figure 6.31 (a-c) shows the cyclic voltammograms for the electrochemical polymerization of DOOPT, DHOPT and DBOPT, respectively, on glassy carbon disk electrodes for the first 10 cycles. Oxidation of DOOPT, DHOPT and DBOPT starts around 1.04 V, 1.02 V and 1.00 V *vs*. Ag/AgCl with peak potentials at 1.16 V, 1.14 V and 1.11 V, respectively. The oxidation of the monomers continue from cycle to cycle, giving more of the polymer films that give peaks for p-doping (oxidation) and dedoping reactions which are reversible.

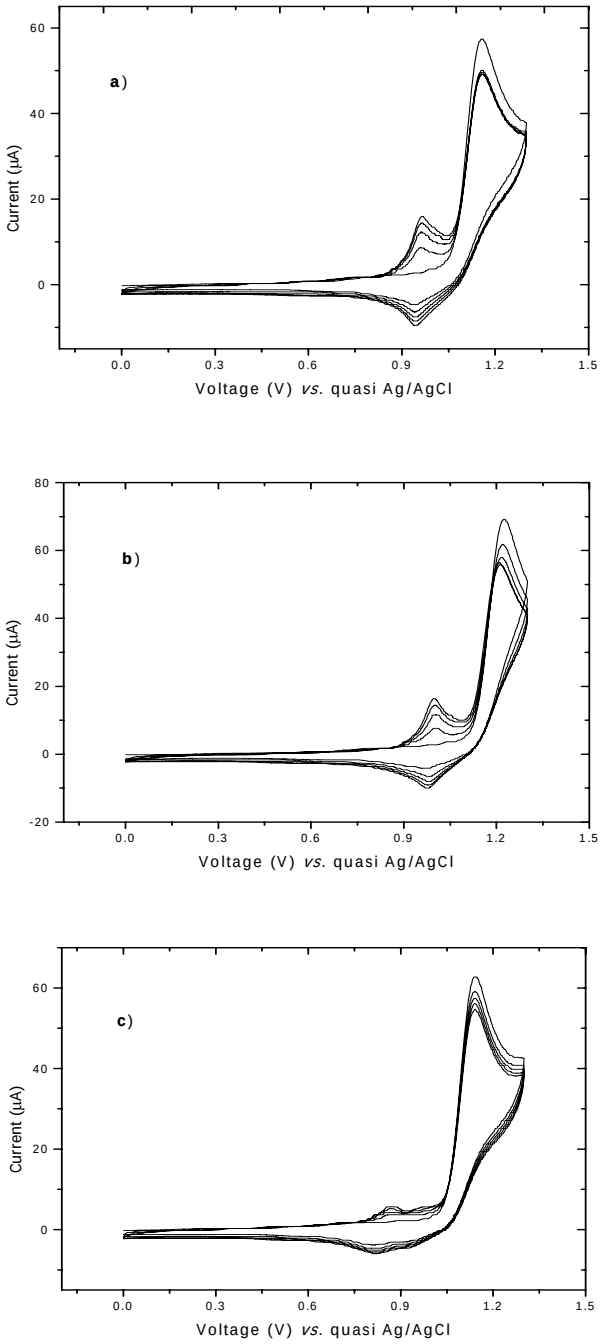

Figure 6.31. Cyclic voltammograms for the electropolymerization of: (**a**) DOOPT, (**b**) DHOPT and (**c**) DBOPT on glassy carbon disk electrode in CH_3CN solution containing 1.0 mM of the monomers and 0.1 M of TEATFB recorded at a scan rate of 10 mV/s.

The cyclic voltammograms for the electrochemical polymerization of the three monomers on glassy carbon are very much similar to the electropolymerization on ITO-glass and on nc-TiO_2 coated ITO-glass. The polymerization on nc-TiO_2 coated ITO-glass takes place on the ITO-glass and the film grows within the pores of nc-TiO_2 film. This results with the formation of uniform thick films. PDOOPT and PDHOPT adhere strongly on nc-TiO_2 coated ITO-glass and on glassy carbon, but slightly less on ITO-glass. PDBOPT, on the other hand, adheres more strongly on nc-TiO_2 coated ITO-glass than the other polymers producing a much better film on the nc-TiO_2 surface. It however adheres slightly on glassy carbon and poorly on ITO-glass where much of the film detaches easily. The detachment from the electrodes may be due to the high stability of the reacted species generated upon monomer oxidation, which diffuse away from the electrodes to form oligomers in solution [75]. The nc-TiO_2 film has been found to be a good matrix for the growth of PDBOPT film on ITO-glass. The strength of adherence to the bare electrodes, as observed during the growth of the polymers, follows the order: PDBOPT < PDHOPT < PDOOPT. The color of all the polymer films changes between blue in their oxidized states and yellow in their neutral states.

Figure 6.32 shows the cyclic voltammograms of PDOOPT, PDHOPT and PDBOPT in a monomer free electrolyte solution that contains 0.1 M tetraethylammoniumtetrafluroborate in acetonitrile.

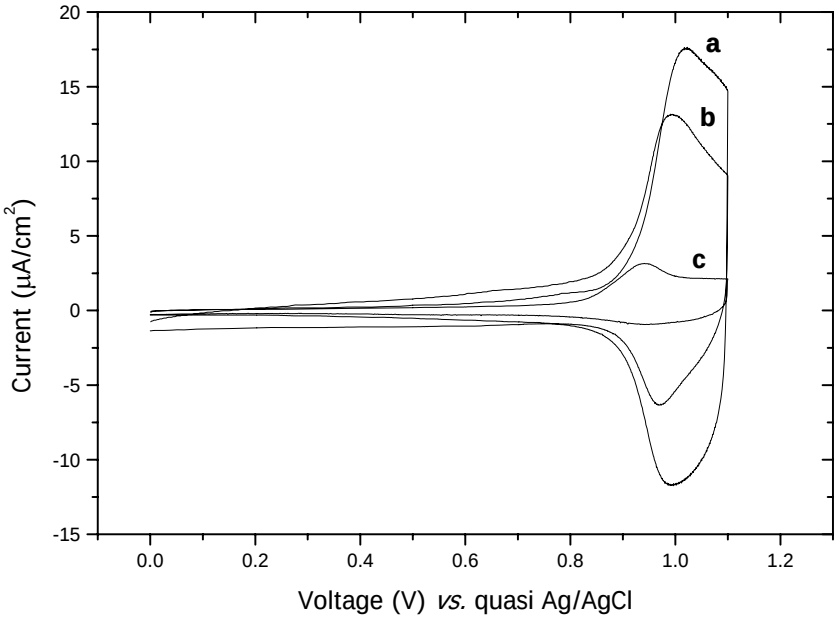

Figure 6.32. Cyclic voltammogram of: (**a**) PDOOPT, (**b**) PDHOPT and (**c**) PDBOPT on glassy carbon disk electrode recorded in a 0.1 M TEATFB/CH_3CN solution at a scan rate of 10 mV/s.

The onset potentials for the oxidation of PDOOPT, PDHOPT and PDBOPT are 0.89 V, 0.86 V and 0.79 V *vs.* Ag/AgCl while the peak potentials are 1.0 V, 0.97 V and 0.92 V, respectively. The quasi Ag/AgCl electrode has been calibrated with standard Ag/AgCl reference electrode by ferrocene in 0.1 M TEATFB/CH_3CN solution. The oxidation potential is thus observed to be directly related to the chain length. This is due to the fact that the density of π-electrons and charges is increasing as the length of the side chain decreases, caused by better π-stacking and improved inter-chain coupling [76], which enhances the donor character and favors oxidation [77].

Figure 6.33 shows the absorption spectra (normalized at 400 nm) of PDOOPT, PDHOPT and PDBOPT films grown on ITO-glass. The estimated optical band gaps of the neutral polymers, as determined from the onset of the UV-Vis absorption peaks, are 2.07 eV, 2.10 eV and 2.14 eV, respectively. These absorption onset values correlating with the energy of π - π* inter-band transition indicate a slightly better planarity of the backbone chains for

PDOOPT than for PDBOPT. This is due to the fact that longer side groups restrict the number of possible conformations [77].

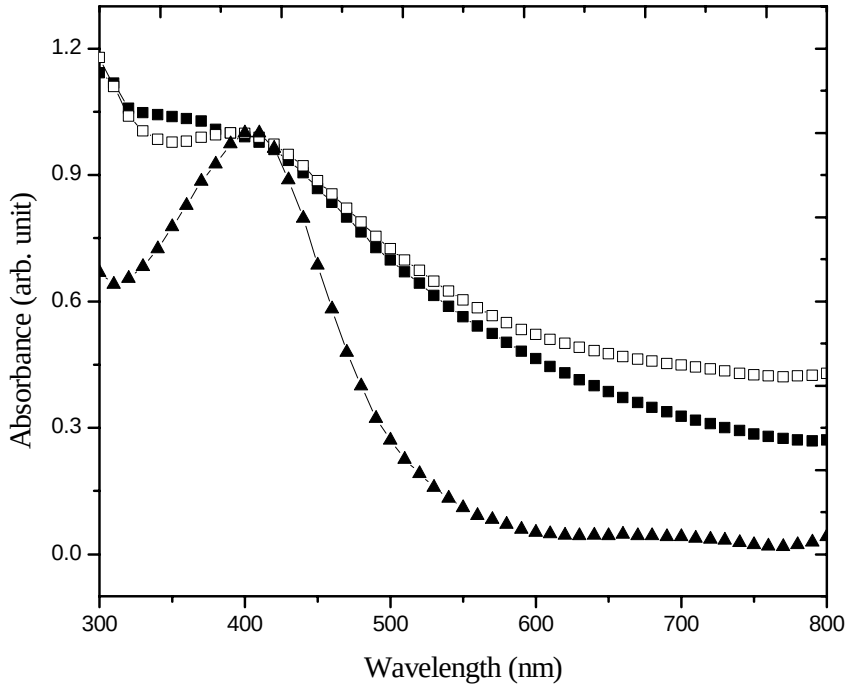

Figure 6.33. UV-Vis Absorption spectra (normalized at 400 nm) of PDOOPT (closed squares), PDHOPT (open squares) and PDBOPT (closed triangles) films electrochemically coated on ITO-glass.

The HOMO level of semiconducting polymers films is determined using the empirical equation proposed by Bredas *et al.* [73] by adding a value of 4.4 to the onset of oxidation measured against the Ag/AgCl reference electrode [41]. Accordingly, the estimated HOMO levels of PDOOPT, PDHOPT and PDBOPT are found to be -5.29 eV, -5.26 eV and -5.19 eV, respectively. The LUMO levels of the polymers are estimated by subtracting the optical band gaps from the HOMO levels and are found to be -3.22 eV, -3.16 eV and -3.05 eV, respectively. These energy positions can allow the transfer of electrons from the excited state of the polymer to the conduction band edge of TiO_2 ($E_{CB\ (TiO2)}$ = -4.2 eV [68] and the transfer of holes from the HOMO of the polymer to I_3^-/I^- redox mediator whose redox

potential is around -4.9 eV [2]. Table 6.3 summarizes the electrochemical and spectroscopic data of the polymers investigated in this study.

Table 6.3. Cyclic voltammetry data, estimated HOMO-LUMO energy levels and optical band gaps (E_g^{opt}) of PDOOPT, PDHOPT and PDBOPT films.

Photoactive electrode	E^{ox}_{onset} *vs.* Ag/AgCl (V)	HOMO (eV)	E_g^{opt} (eV)	LUMO (eV)
PDOOPT	0.89	-5.29	2.07	-3.22
PDHOPT	0.86	-5.26	2.10	-3.16
PDBOPT	0.79	-5.19	2.14	-3.05

b) The photoresponse behaviors of the photoelectrochemical cells

i) Current-voltage characteristics

Figure 6.34 and Figure 6.35 show the current-voltage curves of the photoelectrochemical devices in the dark and under white light illumination at 80 mW/cm^2 light intensity, respectively, where the photoactive electrodes consist of composite films of PDBOPT/nc-TiO_2, PDHOPT/nc-TiO_2 and PDOOPT/nc-TiO_2. The photoelectrochemical characteristics of the devices are summarized in Table 6.4. In Figure 6.34 and Figure 6.35, the forward voltage corresponds to the PEDOT electrode being positive.

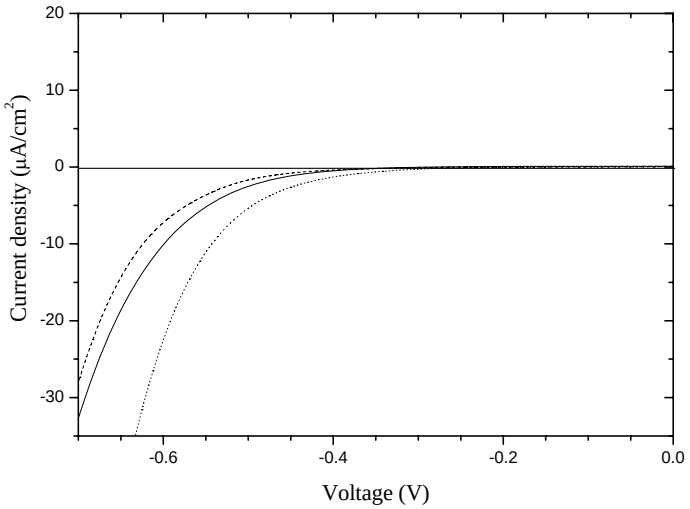

Figure 6.34. Current density *vs.* voltage characteristics of the polymer/nc-TiO_2 based liquid-state PEC in the dark where the polymer is PDHOPT (dot line), PDOOPT (solid line) and PDBOPT (dash line).

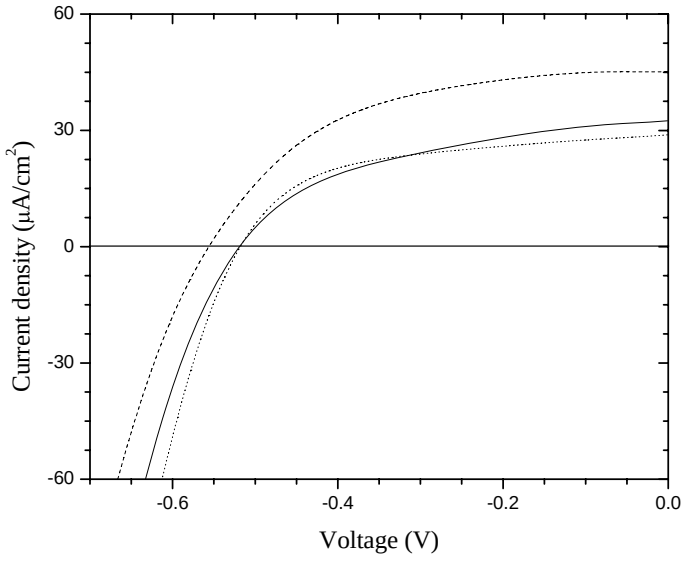

Figure 6.35. Current density *vs.* voltage characteristics of the polymer/nc-TiO_2 based liquid-state PEC under white light illumination from the ITO/nc-TiO_2/polymer side (backside) with light intensity of 80 mW/cm^2 where the polymer is PDHOPT (dot line), PDOOPT (solid line) and PDBOPT (dash line).

Table 6.4. Photoelectrochemical cell performance parameters of PDOOPT/nc-TiO_2, PDHOPT/nc-TiO_2 and PDBOPT/nc-TiO_2 based devices depicted in Figures 6.35 and 6.36.

Photoactive electrode	V_{OC} (V)	I_{SC} (μA/cm^2)	*FF*	η (%)	*IPCE*%
PDOOPT/nc-TiO_2	-0.52	32	0.46	0.01	0.15
PDHOPT/nc-TiO_2	-0.52	28	0.51	0.01	0.11
PDBOPT/nc-TiO_2	-0.56	45	0.52	0.02	0.65

In the dark, the device gave no current until a more negative potential is applied to the photoactive electrodes. Under illumination, the devices produced anodic photocurrents. Devices containing PDBOPT/nc-TiO_2 photoactive electrode showed a better performance producing a V_{OC} of -0.56 V, an I_{SC} of 45 μA/cm^2, a *FF* of 0.52 and η of 0.02%. The PDHOPT/nc-TiO_2 and PDOOPT/nc-TiO_2 devices show nearly similar performances with a V_{OC} of -0.52 V, and η of 0.01%. There is a small difference in I_{SC} and *FF* for the two, 32 μA/cm^2 and 0.46 for PDOOPT/nc-TiO_2 and 28 μA/cm^2 and 0.51 for PDHOPT/nc-TiO_2. The higher value in the V_{OC}, the I_{SC} and the *FF* in PDBOPT/nc-TiO_2 devices may be due to, as suggested by Nazeeruddin *et al.* [78], the suppression of the dark current at the semiconductor-electrolyte junction that arises from the reduction of triiodide by the conduction band electrons of the TiO_2. Since PDBOPT forms a good film on the TiO_2 surface, it can decrease the rate of the reduction of the triiodide ($k_{et}[I_3^-]$) on the TiO_2 surface leading to an increase in the open-circuit voltage according to the following equation:

$$V_{OC} = \left(\frac{kT}{e}\right)\ln\left(\frac{I_{inj}}{n_{CB}k_{et}[I_3^-]}\right) \quad (4)$$

where I_{inj} is the flux of charge resulting from sensitized injection, n_{CB} the concentration of electrons at the TiO_2 surface, k the Boltzmann constant, *T* the absolute temperature and *e* the electronic charge.

Assuming the same regio-regularity for the three polydialkoxy thiophenes, the hole mobility should increase as the length of the side chain decreases due to a better degree of intermolecular order and chain packaging density [77]. Hence, the expected higher hole

mobility in PDBOPT should contribute to the higher short-circuit current observed in PDBOPT/nc-TiO_2 devices. According to our investigation, the HOMO energy level of PDBOPT is higher in energy when compare with PDHOPT and PDOOPT. This allows a less restricted hole injection from the HOMO of PDBOPT to the I_3^-/I^- redox couple, leading to higher short-circuit current.

ii) Spectral response

Figure 6.36 shows the *IPCE*% of PDOOPT/nc-TiO_2, PDHOPT/nc-TiO_2 and PDBOPT/nc-TiO_2 based devices when illuminated from the ITO/nc-TiO_2/polymer side (backside). The maximum *IPCE%* obtained due to absorption by the polymers in the devices are 0.15% (at 440 nm), 0.11% (at 440 nm) and 0.65% (at 430 nm), respectively. The relative values correspond to the values observed in the current-voltage studies under illumination.

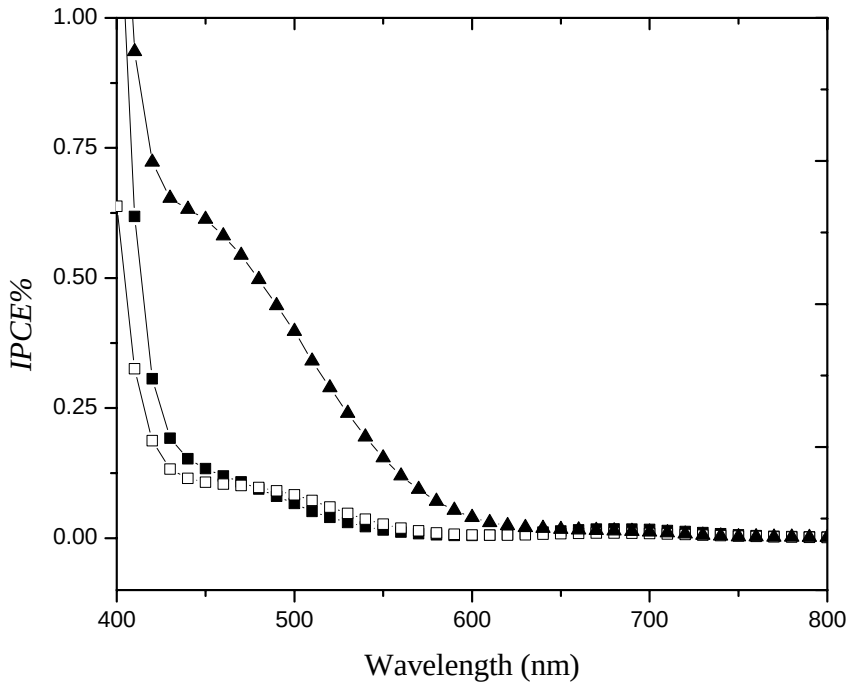

Figure 6.36. Action spectrum of PDOOPT/nc-TiO_2 (solid square), PDHOPT/nc-TiO_2 (open square) and PDBOPT/nc-TiO_2 (closed triangle) based liquid-state PEC under illumination from the backside.

iii) Dependence of *Isc* and *Voc* on incident light intensity

The dependence of V_{OC} and I_{SC} on incident light intensity for PDOOPT/nc-TiO_2, PDHOPT/nc-TiO_2 and PDBOPT/nc-TiO_2 based devices are shown in Figures 6.37 and 6.38, respectively. From the figures it can be observed that the V_{OC} and the I_{SC} increase with increasing light intensity, indicating that both V_{OC} and I_{SC} are affected by the photogenerated charge carriers [79]. The effect is more pronounced in PDBOPT/nc-TiO_2 based devices indicating better charge separation with decreasing side chain length of the substituent [79].

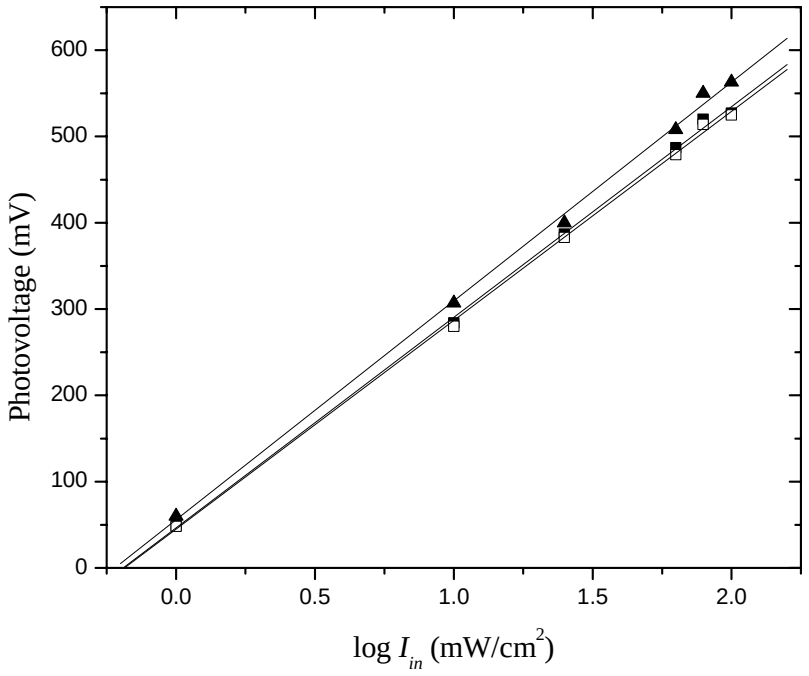

Figure 6.37. Plot of V_{OC} *vs.* log I_{in} of PDOOPT/nc-TiO_2 (solid squares), PDHOPT/nc-TiO_2 (open squares) and PDBOPT/nc-TiO_2 (closed triangles) based liquid-state PECs.

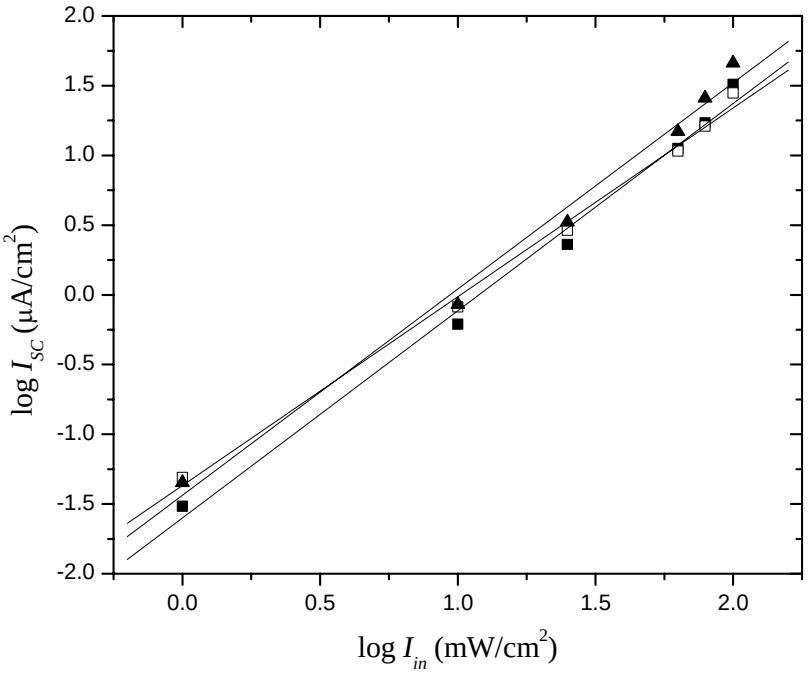

Figure 6.38. Plot of log I_{SC} *vs.* log I_{in} of PDOOPT/nc-TiO_2 (solid squares), PDHOPT/nc-TiO_2 (open squares) and PDBOPT/nc-TiO_2 (closed triangles) based liquid-state PECs.

c) Conclusions

PDOOPT, PDHOPT and PDBOPT, have been prepared electrochemically from their corresponding monomers for solar cell application. The energy levels of the HOMO and the LUMO of the polymers have been estimated from their cyclic voltammograms and UV-Vis optical absorption spectra. Electrochemical polymerization of DOOPT, DHOPT and DBOPT on nc-TiO_2 coated ITO-glass improves the film properties of the corresponding polymers. The polymers that are synthesized electrochemically on nc-TiO_2 coated ITO-glass sensitize nanocrystalline titanium dioxide in liquid-state photoelectrochemical cells.

Polythiophenes with longer dialkoxyphenyl substituents exhibited a lower photoelectrochemical cell performance. Our results show that the expected better exciton and hole mobility of shorter dialkoxyphenyl substituted polythiophenes can be used for solar cell application by improving the film properties of the polymers. It has been observed

that the V_{OC} and the I_{SC} of PDOOPT/nc-TiO_2, PDHOPT/nc-TiO_2 and PDBOPT/nc-TiO_2 based photoelectrochemical cells increase with increasing light intensity indicating that both V_{OC} and I_{SC} are affected by the photogenerated charge carriers.

6.3.3.4. The Photoresponse Behavior of a Solid-state MEH-PPPV - Sensitized Titanium Dioxide Photoelectrochemical Cell

The chemical structure of poly[2-methoxy-5-(2'-ethylhexyloxy)-1,4-phenylenevinylene], MEH-PPV, is shown in Figure 6.39.

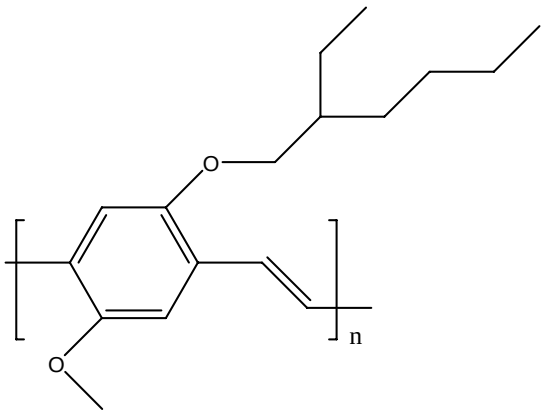

Figure 6.39. The chemical structure of MEH-PPV.

a) Current-voltage characteristics

The current–voltage characteristics of the ITO/nc-TiO_2/MEH-PPV/(I_3^-/I^-)/PEDOT/ITO solid-state PEC in the dark and under white light illumination from the backside at light intensity of 100 mW/cm^2 is shown in Figure 6.40. The device did not give a significant dark current for a certain range of applied voltages. The illuminated cell delivered an anodic short-circuit current (I_{SC}) of 0.145 mA/cm^2 and an open-circuit voltage (V_{OC}) of -410 mV. The fill factor (*FF*) and the power conversion efficiency (η) of the device were 0.5 and 0.03%, respectively.

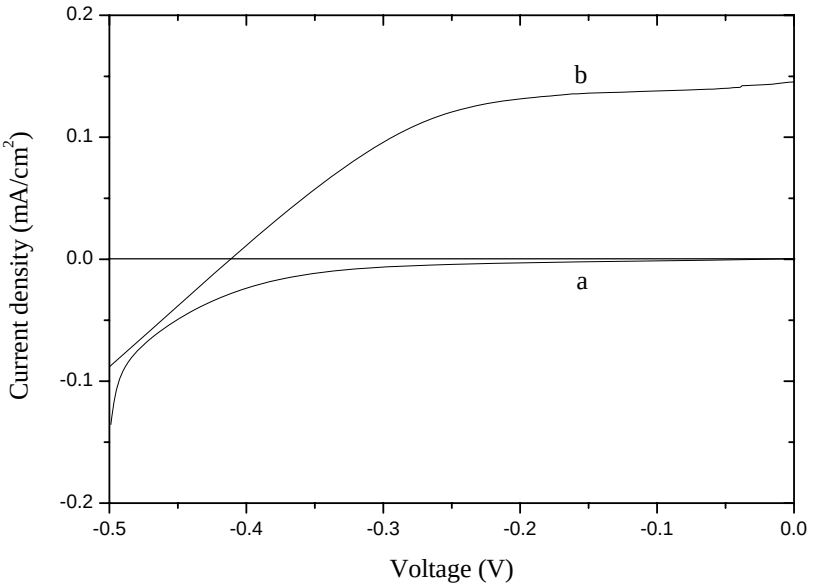

Figure 6.40. Current density *vs.* voltage characteristics of the nc-TiO_2/MEH-PPV based solid-state PEC a) in the dark and b) under white light illumination from the backside at light intensity of 100 mW/cm^2.

b) Time dependence of the short-circuit current density and the open-circuit voltage

The changes in I_{SC} and V_{OC} with and without illumination were measured as a function of time. These measurements were used to observe the transient response of the cell and its stability towards light illumination. The illumination was made from the backside with white light of intensity 100 mW/cm^2 and it was switched on and off periodically by blocking the light path.

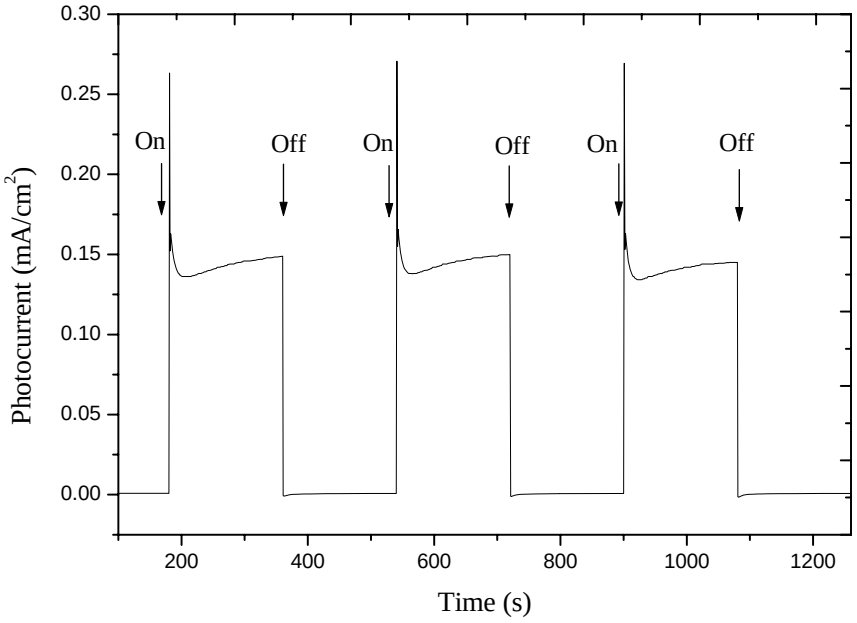

Figure 6.41. Short-circuit photocurrent changes induced by switching illumination on and off from the backside of the nc-TiO_2/MEH-PPV based solid-state PEC with incident light intensity of 100 mW/cm^2.

Upon illumination a transient short-circuit current was immediately generated, probably due to rapid modifications in the electrical properties of the semiconducting polymer [80]. The current then dropped and then slightly increased to a steady-state value of 0.145 mA/cm^2 (Figure 6.41). When the illumination was switched off, the current immediately dropped to zero. An open-circuit photovoltage was also immediately generated with a value of 410 mV and dropped to zero sharply when the illumination was switched off indicating the absence of electron trapping sites on the composite film (Figure 6.42). Such behaviors of I_{SC} and V_{OC} have been observed in a similar photoelectrochemical system without TiO_2 [81].

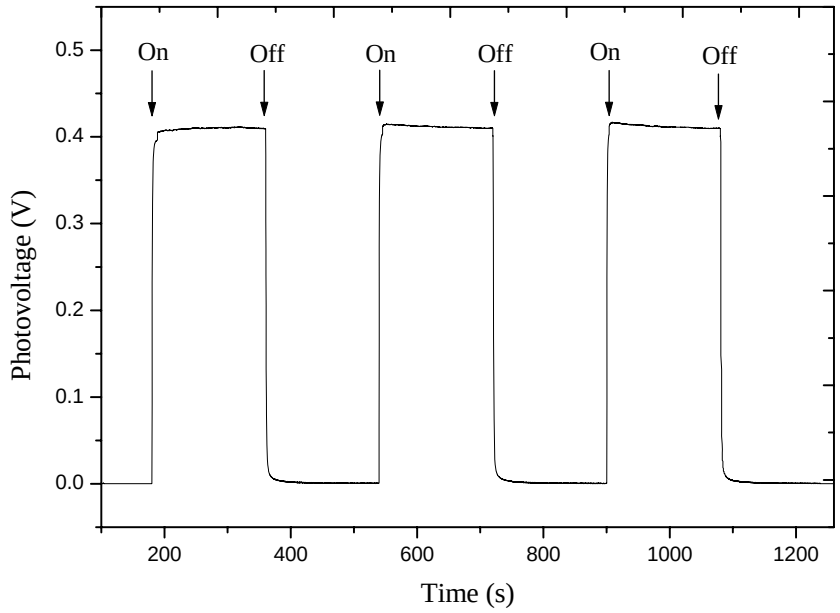

Figure 6.42. Open-circuit voltage response of the nc-TiO_2/MEH-PPV based solid-state PEC to switching illumination on and off from the backside with incident light intensity of 100 mW/cm^2.

c) Spectral response

The photocurrent collected at different wavelengths of the incident light, relative to the number of photons incident on the surface at that wavelength, determines the spectral response of a PEC. The ability of a solar cell to generate photocurrent at a given wavelength of the incident light is measured by the monochromatic incident photon-to-current conversion efficiency (*IPCE*), defined as the number of electrons generated per number of incident photons. Figure 6.43 shows the UV-Visible absorption spectrum of MEH-PPV and the IPCE% spectra for the backside and for the front side illumination of a nc-TiO_2/MEH-PPV based solid-state PEC under short-circuit condition. The Figure shows that the action spectra for backside and front side illuminations closely match the absorption spectrum of MEH-PPV indicating that the photoelectrochemical conversion is achieved through the photosensitization of TiO_2 by MEH-PPV. The *IPCE*% obtained for the backside and for the front side illuminations at the maximum absorption of MEH-PPV (500 nm) were 1.8% and

1.4%, respectively. The higher *IPCE*% for the backside illumination indicates that excitons are generated near the nc-TiO_2/MEH-PPV interface where exciton dissociation takes place [19]. The lowering of the *IPCE*% for front side illumination could be due to electron recombination processes during the transport of electron-hole pair (exciton) from the outer part of the film to the nc-TiO_2/MEH-PPV interface [82].

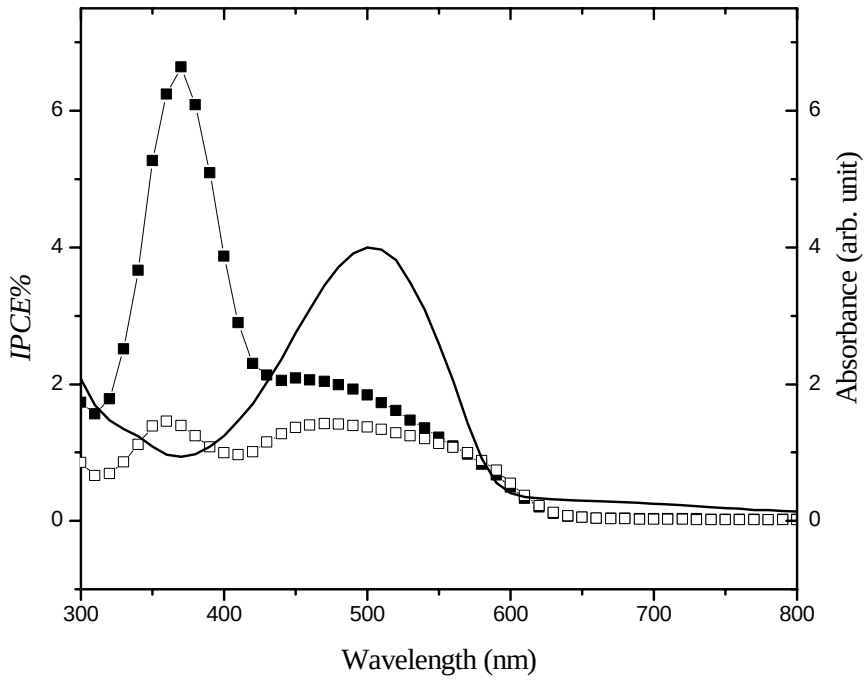

Figure 6.43. Optical absorption spectrum of MEH-PPV film (solid line) on ITO-glass and the photocurrent action spectra of nc-TiO_2/MEH-PPV based PEC under illumination from the backside (solid squares) and front side (open squares).

The *IPCE%* peak observed at shorter wavelengths (around 380 nm) is due to light absorption by the nc-TiO_2. The value is relatively high (especially during backside illumination where exciton dissociation is favored) because of the low light intensities in the short wavelength regions (Figure 6.43). Figure 6.44 (from which the *IPCE%* spectra of Figure 6.43 are obtained) shows the incident light intensity distribution at the sample position and the short-circuit current density which were measured at different wavelengths

while illuminating a calibrated silicon photodiode and the nc-TiO_2/MEH-PPV based solid-state PEC, respectively. From Figure 6.44, it can be observed that much of the current during white light illumination comes from the sensitizing effect of MEH-PPV.

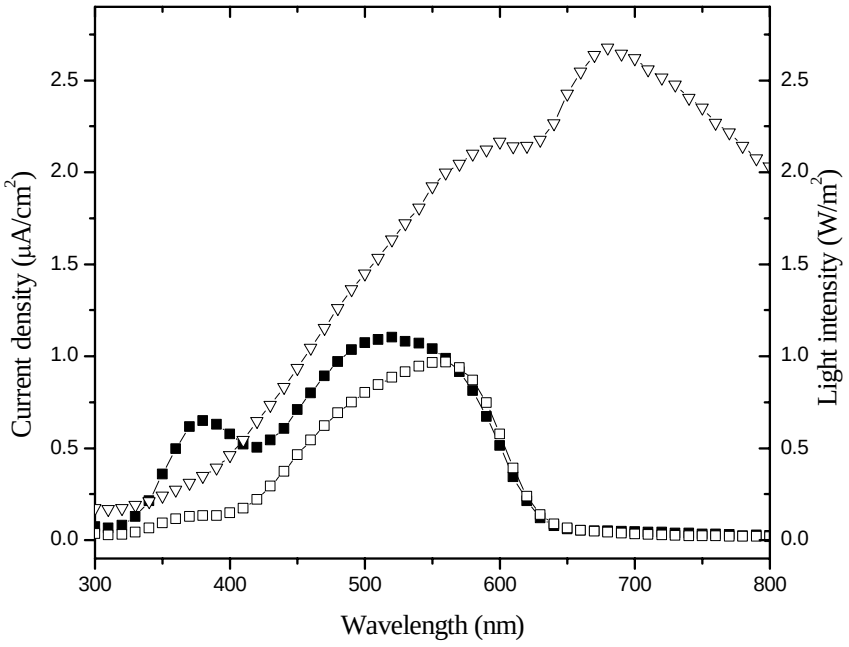

Figure 6.44. Incident light intensity distribution (open triangles) and short-circuit photocurrent density spectra of the nc-TiO_2 /MEH-PPV based solid-state PEC under illumination from the backside (solid squares) and front side (open squares).

The energy levels of the LUMO and the HOMO of MEH-PPV are -2.9 eV and -5.1 eV *vs.* vacuum, respectively [49]. The quasi-Fermi energy level of nc-TiO_2 under illumination is -4.2 eV *vs.* vacuum [83]. Thus photogenerated free electrons can be transferred from the LUMO of MEH-PPV to the low-lying conduction band of TiO_2. In the mean time photogenerated holes can be transferred from the HOMO of MEH-PPV to the electrolyte where they oxidize I^- to I_3^- (E_{redox} (I_3^-/I^-) = -4.9 eV *vs.* vacuum [2]). I^- is regenerated when the I_3^- is reduced at the counter electrode.

d) Dependence of *Isc* and V_{OC} on incident light intensity

The plots of log I_{SC} and V_{OC} *vs.* log I_{in} for nc-TiO_2/MEH-PPV based solid-state PEC are depicted in Figures 6.45 and 6.46, respectively. The plot of log I_{SC} *vs.* log I_{in} yielded a straight line with α = 0.9. An α value less than 1 indicates the presence of some exciton recombination due to surface states that act as recombination centers [69,84].

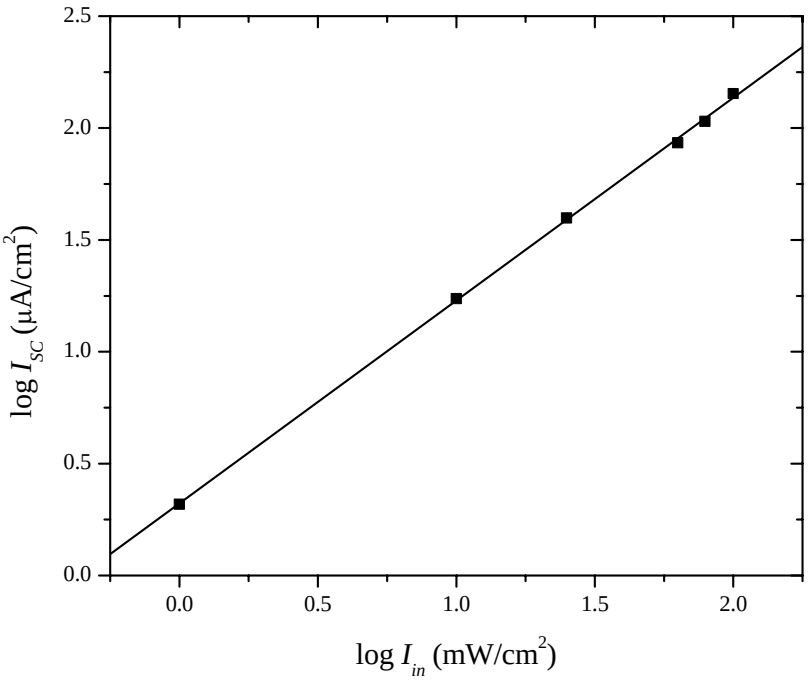

Figure 6.45. Dependence of short-circuit photocurrent on incident light intensity for illumination through the backside of the nc-TiO_2/MEH-PPV based solid-state PEC.

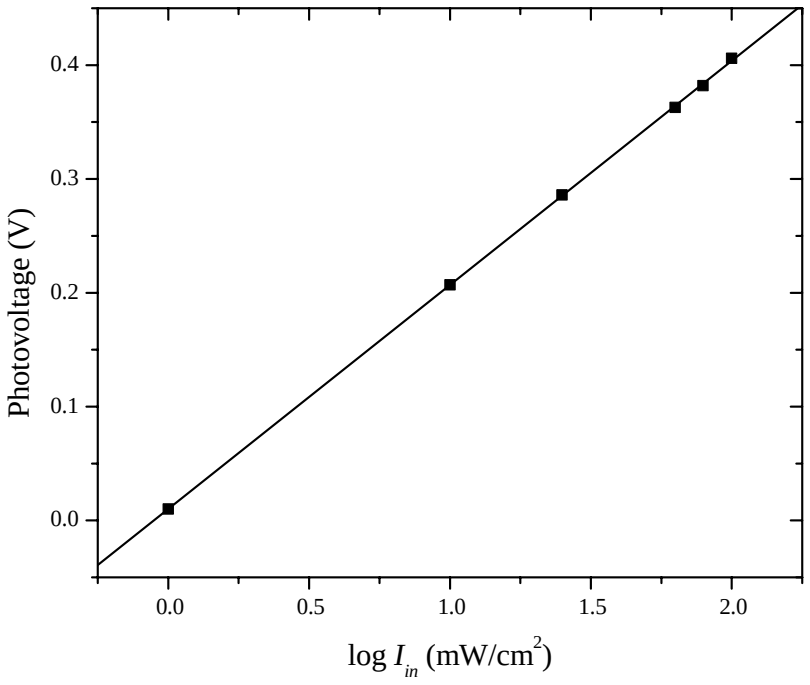

Figure 6.46. Dependence of photovoltage on incident light intensity for illumination through the backside of the nc-TiO_2/MEH-PPV based solid-state PEC.

e) Conclusions

A solid-state PEC based on MEH-PPV-sensitized TiO_2 was constructed and studied for its photoresponse behavior. The solid polymer electrolyte used in the device was POMOE that was complexed with I_3^-/I^- and the counter electrode was oxidized PEDOT on ITO-glass. A short-circuit current of 0.145 mA/cm^2, an open-circuit voltage of 410 mV, a power conversion efficiency of 0.03% and a fill factor of 0.5 were obtained when the device was illuminated with light of intensity 100 mW/cm^2. The *IPCE%* obtained for the backside and for the front side illuminations at the maximum absorption of MEH-PPV (500 nm) were 1.8% and 1.4%, respectively. Exciton recombination may be a limiting factor for the photocurrent generation, as observed from the study of incident light intensity dependence of short-circuit current. Though the performance of the device is low when compared with solid-state dye-sensitized and liquid-state polymer-sensitized nc-TiO_2 photoelectrochemical

cells, the results are still encouraging when considering the advantages of conducting polymers and polymer electrolytes over dyes and liquid electrolytes, respectively. Increasing the interpenetration of the sensitizing polymer and the polymer electrolyte through the pores of the nc-TiO_2 particles, use of a sensitizing polymer that could be adsorbed better on to the nc-TiO_2 particles and use of a polymer electrolyte with better conductivity can increase the power conversion efficiencies of polymer-sensitized solid-state photoelectrochemical cells.

6.3.3.5. A Comparative Study on Solid-state Photoelectrochemical Solar Energy Conversion Based on Poly[2-methoxy-5-(2'-ethylhexyloxy)-1,4-phenylenevinylene], MEH-PPV, and a Blend of MEH-PPV and C_{60}

a) Current-voltage characteristics

Figure 6.47 and Figure 6.48 show the current-voltage curves of the photoelectrochemical devices based on MEH-PPV film and a MEH-PPV/C_{60} composite film, in the dark and under white light illumination at 100 mW/cm^2, respectively. The devices were illuminated from their front side (ITO/PEDOT). The photoelectrochemical characteristics of the devices are compared in Table 6.5. In the dark, the current for both devices was negligible and remained relatively constant in the negative potential range while a larger anodic current was observed in the larger positive potential range. The positive applied potential acts to diminish the effects of the internal barrier field that is set at the polymer/electrolyte junction. As a result, charge carriers acquire enough energy to cross the barrier, resulting with large anodic currents. The increase in the anodic current with increasing positive potential is sharper in MEH-PPV/C_{60} based devices indicating a decrease in the series resistance of the film that may be due to the ease of electron transport through the C_{60} particles. On the other hand, applying a negative potential enhances the barrier potential and only a small current flows.

The current response of the devices to the applied potentials in the dark indicates that the devices exhibit the desirable photoelectrochemical properties. Under illumination, cathodic photocurrents were observed in both devices that extend from the negative potential range up to a positive potential range, which is expressed as the open-circuit voltage. This indicates that the direction of the photoinduced charge separation is the same as that of the charge separation by the applied potential.

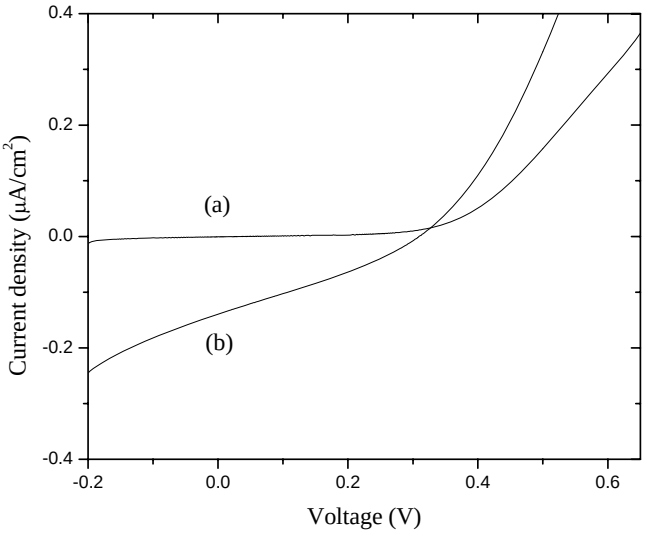

Figure 6.47. Current density *vs*. voltage characteristics of the MEH-PPV based solid-state PEC: (a) in the dark and (b) under white light illumination from the ITO/PEDOT side (front side) at light intensity of 100 mW/cm^2.

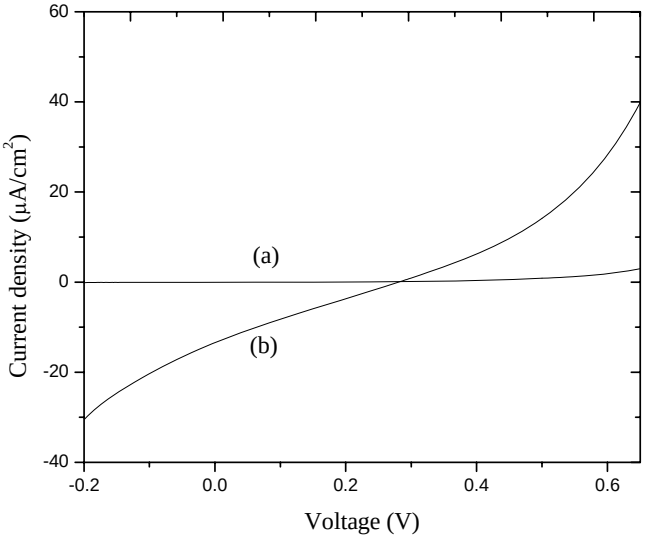

Figure 6.48. Current density *vs*. voltage characteristics of the MEH-PPV/C_{60} based solid-state PEC: (a) in the dark and (b) under white light illumination from the ITO/PEDOT side (front side) at light intensity of 100 mW/cm^2.

Table 6.5: The performance of photoelectrochemical devices based on MEH-PPV and MEH-PPV/C_{60} photoactive electrodes when illuminated with white light intensity of 100 mW/cm^2.

Photoactive electrode	V_{OC} (V)	I_{SC} (μA/cm^2)	*FF*
MEH-PPV	310	0.14	0.30
MEH-PPV/C_{60}	280	13.40	0.24

From Table 6.5, it can be seen that the MEH-PPV/C_{60} based device exhibits nearly a 95-fold improvement in the short-circuit current, but lower V_{OC} when compared with the MEH-PPV based device. The electron transfer from the LUMO of a conjugated polymer to the LUMO of C_{60} takes place much faster than any decaying process of the photoexcitation [85]. The several-fold enhancement in the short circuit current of MEH-PPV/C_{60} based device most likely originates from the enhanced charge carrier separation and improved charge carrier mobility [86]. The fill factor for MEH-PPV/C_{60}-based devices is lower than that of MEH-PPV-based devices, probably due to space-charge effects inherent in bulk heterojunction structures [16].

Figure 6.49 illustrates the schematic of operation of the MEH-PPV and MEH-PPV/C_{60} based solid-state PEC. The energy levels of the LUMO and the HOMO of MEH-PPV are -2.9 eV and -5.1 eV *vs.* vacuum, respectively [49] while those of C_{60} are -3.7 eV and -6.1 eV, respectively [87]. Thus, photogenerated free electrons can be transferred from the LUMO of MEH-PPV to the LUMO of C_{60} and then to the electrolyte where they reduce I_3^- to I^- (E_{redox} (I_3^-/I^-) = -4.9 eV *vs.* vacuum [2]). I_3^- is regenerated when the I^- is oxidized at the counter electrode (anode). In the mean time, the photogenerated holes move to the back contact (ITO) of the PEC through the polymer network.

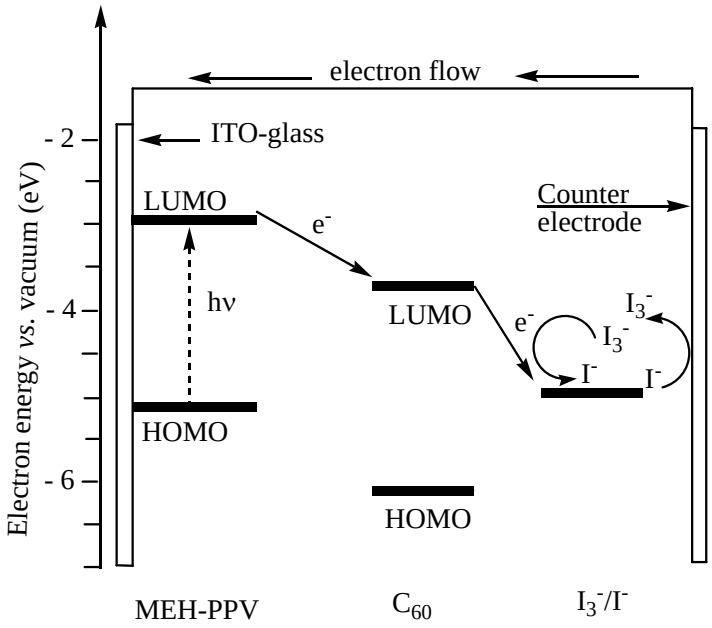

Figure 6.49. Schematic of operation of the MEH-PPV and MEH-PPV/C_{60} based solid-state PEC.

b) Spectral response

The photocurrent action spectra (expressed as *IPCE%*) for the MEH-PPV based and for the MEH-PPV/C_{60} based solid-state PECs are shown in Figure 6.50 and Figure 6.51, respectively. Table 6.6 summarizes the *IPCE%* obtained at the maximum absorbance for the two devices.

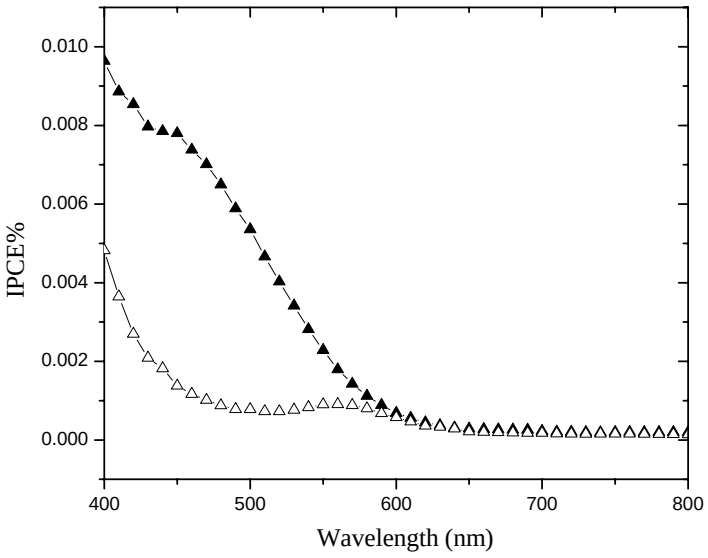

Figure 6.50. Action spectra of MEH-PPV based solid-state PEC under illumination from the front side (closed triangles) and from the backside (open triangles).

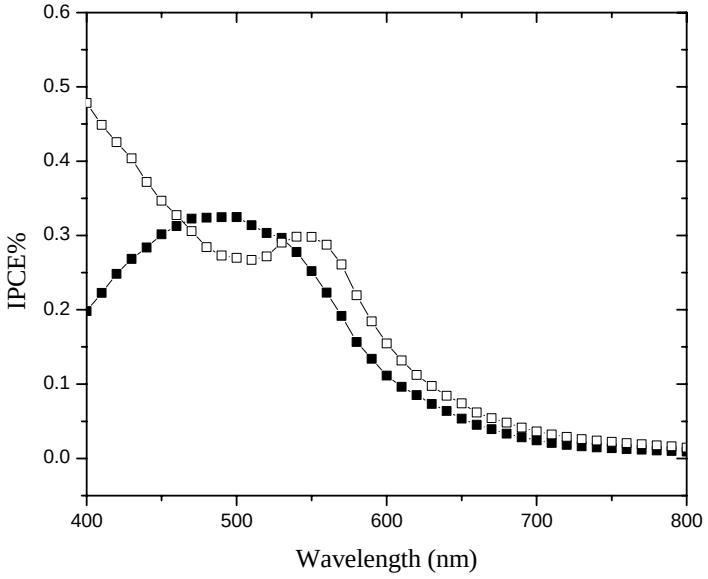

Figure 6.51. Action spectra of MEH-PPV/C_{60} based solid-state PEC under illumination from the front side (closed squares) and from the backside (open squares).

Table 6.6. *IPCE%* for the MEH-PPV based and for the MEH-PPV/C_{60} based solid-state PECs.

Photoactive electrode	*IPCE%* (x10^{-3})	
	Front side illumination	Backside illumination
MEH-PPV	7	0.9
MEH-PPV/C_{60}	320	270

The higher *IPCE%* obtained for the front side illumination of both devices indicates that excitons are generated near the polymer/electrolyte interface where exciton dissociation takes place. The *IPCE%* of MEH-PPV/C_{60} based PEC are higher than those of MEH-PPV based devices, indicating better charge separation and transport in MEH-PPV/C_{60} devices.

The normalized optical absorption spectrum of MEH-PPV film on ITO-glass and the normalized photocurrent action spectra of MEH-PPV based and MEH-PPV/C_{60} based devices for front side illuminations are shown in Figure 6.52. The photocurrent action spectrum of the MEH-PPV/C_{60} based PEC for the front side illumination matched the UV-Vis absorption spectrum of the MEH-PPV/C_{60} than does the MEH-PPV based device, indicating better charge carrier generation and collection.

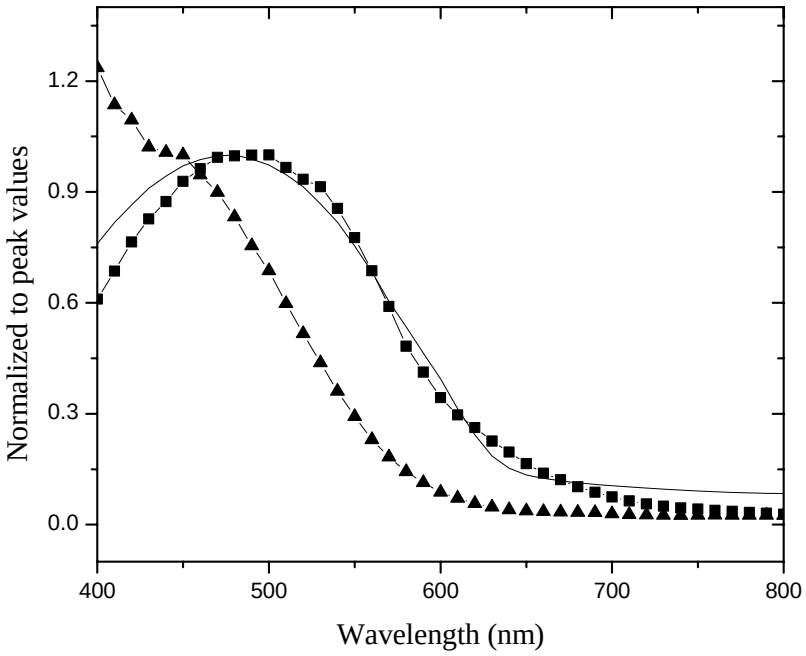

Figure 6.52. Normalized optical absorption spectrum of MEH-PPV/C_{60} film on ITO-glass (solid line) and normalized photocurrent action spectra of MEH-PPV based (closed triangles) and MEH-PPV/C_{60} based (closed squares) devices for front side illuminations.

c) Dependence of *Isc* and V_{OC} on incident light intensity

The dependence of I_{SC} and V_{OC} on incident light intensity for MEH-PPV and MEH-PPV/C_{60} based devices are shown in Figure 6.53 and Figure 6.54, respectively. From the figures it can be observed that the V_{OC} and the I_{SC} increase with increasing light intensity, indicating that both V_{OC} and I_{SC} are affected by the photogenerated carriers [79]. In MEH-PPV/C_{60} based devices, the I_{SC} increases more rapidly with increasing light intensity, indicating better charge separation and collection.

For organic and inorganic solar cells, the short-circuit current density increases with incident light intensity and is proportional to I_{in}^{α} [69], where α is characteristic for the system studied. In Figure 6.53, the photocurrent increases less rapidly than the first power (an ideal value) of the light intensity for both MEH-PPV based (α = 0.60) and MEH-

PPV/C_{60} based (α = 0.71) devices, indicating the presence of bimolecular exciton recombination [70,71] and/or the presence of traps and disorders that act as recombination centers [72,84].

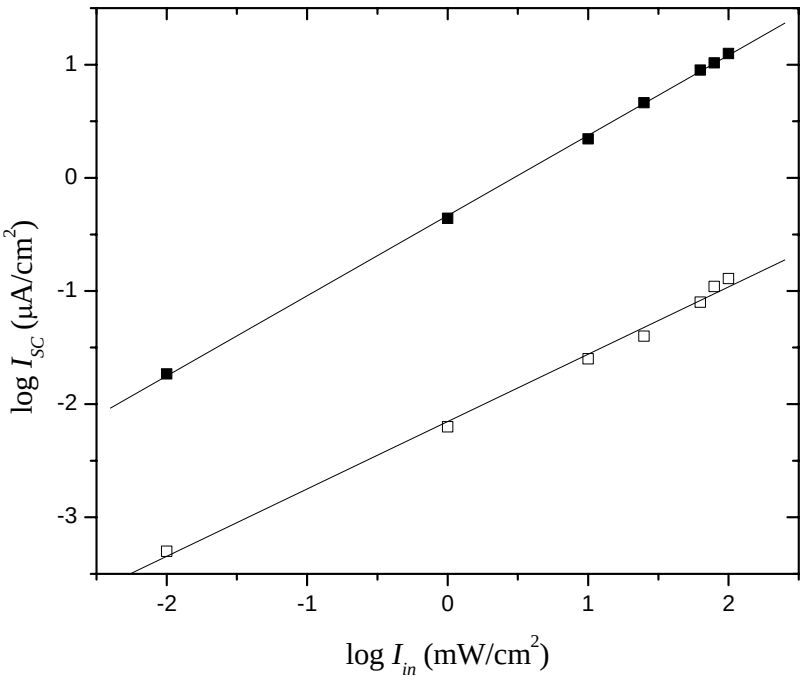

Figure 6.53. Plot of log I_{SC} *vs.* log I_{in} of MEH-PPV based (open squares) and MEH-PPV/C_{60} based (closed squares) solid-state PECs.

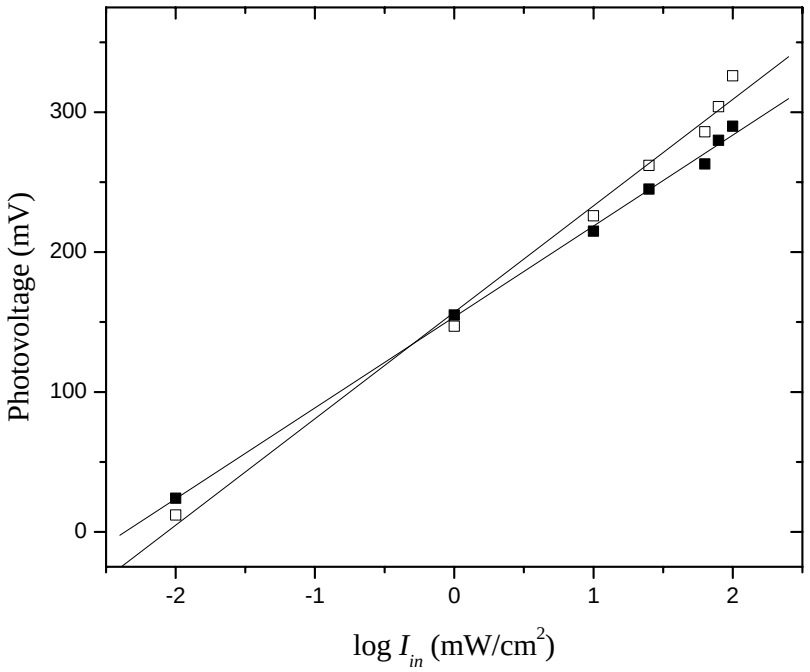

Figure 6.54. Plot of V_{OC} *vs.* log I_{in} of MEH-PPV based (open squares) and MEH-PPV/C_{60} based (closed squares) solid-state PECs.

d) Conclusions

Solid-state photoelectrochemical cells based on MEH-PPV and a blend of MEH-PPV/C_{60} photoactive electrodes were constructed and studied for their photoresponse behavior. The solid polymer electrolyte used in the devices was POMOE that was complexed with I_3^-/I^- and the counter electrode was oxidized PEDOT on ITO-glass. Devices where the photoactive electrode consists of MEH-PPV/C_{60} showed improved short-circuit current and power conversion efficiency over those that consist of MEH-PPV alone. The several-fold enhancement in the short-circuit current of MEH-PPV/C_{60} based devices most likely originates from the improved charge carrier separation and mobility. MEH-PPV based devices exhibit improved IPCE% that follows the UV-Vis absorption spectra.

REFERENCES

[1] B. O'Regan, M. Grätzel, Nature 353 (1991) 737.

[2] A. Hagfeldt, M. Grätzel, Acc. Chem. Res. 33 (2000) 269.

[3] A. Hinsch, J.M. Kroon, R. Kern, I. Uhlendorf, J. Holzbock, A. Meyer, J.A. Ferber, Prog. Photovolt: Res. Appl. 9 (2001) 425.

[4] R. Grünwald, H. Tributsch, J. Phys. Chem. B 101 (1997) 2564.

[5] A.F. Nogueira, J.R. Durrant, M.A. De Paoli, Adv. Mater. 13 (2001) 826.

[6] B. O'Regan, D.T. Schwartz, J. Appl. Phys. 80 (1996) 4749.

[7] U. Bach, D. Lupo, P. Comte, J.E. Moser, F. Weissörtel, J. Salbeck, H. Spreitzer, M. Grätzel, Nature 395 (1998) 583.

[8] D. Gebeyehu, C.J. Brabec, N.S. Sariciftci, D. Vangeneugden, R. Kiebooms, D. Vanderzande, F. Kienberger, H. Schindler, Synth. Met. 125 (2002) 2797.

[9] D. Gebeyehu, C.J. Brabec, F. Padinger, T. Fromherz, S. Spiekermann, N. Vlachopoulos, F. Kienberger, H. Schindler, N.S. Sariciftci, Synth. Met. 121 (2001) 1549.

[10] G.K.R. Senadeera, T. Kitamura, Y. Wada, S. Yanagida, Sol. Energy Mater. Sol. Cells 88 (2005) 315.

[11] Y. Hao, M. Yang, C. Yu, S. Cai, M. Liu, L. Fan, Y. Li, Sol. Energy Mater. Sol. Cells 56 (1998) 75.

[12] P.A. van Hal, M.M. Wienk, J.M. Kroon, R.A.J. Janssen, J. Mater. Chem. 13 (2003) 1054.

[13] P.A. van Hal, M.M. Wienk, J.M. Kroon, W.J.H. Verhees, L.H. Slooff, W.J.H. van Gennip, P. Jonkheijm, R.A.J. Janssen, Adv. Mater. 15 (2003) 118.

[14] D. Gebeyehu, C.J. Brabec, N.S. Sariciftci, Thin Solid Films 403-404 (2002) 271.

[15] T.J. Savenije, J.M. Warman, A. Goossens, Chem. Phys. Lett. 287 (1998) 148.

[16] G. Li, V. Shrotriya, J. Huang, Y. Yao, T. Moriarty, K. Emery, Y. Yang, Nature 4 (2005) 864.

[17] M. Reyes-Reyes, K. Kim, D.L. Carroll, Appl. Phys. Lett.87 (2005) 083506.

[18] W. Ma, C. Yang, X. Gong, K. Lee, A.J. Heeger, Adv. Funct. Mater.15 (2005) 1617.

[19] A.C. Arango, L. Johnson, H. Horhold, Z. Schlesinger, S.A. Carter, Adv. Mater. 12 (2000) 1689.

[20] W.U. Huynh, J.J. Dittmer, A.P. Alivisatos, Science 295 (2002) 2425.

[21] G.P. Smestad, S. Spiekermann, J. Kowalik, C.D. Grant, A.M. Schwartzberg, J. Zhang, L.M. Tolbert, E. Moons, Sol. Energy Mater. Sol. Cells 76 (2003) 85.

[22] E. Arici, H. Hoppe, F. Schäffler, D. Meissner, M.A. Malik, N.S. Sariciftci, Thin Solid Films 451-452 (2004) 612.

[23] W.J.E. Beck, M.M. Wienk, R.A.J. Janssen, Adv. Mater. 16 (2004) 1009.

[24] C.D. Grant, A.M. Schwartzberg, G.P. Smestad, J. Kowalik, L.M. Tolbert, J.Z. Zhang, J. Electroanal. Chem. 522 (2002) 40.

[25] A.J. Breeze, Z. Schlesinger, P.J. Brock, S.A. Carter, Phys. Rev. B 64 (2001) 125205.

[26] L. Bozano, S.A. Carter, J.C. Scott, G.G. Malliaras, P.J. Brock, Appl. Phys. Lett. 74 (1999) 1132.

[27] E.M. Genies, M. Lapkowski, C. Santier, E. Vieil, Synth. Met. 18 (1987) 18.

[28] N.S. Sariciftci, H. Kuzmany, Synth. Met. 21 (1987) 157.

[29] M. Kaneko, H. Nakamura, J. Chem. Soc., Chem. Commun. (1985) 346.

[30] E.M. Genies, M. Lapkowski, Synth. Met. 24 (1988) 69.

[31] P.K. Shen, Z.Q. Tian, Electrochimica Acta, 34 (1989) 1611.

[32] S.das Neves, M.-A. De Paoli, Synth. Met. 96 (1998) 49.

[33] S.X. Tan, J. Zhai, M.X. Wan, L. Jiang, D.B. Zhu, Synth. Met. 137 (2003) 1511.

[34] R.W.T. Higgins, N.A. Zaidi, A.P. Monkman, Adv. Funct. Mater. 11 (2001) 407.

[35] S.-An Chen, Y. Fang, Synth. Met. 60 (1993) 215.

[36] Y. Hao, M. Yang, C. Yu, S. Cai, M. Liu, L. Fan, Y. Li, Sol. Energy mater. Sol. Cells 56 (1998) 75.

[37] D. Carinhana Jr., R. Faez, A.F. Nogueira, M.-A.D e Paoli, Synth. Met. 121 (2001) 1569.

[38] F. Cao, G. Oskam, P.C. Searson, J. Phys. Chem. 99 (1995) 17071.

[39] R. Cervin, X.C. Li, G.W.C. Spencer, A.B. Holmes, S.C. Moratti, R.H. Friend, Synth. Met. 84 (1997) 359.

[40] Y. Liu, M.S. Liu, A.K.-Y. Jen, Acta Polym. 50 (1999) 105.

[41] D.M. de Leeuw, M.M.J. Simenson, A.R. Brown, R.E.F. Einerhand, Synth. Met. 87 (1997) 53.

[42] M. Al-Ibrahim, H.-K. Roth, U. Zhokhavets, G. Gobsch, S. Sensfuss, Sol. Energy Mater. Sol. Cells 85 (2005) 13.

[43] I. Schwendan, J. Hwang, D.M Welsh, D.B. Tanner, J.R. Reynolds, Adv. Mater. 13 (2001) 634.

[44] G.A. Sotzing, J.L. Reddinger, A.R. Katritzky, J. Soloducho, R. Musgrave, J.R. Reynolds, P.J. Steel, Chem. Mater. 9 (1997) 1578.

[45] I. Schwendan, R. Hickman, G. Sönmez, P. Schottland, K. Zong, D.M. Welsh, J.R. Reynolds, Chem. Mater. 14 (2002) 3118.

[46] G.W. Jones, D.M. Taylor, H.L. Gomes, Synth. Met. 85 (1997) 1341.

[47] U. Rammelt, N. Hebestreit, A. Fikus, W. Plieth, Electrochim. Acta 46 (2001) 2363.

[48] F. Cecchet, C.A. Bignozzi, F. Paolucci, M. Marcaccio, Synth. Met. 156 (2006) 27.

[49] Y. Li, Y. Cao, J. Gao, D. Wang, G. Yu, A.J. Heeger, Synth. Met. 99 (1999) 243.

[50] C. Xirochaki, G. Kiriakidis, T.F. Pedersen, H. Fritzsche, J. Appl. Phys. 79 (1996) 9349.

[51] S. Mailis, L. Boutsikaris, N.A. Vainos, C. Xirochaki, G. Vasiliou, N. Garawal, G. Kiriakidis, H. Fritzsche, Appl. Phys. Lett. 69 (1996) 2459.

[52] C. Xirochaki, K. Moschovis, E. Chatzitheodoridis, G. Kiriakidis, P. Morgen, Appl. Phys. A 67 (1998) 295.

[53] S. Pissadakis, S. Mailis, L. Reekie, J.S. Wilkinson, R.W. Eason, N.A. Vainos, K. Moschovis, G. Kiriakdikis, Appl. Phys. A 69 (1999) 333.

[54] H. Spanggaard, F.C. Krebs, Sol. Energy Materials Sol. Cells 83 (2004) 125.

[55] J.S. Kim, M. Granstrom, R.H. Friend, N. Johansson, W.R. Salaneck, R. Daik, W.J. Feast, F. Cacialli, J. Appl. Phys. 84 (1998) 6859.

[56] A.R. Schlatman, D.W. Floet, A. Hilberer, F. Garten, P.J.M. Smulders, T.M. Klapwijk, G. Hadziioannou, Appl. Phys. Lett. 69 (1996) 1764.

[57] S.A. Carter, M. Angelopoulos, S. Karg, P.J. Brock, J.C. Scott, Appl. Phys. Lett. 70 (1997) 2067.

[58] Y. Cao, G. Yu, C. Zhang, R. Menon, A.J. Heeger, Synth. Met. 87 (1997) 171.

[59] J.C. Carter, I. Grizzi, S.K. Heeks, D.J. Lacey, S.G. Latham, P.G. May, O.R. d.l. Panos, K. Pichler, C.R. Towns, H.F. Wittman, Appl. Phys. Lett. 71 (1997) 34.

[60] K. Tennakone, G.R.R.A. Kumara, I.R.M. Kottegoda, K.G.U. Wijayantha, V.P.S. Perera, J. Phys. D: Appl. Phys. 31 (1998) 1492.

[61] Q. Pei, M. Ahlskog, O. Inganäs, Polymer 35 (1994) 1347.

[62] X. Chen, K.-Z. Xing, O. Inganäs, Chem. Mater. 8 (1996) 2439.

[63] H. Randriamahazaka, C. Noël, C. Chevrot, J. Electroanal. Chem. 472 (1999) 103.

[64] M. Granström, K. Petritsch, A.C. Arias, A. Lux, M.R. Andersson, R.H. Friend, Nature 395 (1998) 257.

[65] T. Yohannes, O. Inganäs, Sol. Energy Materials Sol. Cells 51 (1998) 193.

[66] C.V. Nicholas, D.J. Wilson, C. Booth, J.R.M. Giles, Br. Polym. J. 20 (1988) 289.

[67] M. Nekoomanesh, H.S. Nagae, C. Booth, J.R. Owen, J. Electrochem. Soc. 139 (1992) 3046.

[68] Y. Xu, M.A.A. Schoonen, American Mineralogist 85 (2000) 543.

[69] H. Meier, Organic Semiconductors, Verlag Chemi: Berlin, 1974, p. 318.

[70] M. Pientka, V. Dyakonov, D. Meissner, A. Rogach, D. Talapin, H. Weller, L. Lutsen, D. Vanderzande, Nanotechnolorgy 15 (2004) 163.

[71] G. Dellepiane, C. Cuniberti, D. Comoretto, G.F. Musso, G. Figari, A. Piaggi, A. Borghesi, Phys. Rev. B 48 (1993) 7850.

[72] S. Glenis, G. Tourillon, F. Garnier, Thin Solid Films 139 (1986) 221.

[73] J.L. Bredas, R. Silbey, D.S. Boudreaux, R.R. Chance, J. Am. Chem. Soc. 105 (1983) 6555.

[74] F.J. Hyde, *Semiconductors*, Macdonald & Co. (Publishers) Ltd., London, 1965; p 227.

[75] F. Costanzo, D. Tonelli, G. Scalmani, J. Cornil, Polymer 47 (2006) 6692.

[76] A. Heeger, P. Smith, Conjugated polymers, J.L. Bredas, R. Silbey, eds., Kluwer, Dordrcht, 1991, p. 142.

[77] S. Sensfuss, M. Al-Ibrahim, in: Organic Photovoltaics, S-S. Sun, N.S. Sariciftci (eds.), first ed., Crc Press LIc, UK, 2005, p.529.

[78] M.K. Nazeeruddin, A. Kay, I. Rodicio, R. Humphry-Baker, E. Müller, P. Liska, N. Vlachopoulos, M. Grätzel, J. Am. Chem. Soc. 115 (1993) 115.

[79] Y. Fang, S-An. Chen, M.L. Chu, Synth. Met. 52 (1992) 261.

[80] E.M. Genies, M. Lapkowski, Synth. Met. 24 (1988) 69.

[81] T. Yohannes, O. Inganäs, J. Electrochem. Soc. 143 (1996) 2310.

[82] H. Lindström, A. Hagfeldt, H. Rensmo, A. Solbrand, S. Södergren, S.E. Lindquist, SPIE 2531 (1995) 176.

[83] A. Hagfeldt, M. Grätzel, Chem. Rev. 95 (1995) 49.

[84] R.O. Loufty, J.H. Sharp, C.K. Hsiao, R. Ho, J. Appl. Phys.52 (1981) 5218.

[85] L. Smilwitz, N.S. Sariciftci, R. Wu, C. Gettinger, A.J. Heeger, F. Wudl, Phys. Rev. B 47 (1993) 13835.

[86] S.E. Shaheen, C.J. Brabec, F. Padinger, T. Fromherz, J.C. Hummelen, N.S. Sariciftci, Appl. Phys. Lett. 78 (2001) 841.

[87] N.S. Sariciftci, L. Smilowitz, A.J. Heeger, F. Wudl, Science 258 (1992) 1474.